

UCSF

UC San Francisco Electronic Theses and Dissertations

Title

The cooperation of PIK3CA[H1047R] with BRAF[V600E] and KRAS[G12D] in lung tumorigenesis

Permalink

<https://escholarship.org/uc/item/8fs8784n>

Author

Green, Shon

Publication Date

2015

Peer reviewed|Thesis/dissertation

The cooperation of PIK3CA^{H1047R} with
BRAF^{V600E} and KRAS^{G12D} in lung
tumorigenesis

by

Shon Green

DISSERTATION

Submitted in partial satisfaction of the requirements for the degree of

DOCTOR OF PHILOSOPHY

in

Cell Biology

ACKNOWLEDGEMENTS

I thank my advisor, Martin McMahon, for inspiration, guidance, patience, and unrelenting support of my progress and development as a scientist. I thank all members of the McMahon Lab, especially past members Christy Trejo and Roch-Phillip Charles, as well as Jillian Silva, Marian Deuker, Anny Shai, Ed Van Veen, Joseph Juan, Daphne Pringle, Evan Markegard, and Paddy O'Leary for training, advice, and support. I thank members of my thesis committee: Frank McCormick, Trever Bivona, Emmanuelle Passegue and Eric Collisson for feedback and guidance throughout my doctoral studies. I thank the faculty of the Tetrad program at UCSF for teaching, training, and resources. I thank UCSF core facilities: the laboratory for cell analysis, the preclinical therapeutics core, the laboratory animal resource center, and the Nikon imaging center for equipment and training. I thank Tina Yuan for mentorship, and all members of the McCormick lab, Ruggero lab, Balmain lab, Akhurst lab, Toczyski lab, and Collisson lab for reagents, protocols, and friendship.

Reference for published material:

Trejo CL, Green S, Marsh V, Collisson EA, Iezza G, Phillips WA, et al. Mutationally activated PIK3CA(H1047R) cooperates with BRAF(V600E) to promote lung cancer progression. *Cancer research* 2013;73(21):6448-61.

The cooperation of PI3K α ^{H1047R} with BRAF^{V600E} and KRAS^{G12D} in lung tumorigenesis

Shon Green

ABSTRACT

KRAS is a GTPase that transmits external signals into the cell to regulate numerous cellular processes including cell division and apoptosis. Hence mutations in KRAS that render it constitutively active make it a potent oncogene. KRAS driver mutations are found in ~30% of non-small cell lung cancers and are associated with poor prognosis. Because of the significant challenges presented by pharmacological targeting of KRAS, efforts have turned to defining and targeting KRAS-regulated signaling pathways that are required for cancer cell maintenance. Most notable among these are the RAF protein kinases and PI3K α , which have been credentialed both as key effectors of KRAS and *bona fide* human oncogenes. To study the contributions of these pathways to lung tumorigenesis I employed genetically engineered mouse models in which mutationally activated KRAS^{G12D}, BRAF^{V600E}, or PI3K α ^{H1047R} can be conditionally expressed in the lung epithelium. Using these tools and complimentary tissue culture systems I tested the role of PI3K α signaling in BRAF- and KRAS-driven lung cancer formation. My results show that simultaneous expression of oncogenic BRAF and PI3K α is sufficient to form lung cancer in mice in a way that mimics KRAS activation. Thus RAF \rightarrow MEK \rightarrow ERK and PI3K α \rightarrow AKT act synergistically to promote lung

tumorigenesis. In addition, mutational activation of PI3K α dramatically accelerates KRAS-driven lung tumor initiation and progression, showing that despite the known ability of KRAS to directly activate PI3K α , PI3-lipid signaling remains limiting for KRAS-driven lung tumorigenesis. Finally, the cooperation between oncogenic PI3K α and BRAF or KRAS can be partially explained by signals downstream of RAF \rightarrow MEK \rightarrow ERK and PI3K α \rightarrow AKT that converge on activation of the cell division cycle and suppression of apoptosis. However in both BRAF/PIK3CA and KRAS/PIK3CA mutated tumors, PI3K inhibition is cytostatic at best and only moderately slows the growth of cancers, indicating that blockade of this pathway in established tumors suppresses cell division but does not illicit cell death.

TABLE OF CONTENTS

Introduction	page 1
Chapter 1: Mutationally activated PIK3CA ^{H1047R} cooperates with BRAF ^{V600E} to promote lung cancer progression	page 11
Chapter 2: PI3'-kinase signaling is limiting for KRAS ^{G12D} -driven lung tumorigenesis in mice	page 69
Conclusions	page 120
References	page 123

LIST OF FIGURES

Figure I-1.....	page 10
Figure 1-1.....	page 53
Figure 1-2.....	page 54
Figure 1-3.....	page 55
Figure 1-4.....	page 56
Figure 1-5.....	page 57
Figure 1-6.....	page 58
Figure 1-7.....	page 59
Figure 1-S1.....	page 60
Figure 1-S2.....	page 61
Figure 1-S3.....	page 62
Figure 1-S4.....	page 63
Figure 1-S5.....	page 64

Figure 1-S6.....	page 65
Figure 1-S7.....	page 66
Figure 1-S8.....	page 67
Supplementary Table 1-S1.....	page 68
Supplementary Table 1-S2.....	page 68
Figure 2-1.....	page 106
Figure 2-2.....	page 107
Figure 2-3.....	page 108
Figure 2-4.....	page 109
Figure 2-5.....	page 110
Figure 2-6.....	page 111
Figure 2-7.....	page 112
Figure 2-S1.....	page 113
Figure 2-S2.....	page 114
Figure 2-S3.....	page 115
Figure 2-S4.....	page 116
Figure 2-S5.....	page 117
Figure 2-S6.....	page 118
Figure 2-S7.....	page 119

INTRODUCTION

Driver mutations in non-small cell lung cancer

Lung cancer remains to date the most prevalent and deadly cancer, with annual mortality rates surpassing those of the next four most common cancers combined [1]. Adenocarcinoma, the major sub-type of non-small cell lung cancer (NSCLC), accounts for approximately 50% of all cases. Efforts in the past decade to characterize the mutational spectrum of lung adenocarcinomas have identified a central role for receptor-tyrosine kinase (RTK)-RAS signaling in the pathology of this disease. Indeed, practically all known driver mutations found in lung adenocarcinoma occur either in RTKs (e.g. *EGFR*, *ALX1*, and *ROS1*), in *KRAS*, in downstream effectors of RAS (e.g. *BRAF* and *PIK3CA*), or in the negative regulator of RAS, Neurofibromin 1 (*NF1*) [2]. Mutations in *KRAS* alone account for ~30% of cases, which are typically associated with aggressive disease and poor survival [3]. While progress has been made in developing inhibitors against RTKs, BRAF, and PIK3CA, directly targeting RAS has been enormously challenging and largely unsuccessful to date. Therefore efforts have turned to identifying and targeting, whenever possible, effectors of RAS required for cancer cell maintenance.

Signal transduction downstream of RAS

RAS is a GTPase that acts in a switch-like manner to turn on signaling cascades in response to external stimuli (Figure I-1). When receptor tyrosine kinases are activated by ligand binding and dimerization, they autophosphorylate sites in their intracellular portions which recruit proteins containing SH2 domains. One of these is the adaptor protein GRB2 which binds SOS, a guanine nucleotide exchange factor for RAS.

When recruited to the cell membrane, SOS catalyzes the release of GDP from RAS thereby allowing it to bind GTP and adopt an active conformation [4]. In its active conformation RAS-GTP binds and activates its downstream effectors through induction of conformational changes or recruitment to the cell membrane. In order to switch off, RAS must hydrolyze GTP to produce GDP. However RAS has a weak intrinsic GTPase activity and therefore requires GTPase activating proteins (GAPs) to assist in the process. The most common mutations found in *RAS* occur in codon 12, rendering it insensitive to GAPs and thus constitutively active. As mentioned above, mutations that disrupt the function of the RAS GAP NF1 are also found in ~8% of lung adenocarcinomas [2].

Two key RAS effectors that are also credentialed as oncogenic drivers of lung cancer in their own right are the RAF family of protein kinases and the catalytic subunit of class I PI3-lipid kinase alpha, PI3K α /PIK3CA. BRAF, a member of the RAF family, and PIK3CA are each found mutated in about 7% of lung adenocarcinomas [2]. RAF is a serine/threonine kinase that is recruited to the membrane by binding to RAS-GTP, which allows its activation by other membrane-bound kinases. Activated RAF initiates the mitogen-activated-protein-kinase (MAPK) cascade that regulates many important cellular processes (Figure I-1). RAF phosphorylates MEK1/2, which become activated and phosphorylate ERK1/2, which in turn phosphorylate and regulate a large number of transcription factors and other targets. Two major outcomes of MAPK signaling are activation of the cell division cycle and inhibition of apoptosis, both of which are essential for normal biological function and for cancer formation. The most common mutation found in this pathway (not including KRAS mutations) occurs in the activation

loop of the BRAF kinase domain, producing BRAF^{V600E}. This mutation eliminates the requirement for upstream activation and thus renders BRAF constitutively active. Unlike melanomas where the V600E substitution accounts for 80-90% of BRAF mutations, NSCLCs also harbor other point mutations in the kinase domain of BRAF [5].

PI3K α is a lipid kinase that catalyzes the production of phosphatidylinositol (3,4,5)-trisphosphate (PIP3) on the cytoplasmic side of the cell membrane (Figure I-1). PI3K α can either bind activated RTKs directly through an SH2 domain in its p85 regulatory subunit, or can be activated by RAS-GTP through a RAS-binding domain in the catalytic subunit. Both interactions relieve an intrinsic negative feedback which allows PI3K α to phosphorylate its lipid substrate. PTEN is a lipid phosphatase that catalyzes the removal of phosphate groups from PIP3, thereby negatively regulating PI3K α signaling. PIP3 recruits proteins containing pleckstrin homology domains which include the AKT (PKB) family of kinases and their regulators PDK-1 and mTORC2. Through this recruitment to the membrane AKT1-3 become phosphorylated and activated by PDK-1 and mTORC2 at residues T308 and S473 respectively. Once active, AKT1-3 phosphorylate a diverse set of targets that regulate many cell activities including proliferation, survival, motility, and metabolism (Figure I-1) [6]. *PIK3CA* is one of the most commonly mutated genes in human cancers. In addition to mutations in *PIK3CA* which are found in ~7% of lung adenocarcinomas, the PI3K pathway as a whole is activated in ~25% of cases (by copy number alterations, *PTEN* loss, mutations in *AKT1*, and other mechanisms) [2]. The H1047R substitution modeled in this work occurs in the kinase domain of *PIK3CA* and causes a conformation change that blocks

the auto-inhibitory binding of the C-terminus tail, thus maintaining PIK3CA in a constitutively active state [7].

The MAPK and PI3K pathways coordinately control many processes and also exhibit complex cross-talk with each other through positive and negative feedback loops [8]. When simultaneously activated, the RAF→MEK→ERK and PI3Kα→AKT pathways have been shown to act synergistically to drive cancer in various models [9, 10].

Genetically engineered mouse models of lung cancer

Genetically engineered mouse (GEM) models of mutationally activated oncogenes or loss of tumor suppressors have been valuable tools in the study of lung cancer initiation and progression. To gain a better understanding of KRAS-driven NSCLC and investigate the role of its downstream effectors I have utilized previously described GEM models in which oncogenic forms of KRAS (*KRas^{LSL-G12D}*), BRAF (*BRAF^{CA-V600E}*), or PIK3CA (*Pik3ca^{Lat-H1047R}*) can be conditionally expressed in the adult mouse epithelium, in a way that recapitulates the acquisition of a somatic mutation as it might occur in a human lung [11-13]. In such mice, a genetic element has been knocked in to the endogenous locus of the gene that includes LoxP sites flanking a portion of the gene. These sequences are recognized by the enzyme Cre recombinase (Cre) which recombines this element, resulting in expression of a mutated form of the gene that is subject to all normal regulation and splicing. In the *KRas^{LSL-G12D}* mouse model, no protein is expressed prior to Cre-mediated recombination, however these mice are normal and healthy with one wild type copy of *KRas*. In the *BRAF^{CA-V600E}* and *Pik3ca^{Lat-H1047R}* models, a wild type form of the protein is expressed prior to expression of Cre. As previously described, the mutationally activated proteins expressed in these mice, KRAS^{G12D},

BRAF^{V600E} and PIK3CA^{H1047R}, are commonly found in human cancers and render these proteins constitutively active.

In order to express Cre recombinase in the lung epithelium of adult mice their lungs are infected intra-nasally with an adenovirus encoding Cre recombinase (Ad-Cre). When the virus infects lung cells, Cre is transiently expressed and recombines the genetically-engineered cassette. This permanently changes the genomic DNA in that given cell to carry the oncogenic mutation. Another method used in this work to activate Cre expression in the adult mouse lung is through a knock-in allele to the surfactant-protein-c (SPC) gene that expresses a Cre:ER fusion under control of the SPC promoter [14]. In such mice Cre expression can be induced in type II pneumocytes, which express SPC, by administering tamoxifen to the mouse. Type II pneumocytes are reported to be the cell of origin for KRAS-driven adenocarcinoma, and both KRAS and BRAF-driven tumors invariably express SPC. Thus the *SPC^{CreER}* allele can be used to initiate the expression of oncogenes in a subset of lung cells and in existing tumors that were initiated by means other than Cre [14-16].

The roles of oncogenes in the RAS pathway in lung cancer

The *KRas^{LSL}* mouse model of lung cancer has been previously characterized [11]. After initiation with Ad-Cre and a variable latency period, mice develop abnormal proliferation of cells along the alveolar framework, termed atypical adenomatous hyperplasia (AAH), and papillary growths of cells that line the bronchioles, termed epithelial hyperplasia (EH). Some of these hyperplasias develop into solid tumors termed adenomas over a period of several weeks. The majority of adenomas grow slowly or become growth-arrested and remain histopathologically benign even at 6

months post initiation. A fraction of these tumors (10-20%) progress to adenocarcinomas that display certain features that resemble the human disease. It has been reported that negative feedback signals activated by aberrant RAS signaling are responsible for the growth arrest observed in KRAS mutated lung tumors [17]. This has been termed oncogene-induced senescence, and implies that high levels of signaling downstream of KRAS must be sustained in order for tumors to evade senescence and progress to cancer.

Genetic and pharmacological studies of effector pathways downstream of KRAS using GEMs have established that both $\text{RAF} \rightarrow \text{MEK} \rightarrow \text{ERK}$ and $\text{PI3K}\alpha \rightarrow \text{AKT}$ pathways are required for KRAS-driven lung tumorigenesis [18-20]. However whether both pathways are coordinately and fully activated by oncogenic KRAS has not been established and their respective roles in promoting the various stages of cancer formation are unclear. In addition, despite the knowledge that signaling through MAPK and PI3K cooperate to drive cancer, the biochemical mechanisms of tumor initiation and progression remain poorly understood.

In contrast to the KRas^{LSL} GEM model in which a small fraction of initiated cells sporadically give rise to tumors over a long period of time, oncogenic $\text{BRAF}^{\text{V600E}}$ expression in the lungs of mice results in more rapid and uniform benign tumor growth. Although initially growing more rapidly than KRAS tumors, $\text{BRAF}^{\text{V600E}}$ -driven tumors uniformly become growth-arrested around 12 weeks post initiation and do not progress to cancer [12, 16]. This suggests that activation of MAPK signaling alone is not sufficient to drive continued tumor growth and progression to cancer in this model, since BRAF mutated tumors cannot escape oncogene-induced senescence as a fraction of KRAS

mutated tumors do. It has been shown that WNT→ β -catenin→Myc signaling is one of the limiting factors that prevents further expansion and progression of BRAF mutated lung tumors [21]. Another pathway that might cooperate with BRAF signaling to drive tumor progression is the PI3K pathway. Since KRAS is capable of turning on both MAPK and PI3K signaling and is capable of driving the formation of malignant tumors, it seems likely that BRAF's inability to turn on PI3K signaling might be one of the factors limiting the progression of BRAF mutated tumors.

Despite being a potent oncogene, expression of mutationally activated KRAS at physiological levels does not induce proliferation in the majority of initiated cells, as evidenced by the fact that many KRAS^{G12D}-expressing lung cells in GEMs never divide [22]. Furthermore, the lungs of healthy humans have been reported to harbor KRAS mutations [23]. These observations suggest that additional factors are required to promote the proliferation and malignant progression of KRAS^{G12D}-initiated lung tumors. Indeed, there are reports that elevated expression of RAS oncoproteins is required for their oncogenic effects [24-26], and that external signals are required to activate mutated KRAS through upstream receptors [27]. In addition, various factors have been found to influence progression of KRAS^{G12D} expressing lung tumors, including alterations in TP53, CDKN2A, APC, LKB1 or PTEN tumor suppressors [28-33]. Interestingly, despite PIK3CA being a direct effector of KRAS and their interaction being required for tumor formation [20], it is reported that concomitant activation of PIK3CA through IGF1R is necessary for KRAS-driven lung tumorigenesis [34]. The latter suggests that mutated KRAS does not activate PIK3CA to the full extent possible and

may explain the co-mutation of *KRAS* and *PIK3CA* in a number of cancer types, including lung [5, 35, 36].

Hypothesis

I hypothesized that PI3-lipid signaling is limiting for both BRAF- and KRAS-driven lung tumorigenesis. To test this hypothesis I combined the expression of *KRAS*^{G12D} or *BRAF*^{V600E} with *PIK3CA*^{H1047R} in the lungs of GEMs to generate *KRAS*^{G12D} or *BRAF*^{V600E} lung tumor models with elevated PIK3CA signaling. I also generated complementary cell culture and lung slice models to study how signaling downstream of RAS→RAF→MEK→ERK cooperates with PI3Kα→AKT to regulate cellular processes that drive lung cancer. My results show that elevated PI3-lipid signaling achieved through expression of mutationally activated *PIK3CA*^{H1047R} is sufficient to overcome the growth-arrest of BRAF mutated lung tumors in mice and promote their progression to lung cancer. In addition I discovered that PI3-lipid signaling is limiting for KRAS-driven lung tumor initiation and progression in mice. Lastly, I found that both results can be explained in part by PIK3CA-mediated regulation of components of the cell cycle and apoptotic machinery that act synergistically with signals downstream of the MAPK pathway to promote cell cycle progression and suppress apoptosis.

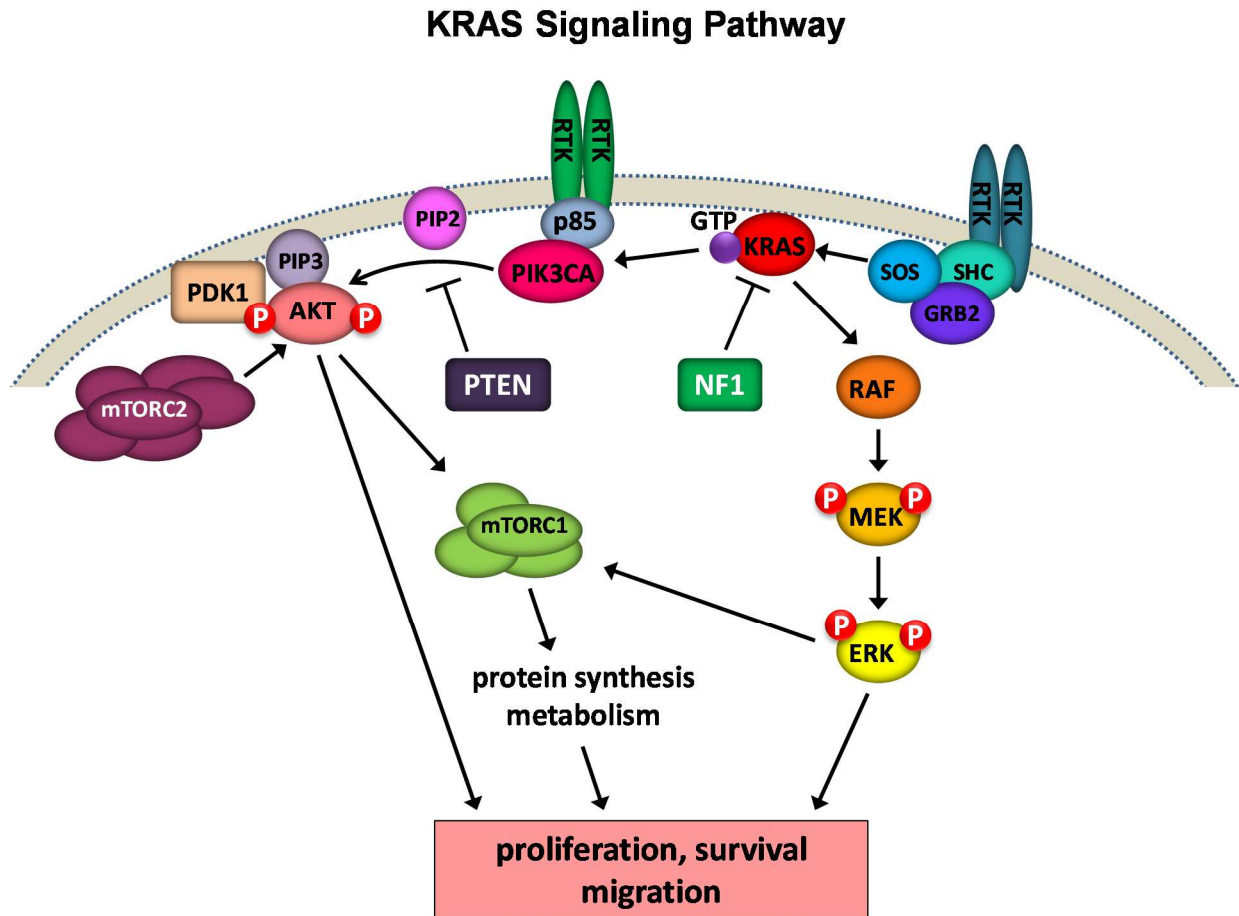
Thesis outline

Chapter 1 describes how oncogenic BRAF and PIK3CA cooperate to drive lung cancer in GEM models and the efforts I have made to try and identify the signaling events that are responsible for this cooperation. This chapter consists of published material and my contributions to this work are listed on page 1 of this chapter.

Chapter 2 describes the discovery that PIK3CA signaling is limiting for KRAS-driven lung tumorigenesis, an analysis of how these oncogenes cooperate in mouse models, and the identification of signals downstream of RAS→RAF→MEK→ERK and PI3K→AKT that converge on regulating the cell division cycle and apoptosis.

The Conclusions section summarizes the major findings of this work and its implications for understanding the biochemical signals that drive lung cancer.

Figure I-1



KRAS signaling pathway: KRAS is activated by SOS which is recruited to activated receptor tyrosine kinases at the membrane. Active KRAS binds and activates many effectors including RAF and PIK3CA. RAF kinase phosphorylates and activates MEK which phosphorylates and activates ERK. PIK3CA lipid kinase produces PIP3 in the membrane which recruits and activates AKT. ERK and AKT are both kinases with multiple targets in the cytoplasm and nucleus that regulate numerous processes including proliferation, survival, migration, transcription, translation, metabolism, and others.

CHAPTER 1:

Mutationally activated PIK3CA^{H1047R} cooperates with BRAF^{V600E} to promote lung cancer progression

My contributions to this work include:

- Pharmacological inhibition of PIK3CA or BRAF in mice (Figure 1-4)
- Analysis of malignant progression of tumors in *BRAF^{CA}* vs. *BRAF^{CA} /Pik3ca^{HR}* mice (Figure 1-5 and Figure 1-S3)
- Cell growth assays and cell cycle analysis with BrdU incorporation, analysis of RPPA results and confirmation of RPPA results by western blotting (Figure 1-7, Figure 1-S7, Figure 1-S8, and Table 1-S2)
- Examination of tumorigenesis in confetti mice to determine clonal origin of tumors (Figure 1-S2)
- Comparison of tumorigenesis initiated by Adeno-cre viruses that express Cre under control of cell-type-specific promoters (Figure 1-S4)
- Authorship of all of the text relating to the work described above as well as the figures related to this work and statistical analyses

Reference:

Trejo CL, Green S, Marsh V, Collisson EA, Iezza G, Phillips WA, et al. Mutationally activated PIK3CA(H1047R) cooperates with BRAF(V600E) to promote lung cancer progression. *Cancer research* 2013;73(21):6448-61.

INTRODUCTION

Non-small cell lung cancer (NSCLC) is a leading cause of cancer mortality and adenocarcinoma is its most common subtype [37]. Recently identified driver mutations in proto-oncogenes in NSCLC have provided strategies for the development of pathway-targeted therapies [38]. However, despite the success of agents such as erlotinib and crizotinib in the treatment of lung cancers expressing mutationally activated EGF receptor, ROS1 or AML4-ALK fusion proteins, most NSCLC patients do not have recourse to the use of such agents.

Of the various oncogenic drivers identified in NSCLC, mutant KRAS remains the most common ($\geq 25\%$) and the most pharmacologically intractable [38]. Consequently, attention has turned to identifying and inhibiting key downstream signaling pathways required for maintenance of *KRAS* mutated NSCLC. Moreover, certain KRAS effectors are also directly implicated as *bona fide* human lung cancer genes. For example, *BRAF* is mutated in $\sim 10\%$ of NSCLC, with one quarter of such mutations encoding the constitutively active BRAF^{V600E} oncoprotein [38, 39]. In addition, PI3'-kinase signaling is also deregulated in $\sim 10\%$ of NSCLC either through mutational activation/amplification of *PIK3CA* (encoding the catalytic subunit of PI3'-kinase- α) or through silencing of *PTEN* (encoding a PI3'-lipid phosphatase) [40]. Finally, AKT, the most widely studied protein kinase effector of PI3'-lipid signaling, is reportedly over-expressed or amplified in a variety of human tumors [41].

One pertinent question is, what pathways downstream of oncogenic KRAS^{G12D} are required for the development and maintenance of lung cancer in GEM models?

Whereas expression of BRAF^{V600E} in the lung epithelium rapidly elicits multifocal lung tumors, lesions are invariably benign and rarely progress to malignancy due to a senescence-like growth arrest [12]. However, treatment of mice bearing KRAS^{G12D}-initiated lung tumors with a MEK1/2 inhibitor elicited tumor regression indicating the importance of RAF→MEK→ERK signaling for tumor maintenance [16, 42]. By contrast, although transgenic expression of mutationally activated PIK3CA^{H1047R} in the lung epithelium was reported to promote lung tumorigenesis, combined inhibition of PI3'-kinase/mTorc had no effect on established KRAS^{G12D}-initiated lung tumors [43]. Moreover, it has been suggested that senescence induced by ERK1/2 MAP kinase pathway activation may be due to feedback inhibition of PI3'-kinase signaling [17]. Consequently, we decided to test whether mutationally activated BRAF^{V600E} and PIK3CA^{H1047R} might cooperate in promoting lung carcinogenesis using mice carrying conditional alleles of *BRAF* and *Pik3ca* [12, 13].

Perhaps surprisingly, we failed to substantiate reports that PIK3CA^{H1047R} can initiate lung tumorigenesis even when two copies of conditional *Pik3ca^{lat}* allele were combined with PTEN silencing. By contrast, concomitant expression of both BRAF^{V600E} and PIK3CA^{H1047R} led to rapid onset of lung tumorigenesis with evidence of malignant progression observed six months after tumor initiation. The cooperative effects of PIK3CA^{H1047R} *in vivo* were AKT dependent and could be modeled *in vitro* by expression of oncogenic *PIK3CA* or *AKT1* alleles in BRAF^{V600E} expressing lung tumor cell lines. Finally, we demonstrate that both BRAF^{V600E} and PIK3CA signaling is necessary for proliferation and survival of mouse BRAF^{V600E}/PIK3CA^{H1047R} expressing lung cancer derived cell lines and demonstrate that these signaling pathways cooperate to regulate

the cell division cycle and apoptosis. These experiments demonstrate that PIK3CA^{H1047R}, whilst insufficient to initiate lung tumorigenesis, is sufficient to overcome the barrier to cancer progression displayed by lung tumors initiated by BRAF^{V600E} in a manner that bears similarity to the effects of KRAS^{G12D}.

MATERIALS AND METHODS

Mice and Adenovirus delivery

All animal experiments were conducted in accordance with protocols approved by the UCSF Institutional Animal Care and Use Committee (IACUC). *BRAF^{CA}* (*Braf^{tm1Mmcm}*), *Trp53^{lox}* (*Trp53^{tm1Brn}*), *PIK3CA^{lat-H1047R}* and *Pten^{lox}* mice were bred and genotyped as previously described [11-13, 44, 45]. Stocks of Adenovirus encoding Cre recombinase (Ad-CMV-Cre) were purchased from Viraquest (North Liberty, IA). Adenoviruses with cell specific expression of Cre recombinase (Ad-SPC-Cre, Ad-CCSP-Cre and Ad-CGRP-Cre) were generously provided by Kate Sutherland and Anton Berns (NKI, Amsterdam) and purchased from the University of Iowa, Gene Transfer Vector Core [46]. Intranasal instillation of adenovirus for infection of the mouse lung epithelium was performed as previously described [47]. Tumor bearing mice were euthanized for analysis either at a pre-determined time point or when their body conditioning score (BCS) was ≤ 2 [48].

Histology and quantification of lung tumor burden

Lungs were removed and fixed in zinc buffered formalin and stored in 70%(v/v) ethanol prior to paraffin embedding. 6 μ m sections were cut and slides were stained with Hematoxylin and Eosin (H&E). H&E stained slides were scanned with an Aperio

ScanScope scanner. Quantification was performed using Aperio Spectrum ImageScope viewing software. Tumor number and size were measured per lobe and overall tumor burden was calculated as (area of lung lobe occupied by tumor)/(total area of lobe) in μm^2 .

Treatment of mice with pathway-targeted therapeutics

For the treatment of mice with pathway-targeted therapeutics, PD325901 (Hansun Trading Co.) was formulated in 0.5%(w/v) Hydroxy-Propyl-Methylcellulose (HPMT, Sigma) and administered by oral gavage (po) at 12.5 mg/kg per mouse once per day (q.d.). MK-2206 (Merck) was formulated in 30%(w/v) Captisol (Ligand Technology, La Jolla, Ca.) and mice were dosed at 120 mg/kg q.d. po. LGX-818 and BKM-120 (Novartis) were formulated in 0.5% carboxymethylcellulose (Sigma) plus 0.5% Tween 80 (Sigma) and mice were dosed q.d. po at 30 mg/kg and 60 mg/kg, respectively.

Immunostaining of mouse lung tissue and immunoblotting

Mouse lungs were fixed in zinc-buffered formalin, processed and embedded in paraffin, cut into 6 μm sections and mounted on glass slides. Citrate-mediated antigen retrieval was performed and then the following antibodies were used for detection: anti-pS473-AKT, anti-Vimentin, anti-PTEN (Cell signaling technology), anti-NKX2.1, anti-Ki67, anti-SP-C and anti-p63 (Santa Cruz Biotechnology).

50 μg aliquots of cell or lung/tumor lysates were probed with antisera against phospho-AKT (pS473 or T308), phospho-ERK1/2 (pT202/pY204), total ERK1/2, total AKT, Cyclin D1, Cleaved Caspase 3 or 7, phospho-4E-BP1 (pS65), phospho-GSK3 β

(pS9), phospho-RP-S6 (pS235/236 or pS240/244), phospho-PRAS40 (pT246), phospho-FOXO1 (pT24), p27^{KIP1} (Cell Signaling technology); BIM, c-MYC (Epitomics), Cyclin A, CDK4 (Santa Cruz), and β -actin (Sigma). Immunoblots were visualized using the Odyssey FC system (Li-Cor) and Image Studio software.

Lung tumor cell isolation, culture and analysis

Lungs of tumor bearing mice were perfused with dispase (BD) and individual lobes were minced and incubated with 2mg/ml dispase/collagenase (Roche). Cell suspensions from either BRAF^{V600E}/TP53^{Null} or BRAF^{V600E}/PIK3CA^{H1047R}/TP53^{Null} induced lung cancers were then filtered and plated directly into culture in Hams-F12/Glutamax media supplemented with 10%(v/v) fetal bovine serum. Following the outgrowth of a mixed population of lung cancer derived cells, a series of single cell-derived clones were isolated by limiting dilution and then expanded. Recombination of the *BRaf^{CA}*, *Trp53^{lox}* and *Pik3ca^{lat}* alleles was verified by PCR [13]. Expression of oncogenic BRAF^{V600E} was determined by immunoblotting cell extracts with a monoclonal antibody (VE1) that is specific to V600E BRAF oncoprotein [49].

A proliferation assay was established in which cells were seeded in triplicate at 10⁴ cells/ml and treated with a range of inhibitors: DMSO control, MEK1/2 inhibitor (PD325901, 15.6nM-1 μ M), ERK1/2 inhibitor (SCH772984, 7.8nM-5 μ M), AKT1-3 inhibitor (MK-2206, 80nM-5 μ M) or class 1 PI3'-kinase inhibitor (GDC-0941, 80nM-5 μ M). Cells were treated with combinations of MEKi plus PI3Ki (PD325901 + GDC-0941) or ERKi plus AKTi (SCH772984 + MK-2206). 72 hours after initial treatment, a Cell Titre-Glo viability assay was performed. Luminescence was detected using a Glo-Max

microplate reader (Promega). Crystal Violet stains were performed by incubating methanol-fixed cells with 0.5%(w/v) Crystal Violet in 25%(v/v) methanol for 10 minutes and subsequently washing in water. Cell cycle analysis was performed by incubating cells at 50% confluency with pathway-targeted inhibitors for 24 hours and 10 μ M BrdU (Becton-Dickinson) added for the final 3 hours. Floating and adherent cells were collected, fixed in ethanol, and stained with anti-BrdU-FITC (Becton-Dickinson) and propidium iodide (Sigma).

Cell sorting was performed using a FACS-Calibur (Becton Dickinson). Control, PIK3CA^{H1047R} or HA tagged-M+AKT1 encoding pBabePuro vectors were a gift from Xiaolin Nan (OHSU), Dr. Frank McCormick (UCSF) or purchased from Addgene (Cambridge, MA) respectively. Ecotropic virus was produced by transient transfection of Plat-E cells [50] and used to generate BRAF^{V600E}/TP53^{Null} cells expressing mCherry, PIK3CA^{H1047R} or M+AKT1 by standard techniques [51]. Anchorage-independent colony formation was performed by plating 5x10³ cells in 1.4%(w/v) Sea-Plaque low melting temperature agarose (Cambrex, Rockland, ME) and culturing them for three weeks at which time colony formation was enumerated using dissecting microscope. PD325901 (Hansun Trading Co.), MK-2206 (Merck), and GDC-0941 (Genentech) were dissolved in dimethylsulfoxide (DMSO) and added to the cultures at the appropriate concentrations.

Reverse Phase Protein Array (RPPA) Analysis

Reverse phase protein array (RPPA) analysis (Functional Proteomics Core Facility at M.D. Anderson Cancer Center) was performed as previously described [52, 53]. Cellular proteins were denatured by 1%(w/v) SDS in the presence of β -mercaptoethanol

and adjusted to a final concentration of 1mg/ml. Samples were diluted in five serial 2-fold dilutions in dilution buffer (lysis buffer containing 1% SDS) and arrayed on nitrocellulose-coated slides (Grace Biolab) using an Aushon 2470 Arrayer (Aushon BioSystems). Each slide was probed with a validated primary antibody plus a biotin-conjugated secondary antibody. The signal obtained was amplified using a DakoCytomation–catalyzed system (Dako) and visualized by DAB colorimetric reaction. Slides were scanned, analyzed and quantified using a customized-software Microvigene (VigeneTech Inc.) to generate spot intensity. Each dilution curve was fitted with a logistic model (“Supercurve Fitting” developed by the Department of Bioinformatics and Computational Biology in MD Anderson Cancer Center, <http://bioinformatics.mdanderson.org/OOMPA>) that fits a single curve using all the samples (i.e. dilution series) on a slide with the signal intensity as the response variable and the dilution steps as independent variables. The fitted curve is plotted with the signal intensities – both observed and fitted - on the y-axis and the log₂-concentration of proteins on the x-axis for diagnostic purposes. The protein concentrations of each set of slides were then normalized by median polish, which was corrected across samples by the linear expression values using the median expression levels of all antibody experiments to calculate a loading correction factor for each sample. Results for each antibody were then mean-centered to facilitate visualization. A list of antibodies, including source and catalog number, may be found at: <http://www.mdanderson.org/education-and-research/resources-for-professionals/scientific-resources/core-facilities-and-services/functional-proteomics->

rppa-core/antibody-lists---protocols/corestdablist-5-3-13.pdf). Unsupervised hierarchical clustering was performed using GENE-E (broadinstitute.org).

RESULTS

Expression of PIK3CA^{H1047R} combined with PTEN silencing fails to induce lung tumors in mice

Whereas over-expression of a tetracycline regulated PIK3CA^{H1047R} under the control of a *CCSP::rtTA* driver results in clonal, benign lung tumors, the effects of physiological levels of expression of the same protein induced stochastically throughout the distal lung epithelium has not been evaluated [43]. To do so, we employed *Pik3ca^{lat-H1047R}* mice (*Pik3ca^{lat}*) carrying a genetically modified *Pik3ca* allele that expresses normal PIK3CA prior to Cre-mediated recombination after which PIK3CA^{H1047R} is expressed at normal physiological levels under the control of the gene's chromosomal regulatory elements [13]. To elicit genetic alterations in the lung epithelium we employed an adenovirus expressing Cre recombinase (Ad-Cre) [12]. In the event that expression of PIK3CA^{H1047R} from a single recombined *Pik3ca^{lat}* allele might be insufficient for lung tumorigenesis, we generated mice encompassing every possible heterozygous or homozygous combination of the *Pik3ca^{lat}* allele, either alone or in combination with a conditional null allele of *Pten* (*Pten^{lox}*) [45]. In total, we tested eight different *Pik3ca^{lat}/Pten^{lox}* genotypes for lung tumorigenesis.

Adult mice of the various *Pik3ca^{lat}/Pten^{lox}* genotypes were intranasally instilled with Ad-Cre and then euthanized for analysis at three, six or ≥ 12 months after infection. As a parallel control for successful tumor induction, we initiated BRAF^{V600E} expression in

the lung epithelium of *BRaf^{CA}* mice [12]. As expected, Ad-Cre infected *BRaf^{CA}* mice developed benign lung adenomas at high multiplicity requiring mice to be euthanized ~12 weeks after initiation (Fig. 1-1A, right panel). By contrast, we failed to detect lung tumors in mice carrying conditional alleles of *Pik3ca* or *Pten*, either alone or in any combination, at three or six months after Ad-Cre infection (Fig. 1-1A, left and middle panels). That PTEN silencing was insufficient for lung tumorigenesis was consistent with previous observations, but the lack of lung tumorigenesis in the compound *Pik3ca^{lat}/Pten^{lox}* mice was surprising [31]. At ≥ 12 months we detected benign adenomas in *Pik3ca^{lat/lat}; Pten^{lox/lox}* mice however these were rare (< one tumor/mouse). The majority of these tumors stained positive for PTEN expression and negative for phospho (p)-AKT suggesting that they may be spontaneously arising lung tumors unrelated to the underlying genotype. However, we also detected very rare lung tumors in *Pik3ca^{lat/lat}; Pten^{lox/lox}* mice that stained brightly for pAKT and that may therefore be driven by this combination of genetic abnormalities (Fig. 1-1T). Immunofluorescence analysis of Ad-Cre infected *Pik3ca^{lat}* or *Pik3ca^{lat/lat}* mice failed to detect any evidence of cells with elevated pAKT or expression of Ki67 above that detected in normal mouse lung at either three, six (not shown) or ≥ 12 months (Fig. 1-1F-M). However, in *Pik3ca^{lat}* mice carrying either one or two conditional *Pten^{lox}* alleles, small numbers of epithelial hyperplasias were observed within the airways (Fig. 1-1N-U). Most prevalent in the *Pik3ca^{lat/lat}; Pten^{lox/lox}* mice, these lesions comprised small numbers of cells that stained negative for PTEN and positive for pAKT, with the strongest pAKT signal detected in lesions found in *Pik3ca^{lat/lat}; Pten^{lox/lox}* mice (Fig. 1-1R). These lesions were generally $\leq 50\mu\text{m}$ in diameter and did not express Ki67 suggesting that they were not actively

proliferating (Fig. 1-S1). Hence, despite evidence of occasional airway hyperplasia, there was no combination of conditional *Pik3ca^{lat}* or *Pten^{lox}* that elicited lung tumors in mice within 6 months after Ad-Cre, which stands in stark contrast to the robust lung tumorigenesis induced by KRAS^{G12D} or BRAF^{V600E} [11, 12, 43].

PIK3CA^{H1047R} dramatically accelerates BRAF^{V600E} driven lung tumorigenesis

To determine if PIK3CA^{H1047R} would cooperate with BRAF^{V600E} in lung tumorigenesis, we infected adult *BRaf^{CA}* or compound *BRaf^{CA}; Pik3ca^{lat}* heterozygous mice with either 5x10⁶ or 10⁷ pfu Ad-Cre. Kaplan-Meier survival analysis of mice infected with 5x10⁶ pfu Ad-Cre indicated that all of the *BRaf^{CA}; Pik3ca^{lat}* mice required euthanasia by ~50 days based on their body conditioning score (per IACUC regulations), a time at which all of the *BRaf^{CA}* mice remained healthy (Fig. 1-2A) [48]. Overall, *BRaf^{CA}* mice lived more than twice as long as *BRaf^{CA}; Pik3ca^{lat}* littermates after initiation (median survival 100 vs. 39 days, $p = 1.25 \times 10^{-5}$, Fig. 1-2B). Furthermore, three weeks after infection with 10⁷ pfu Ad-Cre, many of the *BRaf^{CA}; Pik3ca^{lat}* mice displayed labored breathing and reduced body weight indicating the onset of lethal lung tumorigenesis. Representative mice of both genotypes were euthanized at this time for necropsy (Materials and Methods). Compared to control *BRaf^{CA}* mice, *BRaf^{CA}; Pik3ca^{lat}* mice presented with significantly more tumors (96 vs. 54, $p=0.025$) and BRAF^{V600E}/PIK3CA^{H1047R} expressing lung tumors were significantly larger than their BRAF^{V600E} expressing counterparts (52,516 μm^2 vs. 6,782.5 μm^2 , $p=0.004$, Fig. 1-2B). Three weeks after initiation, BRAF^{V600E}/PIK3CA^{H1047R} expressing lung lesions in manifested as large adenomas, whereas *BRaf^{CA}* mice displayed only alveolar and airway hyperplasias (Fig. 1-2B). Overall, *BRaf^{CA}; Pik3ca^{lat}* mice displayed a 14-fold

higher tumor burden at three weeks post-initiation compared to control *BRaf^{CA}* mice (16.8% vs. 1.2%, $p=0.01$, Fig. 1-2A).

PTEN silencing enhances BRAF^{V600E}-induced lung tumorigenesis

To complement analysis of the effects of PIK3CA^{H1047R} on BRAF^{V600E}-induced lung tumorigenesis, we tested if deregulation of PI3'-kinase signaling through PTEN silencing might have similar effects. Indeed, this is a combination of alterations commonly found in human melanoma and which cooperate in GEM models of the disease [10, 41]. We backcrossed *Pten^{lox}* mice for five generations with FVB/N mice, the same background as the *BRaf^{CA}* and *Pik3ca^{lat}* mice to minimize potentially confounding effects of genetic background on the experiments. We then infected *BRaf^{CA}*, *BRaf^{CA}; Pik3ca^{lat/+}* or compound *BRaf^{CA}; Pten^{lox/lox}* with 10⁶ pfu Ad-Cre with mice euthanized four weeks after initiation. Compared to control *BRaf^{CA}* mice, *BRaf^{CA}; Pik3ca^{lat}* and *BRaf^{CA/+}; Pten^{lox/lox}* mice displayed a ≥ 10 -fold and a 4-fold increase in overall tumor burden respectively (2.8% vs. 31.2% vs. 10.8%, Fig. 1-3A). To test for the efficiency of Cre-mediated PTEN silencing in *BRaf^{CA/+}; Pten^{lox/lox}* mice, lung tumors were stained with antisera against PTEN (Fig. 1-3B). Whereas most lung tumor cells arising in *BRaf^{CA}* mice displayed readily detectable PTEN expression, the vast majority of tumor cells in *BRaf^{CA}; Pten^{lox/lox}* mice were PTEN negative. These data indicate that the statistically significant difference between lung tumorigenesis in *BRaf^{CA}; Pik3ca^{lat}* vs. *BRaf^{CA/+}; Pten^{lox/lox}* mice is not due to inefficient PTEN silencing. Overall, these data support the hypothesis that activation of PI3'-kinase signaling, either by co-expression of PIK3CA^{H1047R} or PTEN silencing, cooperates with BRAF^{V600E} in lung tumorigenesis [31].

Immunohistochemical staining and analysis of early-onset BRAF^{V600E}, BRAF^{V600E}/PIK3CA^{H1047R} and BRAF^{V600E}/PTEN^{Null} expressing lung tumors indicated that they were generally benign and that they expressed both Aquaporin V (AQP5) and Surfactant Protein C (SP-C), markers of alveolar type I and II pneumocytes respectively as described previously [16]. Hence, despite the dramatic onset of tumor growth, we detected no signs of malignant progression in these lesions at early time points after tumor initiation.

Pharmacological blockade of MEK or AKT prevents the growth of BRAF^{V600E}/PIK3CA^{H1047R} lung tumors

To assess the role of downstream signaling components on the cooperation between BRAF^{V600E} and PIK3CA^{H1047R}, we employed pharmacological inhibitors of either MEK1/2 (PD325901) or AKT (MK-2206) [54, 55]. These agents are non-substrate competitive, allosteric inhibitors with high specificity and selectivity. *BRaf^{CA}* or *BRaf^{CA}; Pik3ca^{lat}* mice were infected with 10⁶ Ad-Cre and then separated into two groups for treatment with either vehicle control or MK-2206 (120 mg/kg, q.d., po) to inhibit AKT for an additional 4-5 weeks at which time mice were euthanized.

MK-2206 treatment had no effect on BRAF^{V600E}-initiated lung tumor burden (vehicle - 25% vs. MK-2206 - 22%, $p=0.63$, Fig. 1-S1A). By contrast, consistent with previous results, MEK1/2 inhibition largely abolished BRAF^{V600E}-induced lung tumorigenesis (not shown) [12, 16]. These data strongly suggest that BRAF^{V600E}-induced lung tumors are AKT independent for their initial growth.

By contrast to BRAF^{V600E} driven tumors, MK-2206 had a significant effect on BRAF^{V600E}/PIK3CA^{H1047R} driven lung tumorigenesis (Figs. 1-4A&B). Although four weeks of MK-2206 dosing had no effect on overall tumor number (vehicle = 31.8 vs. MK-2206 = 28.7; $p=0.76$), both tumor size (vehicle = 121,413 μm^2 vs. MK-2206 = 30,083 μm^2 , $p<0.0001$) and overall tumor burden (vehicle = 20.7%, MK-2206 = 5%, $p=0.004$), were significantly reduced following AKT inhibition (Figs. 1-4B). Indeed, tumor sizes and overall tumor burden that developed in *BRaf^{CA}; Pik3ca^{lat}* mice in the presence of MK-2206 were roughly equivalent to that observed in *BRaf^{CA}* mice. These data support the hypothesis that AKT activity is required for the cooperation between BRAF^{V600E} and PIK3CA^{H1047R} in lung tumorigenesis but largely dispensable for the growth of BRAF^{V600E}-induced lung tumors. Successful inhibition of pS473-AKT by MK-2206 was confirmed by immunoblot analysis of lysates of BRAF^{V600E} or BRAF^{V600E}/PIK3CA^{H1047R} expressing lung tumors treated with either vehicle or MK-2206 two hours prior to euthanasia (Fig. 1-S1B & 1-S1C respectively).

Previous studies have indicated the exquisite sensitivity of BRAF^{V600E} driven lung tumors to MEK1/2 inhibition with PD325901 [12, 16]. However, analysis of lung, pancreas and colon cancer cell lines suggest that PI3'-kinase signaling, either by mutation of *PIK3CA* or *PTEN* silencing, can render cells less sensitive to MEK inhibition possibly by sustaining the expression of D-type cyclins [56, 57]. Hence, we sought to determine if BRAF^{V600E}/PIK3CA^{H1047R} lung tumors remained sensitive to MEK1/2 inhibition *in vivo*. Lung tumors were initiated in *BRaf^{CA}; Pik3ca^{lat}* mice and two weeks later mice were dosed with vehicle or PD325901 (12.5mg/kg, q.d. po) for a further four weeks at which time mice were euthanized and lung tumor burden assessed (Figs. 1-

4A&B). Compared to controls, MEK1/2 inhibitor treated mice displayed a 15-fold reduction in tumor number (31.8 vs. 2.0, $p=0.005$). Lesions detected in PD325901 treated *BRAF^{CA}; Pik3ca^{lat}* mice were largely small alveolar or airway hyperplasias and no fully formed adenomas were present in these mice. This resulted in a ~12-fold reduction in average tumor size (vehicle = 121,413 μm^2 vs. PD325901 = 10,914 μm^2 for drug treated mice, $p<0.0001$) and a >20,000-fold reduction in overall tumor burden (vehicle = 20.7% vs. PD325901 = 0.001%, $p=0.0004$) compared to controls (Fig. 1-4B). Consequently, these data indicate that $\text{BRAF}^{\text{V600E}}/\text{PIK3CA}^{\text{H1047R}}$ lung tumors remain sensitive to the anti-tumor effects of MEK1/2 inhibition and highlight the central importance of $\text{BRAF}^{\text{V600E}} \rightarrow \text{MEK} \rightarrow \text{ERK}$ signaling in the growth of $\text{BRAF}^{\text{V600E}}/\text{PIK3CA}^{\text{H1047R}}$ -induced lung tumors.

Enhanced therapeutic benefit of combined $\text{BRAF}^{\text{V600E}}$ plus $\text{PIK3CA}^{\text{H1047R}}$ inhibition against $\text{BRAF}^{\text{V600E}}/\text{PIK3CA}^{\text{H1047R}}$ expressing lung tumors

To examine the requirement for sustained signaling in the maintenance of $\text{BRAF}^{\text{V600E}}/\text{PIK3CA}^{\text{H1047R}}$ expressing lung tumors, we initiated tumorigenesis (2×10^7 pfu Ad-Cre) in 34 *BRAF^{CA}; Pik3ca^{lat}* mice and monitored them prospectively for five weeks until they were close to end-stage as defined by signs of labored breathing and loss of $\leq 10\%$ of their body weight. At this time two mice were euthanized for lung histology and the remaining were divided into four cohorts for the following interventions: 1. No treatment; 2. Class 1 PI3'-kinase inhibitor (BKM-120, 60mg/kg, q.d., po); 3. $\text{BRAF}^{\text{V600E}}$ inhibitor (LGX-818, 30mg/kg, q.d., po) or; 4. Combination of BKM-120 and LGX-818 (60 and 30mg/kg respectively, q.d., po) [58, 59]. Response to intervention was assessed by Kaplan-Meier survival analysis where mice were euthanized when their body

conditioning score (BCS) was ≤ 2 [48] (Fig. 1-4C). In addition we monitored mouse body weight, which correlates with changes in tumor burden (Fig. 1-4D).

Kaplan-Meier analysis revealed no statistical difference in survival between untreated (n=6) or BKM-120 treated (n=8) mice as these mice continued to lose weight requiring euthanasia within five days after initiation of dosing (Figs. 1-4C&D). By contrast, mice treated with LGX-818 (n=8) or the combination of LGX-818 plus BKM-120 (n=8) displayed increased survival (Fig. 1-4C). Indeed, no mice in the LGX-818 plus BKM-120 treatment arm required euthanasia. Consistent with this, LGX-818 treated mice continued to lose weight albeit at a reduced rate such that only 1/8 mice developed end-stage disease following four weeks of drug treatment. Finally, mice treated with combination LGX-818 plus BKM-120 displayed immediate signs of improvement in their BCS including increased body weight that continued throughout the treatment period until the mice were euthanized for analysis (Fig. 1-4D).

Histological analysis of lungs from mice of each group indicated that untreated and BKM-120 treated mice displayed a substantial tumor burden (average of ~28% and ~23%) with no statistical difference between these two groups, consistent with the lack of therapeutic benefit afforded by BKM-120 treatment (Figs. 1-4E&F). By contrast, LGX-818 treated mice displayed a statistically significant reduction in tumor burden (~10%) compared to control or BKM-120 treated mice. The therapeutic benefit afforded LGX-818 treated mice was further enhanced by combined treatment with BKM-120 (~3% tumor burden) consistent with the survival and health benefits afforded these mice by combination therapy. Taken together, these data suggest that combined blockade of

BRAF^{V600E} and PIK3CA^{H1047R} signaling in BRAF^{V600E}/PIK3CA^{H1047R} expressing lung tumors was significantly superior to blockade of BRAF^{V600E} or PIK3CA^{H1047R} alone.

PIK3CA^{H1047R} promotes malignant progression of BRAF^{V600E}-induced tumors

KRAS^{G12D}-induced lung tumorigenesis in GEM models is dependent upon both RAF→MEK→ERK, PI3'-kinase, RAC1 and NF-κB signaling [16, 43, 60-63]. However, to date, activation of single biochemical nodes downstream of KRAS.GTP has failed to recapitulate the propensity for malignant progression displayed by KRAS^{G12D}-initiated lung tumors. Although BRAF^{V600E} induces benign lung tumors with enhanced efficacy compared to KRAS^{G12D}, such lesions are low grade, benign and fail to progress to lung cancer [12, 16]. As demonstrated here, although PIK3CA^{H1047R} is unable to initiate lung tumorigenesis, it strikingly promotes the growth BRAF^{V600E}-initiated early-stage lung tumors. This prompted us to evaluate whether BRAF^{V600E} and PIK3CA^{H1047R} might cooperate for late-stage malignant lung cancer progression. To that end, lung tumors was initiated in either *BRaf^{CA}* or *BRaf^{CA}; Pik3ca^{lat}* mice with a low dose of Ad-Cre (5x10⁵ pfu) with mice euthanized 25 weeks later for evaluation of lung tumor burden and grade [16, 64].

By contrast with early time points, overall tumor number was not significantly different in *BRaf^{CA}* versus *BRaf^{CA}; Pik3ca^{lat}* mice with an average of 30 tumors per lobe recorded in both genotypes (Fig. 1-5A). However, individual lung tumors in *BRaf^{CA}; Pik3ca^{lat}* mice were significantly larger compared to those in *BRaf^{CA}* mice (35,000μm² vs. 5,000μm², *p*=0.0005). This difference in tumor size was reflected by overall increased tumor burden in *BRaf^{CA}; Pik3ca^{lat}* mice (24% vs. 6%, *p*=0.0001, Fig. 1-5A).

These data suggest that PIK3CA^{H1047R} does not influence the frequency of BRAF^{V600E} initiated cells in the distal lung epithelium but decreases the latency period prior to the cells committing to tumorigenesis and also increases their overall proliferative potential.

One possible explanation for the larger tumors observed in *BRaf^{CA}; Pik3ca^{lat}* mice is that each tumor arises in a polyclonal manner from more than one initiated cell. Hence, to test the clonality of BRAF^{V600E}/PIK3CA^{H1047R} lung tumors we generated *BRaf^{CA}; Pik3ca^{lat}* mice that also contained the “Confetti” reporter (*Gt(ROSA)26Sor^{tm1}(CAG-Brainbow2.1)Cre, R26^{Confetti}* hereafter) (Supp. Fig. 1-S2) [65]. The action of Cre recombinase on the *R26^{Confetti}* reporter elicits a recombination event that stochastically places one of four different fluorescent proteins (FP) into position downstream of the CAG promoter. Hence, if BRAF^{V600E}/PIK3CA^{H1047R}-induced lung tumors are clonally derived, each tumor should express a single FP. However, if tumors are polyclonal in origin, they will contain a mixture of cells with different FP expression. To that end, *BRaf^{CA}; Pik3ca^{lat}; R26^{Confetti}* mice were infected with 10⁷ pfu Ad-Cre with lung tumors analyzed by fluorescence microscopy 9 weeks later. Individual BRAF^{V600E}/PIK3CA^{H1047R} lung tumors were uniformly positive for a single FP, indicating that each tumor is clonally derived from a single initiated cell (Supp. Fig. 1-S2).

To assess tumor progression in our models, we employed a grading scheme based on previously published classifications of lung lesions in GEM models to assess the grade of >250 tumors from mice of each genotype (Fig. 1-5B and Supp. Figs. 1-S3A&B) [11, 64]. Regions of hyperplasia were designated Grade 1, benign adenomas as Grade 2, larger adenomas as Grade 3 and adeno-squamous or adenocarcinomas as Grade 4. As described previously, BRAF^{V600E}-induced lung lesions were predominantly Grade 1

or 2 with rare examples of Grade 3 detected. By contrast, BRAF^{V600E}/PIK3CA^{H1047R}-induced lung lesions were generally Grade 2 or 3 adenomas but ~3% of tumors were malignant Grade 4 adeno-squamous or adenocarcinoma lesions. These data indicate that BRAF^{V600E} cooperates with PIK3CA^{H1047R} to both accelerate early-stage lung tumorigenesis and to promote late-stage malignant progression [11].

To determine if the cell of origin might influence the spectrum of lung tumors initiated in these mice we employed adenovirus vectors in which expression of Cre recombinase is controlled by lung cell specific promoters [46]. Ad-SPC-Cre, Ad-CCSP-Cre and Ad-CGRP-Cre direct Cre recombinase expression to Alveolar type II pneumocytes, Clara cells or neuroendocrine cells respectively. Of these, we noted that Ad-SPC-Cre was the most potent inducer of lung tumorigenesis in either *BRaf^{CA}* or *BRaf^{CA}; Pik3ca^{lat}* mice and was equivalent in potency to Ad-CMV-Cre, the virus commonly used for these experiments. Moreover, lung tumor cells emerging in either *BRaf^{CA}* or *BRaf^{CA}; Pik3ca^{lat}* mice induced with either Ad-CCSP-Cre or Ad-CGRP-Cre, which were significantly less potent in inducing lung tumorigenesis, displayed the typical cuboidal morphology and expression of SP-C that is characteristic of AT2 cells (data not shown).

In these experiments we assessed tumor grade at 22 weeks in a group of *BRaf^{CA}* or *BRaf^{CA}; Pik3ca^{lat}* mice initiated with Ad-SPC-Cre to confirm the ability of PIK3CA^{H1047R} to promote malignant progression of BRAF^{V600E}-initiated lung tumors (Supp. Fig. 1-S4). As before, the majority of BRAF^{V600E} expressing lung tumors were small, grade 2 adenomas. By contrast, >50% of lung tumors in the Ad-SPC-Cre initiated *BRaf^{CA}; Pik3ca^{lat}* mice were high-grade adenomas (Grade 3) and 8.5% were either grade 4 adeno-squamous cancers or adenocarcinomas. These data confirmed observations

made with Ad-CMV-Cre as the initiating agent and further suggest that the cell of origin for both low- and high-grade BRAF^{V600E}-induced lung tumors expresses SP-C and is likely to be the AT2 cell [15].

TP53 constrains malignant progression of BRAF^{V600E}/PIK3CA^{H1047R} lung tumors

TP53 mutations frequently coexist with mutations in *KRAS*, *BRAF* or *PIK3CA* mutations in human lung adenocarcinomas and TP53 mutation or silencing promotes malignant progression of either KRAS^{G12D} or BRAF^{V600E}-driven lung tumors [11, 12]. In the case of BRAF^{V600E}, high grade, invasive tumors were typically seen at late time points (>8 weeks). We sought to determine if TP53 loss would further enhance the effects of combined expression of BRAF^{V600E} and PIK3CA^{H1047R} in the lung. To that end, we initiated tumorigenesis in a *BRaf^{CA/CA}; Pik3ca^{lat}, Trp53^{lox/lox}* mouse with a *BRaf^{CA}; Trp53^{lox/lox}* mouse as a littermate control. Within four weeks the *BRaf^{CA/CA}; Pik3ca^{lat}, Trp53^{lox/lox}* mouse displayed weight loss and labored breathing requiring euthanasia. Whereas the control *BRaf^{CA}; Trp53^{lox/lox}* mouse had a tumor burden of 0.2% made up of mainly small hyperplasias with a solitary benign adenoma detected (Supp. Fig. 1-S5A), the lungs of the *BRaf^{CA/CA}; Pik3ca^{lat}, Trp53^{lox/lox}* mouse had a tumor burden of 41% made up of high grade, anaplastic adenocarcinoma. Moreover, these aggressive, high-grade tumors stained positive for Vimentin, a marker of epithelial-mesenchymal transition, failed to express TTF-1/NKX2-1, a marker of the distal lung epithelium and displayed a high proliferative index (Ki67, Supp. Fig. 1-S5B). One lung lobe was removed from the *BRaf^{CA/CA}; Pik3ca^{lat}, Trp53^{lox/lox}* mouse and used to establish cell lines for further analysis. This experiment was repeated using a second *BRaf^{CA/+}; Pik3ca^{lat}, Trp53^{lox/lox}* mouse and yielded similar results indicating that PIK3CA^{H1047R}

accelerates the progression of BRAF^{V600E}/TP53^{Null} tumors to malignant lung cancer.

PIK3CA^{H1047R} promotes BRAF^{V600E}-induced oncogenic transformation *in vitro*

There is a dearth of BRAF^{V600E} expressing human lung cancer derived cell lines available for study. One advantage of GEM models of lung cancer is the ability to engineer defined genetic alterations and then generate cell lines for *in vitro* analysis. Consistent with previous observations, we note that successful establishment of lung cancer derived cell lines requires silencing of either *Trp53* or *Cdkn2a* (encoding INK4A & ARF) tumor suppressors. To that end, we generated BRAF^{V600E}/TP53^{Null} and BRAF^{V600E}/PIK3CA^{H1047R}/TP53^{Null} mouse lung cancer derived cell lines (BT and BPT cells hereafter) from suitably manipulated mice [16].

Although lung cancer-derived, BT cells display a limited capacity for anchorage independent growth. To test whether activation of PI3'-kinase signaling might cooperate with BRAF^{V600E} to influence the behavior of BT cells, they were engineered to express either mCherry (control), PIK3CA^{H1047R} or a myristoylated, constitutively activated AKT1 (M⁺AKT1) (Fig. 1-6). Following selection, cell extracts were analyzed by immunoblotting for the activation status of key nodes in the PI3'-kinase signaling pathway (Fig. 1-6A and Supp. Fig. 1-S8A). Compared to control, cells expressing either PIK3CA^{H1047R} or M⁺AKT1 displayed elevated pPRAS40 and pRP-S6 while M⁺AKT1 expressing cells displayed elevated levels of pAKT, p4E-BP1, pFOXO1 and pGSK3 β . PIK3CA^{H1047R} and M⁺AKT1 cells also showed a modest decrease in the expression of p27^{KIP1}. Consistent with the ability of PIK3CA^{H1047R} to cooperate with BRAF^{V600E} in lung tumorigenesis in an AKT dependent manner *in vivo*, expression of either PIK3CA^{H1047R}

or M⁺AKT1 led to a significant increase in anchorage independent colony formation *in vitro* (Fig. 1-6B). Indeed, the parental and mCherry control BT lung cancer cells failed to form colonies in agarose even when cultured for ~8 weeks. By contrast, the PIK3CA^{H1047R} or M+AKT1 expressing cells cloned with an efficiency of 1% and 1.4%, respectively, after three weeks. These data indicate that PI3'-kinase→AKT signaling can cooperate with BRAF^{V600E} in oncogenic transformation of cultured lung cancer derived cell lines.

In conjunction with experiments described above, the ability of BPT lung cancer cells to form anchorage independent colonies was tested in the absence or presence of various pathway-targeted inhibitors. Unlike BT cells, BPT cells are capable of anchorage-independent colony formation (Vehicle, Fig. 1-6C). However, when cultured in the presence of a MEK inhibitor (PD325901 @ 1μM), a class 1 PI3'-kinase inhibitor (GDC-0941 @ 5μM) or an AKT inhibitor (MK-2206 @ 5μM) colony formation was entirely abolished even when the cultures were maintained for 8 weeks (Fig. 1-6C) [66]. Cumulatively, these data indicate the ability of PI3'-kinase→AKT signaling to cooperate with BRAF^{V600E} in conferring key features of the transformed state on lung tumor derived cells.

BRAF^{V600E}/PIK3CA^{H1047R}/TP53^{Null} lung cancer cell lines are sensitive to combined pharmacological inhibition of RAF or PI3'-kinase pathway inhibition

We have documented the striking ability of BRAF^{V600E} and PIK3CA^{H1047R} to cooperate both *in vivo* and *in vitro* in the tumorigenic conversion of mouse lung epithelial cells. To assess the mechanism(s) of cooperation between BRAF^{V600E} and

PIK3CA^{H1047R} on the behavior of BPT cells they were treated with various pathway-targeted inhibitors of BRAF^{V600E} or PIK3CA^{H1047R} signaling at different concentrations, either alone or in combination, at which time effects on cell viability or the cell division cycle were assessed (Figs. 1-7A-C).

As expected, single agent inhibition of MEK1/2 (PD901) or class 1 PI3'-kinases (GDC-0941) was effective in decreasing cell proliferation after 72 hours. Moreover, the combination of these agents had the strongest anti-proliferative effects, demonstrating at least an additive effect particularly in the mid-range of concentrations of both drugs (Fig. 1-7A). Given its potency *in vivo*, single agent AKT inhibition (MK-2206) was surprisingly ineffective at preventing the short-term growth of these cells (Fig. 1-7B). Even at 5 μ M, MK-2206 displayed not even a modest cytostatic effect on cell proliferation/viability. Single agent ERK1/2 inhibition (SCH772984) also exerted a cytostatic effect, only promoting decreased cell viability at higher concentrations (>250nM) [67]. However, in this case, the combination of ERK1/2 and AKT inhibition displayed remarkable cooperativity such that concentrations of ERK1/2 (250nM) or AKT (125nM) that had no effect on cell viability as single agents had striking inhibitory effects on cell proliferation when combined (Fig. 1-7B). These data were confirmed using a cell growth assay in which cells were cultured in the presence of the various agents with effects on cell proliferation quantified by Crystal Violet staining (Supp. Fig. 1-S6A).

Finally, the ability of combined RAF or PI3'-kinase pathway-targeted inhibitors to elicit cell death was tested using a clonogenic assay. Cells were treated with the indicated drug concentrations for 24 hours at which time both adherent and non-adherent cells were collected and viable cells enumerated (Non-adherent cells were

only observed in cells treated with the combination of MEK1/2 plus PI3'-kinase or ERK1/2 plus AKT inhibitors). Clonogenicity was estimated by plating 10^2 - 10^4 cells and counting the number of colonies visible 5 days later. Cells treated with single agent MEK1/2, ERK1/2, PI3'-kinase or AKT inhibitors remained viable and generated colonies with an efficiency of 65-85%. By contrast, only 10% of adherent and <1% of non-adherent cells treated with combined MEK1/2 plus PI3'-kinase inhibitors formed colonies when re-plated in the absence of drug. Approximately 70% of adherent but less than 1% of non-adherent cells treated with combined ERK1/2 plus AKT inhibitors formed colonies when re-plated in the absence of drug. These data suggest that, over 24 hours, single agent blockade of BRAF^{V600E} or PIK3CA^{H1047R} signaling is largely cytostatic with little effect on cell viability. By contrast, combined inhibition of both pathways elicits cell detachment and cell death with the combination of MEK1/2 plus class 1 PI3'-kinase inhibition being most effective (data not shown).

To assess the effects of the various agents on the cell division cycle, we incubated BPT cells with the various pathway-targeted inhibitors either alone or in combination and then labeled cells with BrdU to assess S phase progression (Fig. 1-7C, see Table 1-S1 for drug concentrations). Vehicle-treated cells displayed a remarkable and highly reproducible proliferative index with >75% of cells incorporating BrdU over the labeling period. As expected, single agent blockade of MEK1/2, ERK1/2, PI3'-kinase or AKT reduced the percentage of cells that transited S phase and increased the G1 population with the PI3'-kinase inhibitor displaying the most potent effects, the MEK and ERK inhibitors roughly equipotent and the AKT inhibitor the least potent. Cells treated with combined MEK1/2 plus PI3'-kinase or ERK1/2 plus AKT inhibitors displayed the most

profound effects on the cell division cycle in addition to displaying evidence of cell death manifest by a large number of non-adherent cells and cells with a sub-G1 DNA content (Fig. 1-7C and Table 1-S2). Taken together, these data indicate that BRAF^{V600E} and PIK3CA^{H1047R} cooperatively regulate the cell division cycle and cell death *in vitro*.

It is likely that BRAF^{V600E} and PIK3CA^{H1047R} cooperatively regulate many biochemical processes in the cell to influence cell proliferation *in vitro* and tumorigenesis *in vivo*. To assess the molecular mechanism(s) of oncogenic cooperation between BRAF^{V600E} and PIK3CA^{H1047R} we employed reverse phase protein array (RPPA) analysis to quantify protein expression/modification in samples of BPT cell lysates treated with inhibitors as described above (Fig. 1-7D). Triplicate cultures of BPT cells were treated with inhibitors of MEK1/2 (PD), ERK1/2 (SCH), class 1 PI3'-kinases (GDC) or AKT1-3 (MK) either alone or in combination as indicated (Fig. 1-7D). Prior to RPPA analysis, we confirmed that each of the agents had the anticipated biochemical effects (Supp. Fig. 1-S6B). As expected, inhibition of MEK1/2 or ERK1/2 led to strongly diminished pERK1/2 and promoted a modest increase in pAKT. Inhibition of PI3'-kinases or AKT led to strongly diminished pAKT with no obvious effects on pERK. Finally, the combinations of inhibitors potently suppressed both pERK1/2 and pAKT.

The biological triplicate samples were then analyzed by RPPA with antisera against >150 proteins or protein modifications as described previously [52, 53]. Unsupervised hierarchical clustering of the results of these analyses indicated that samples clustered based on the pathway inhibited such that MEKi or ERKi treated samples clustered together as did PI3Ki and AKTi treated samples (Fig. 1-7D and Supp. Fig. 1-S7). Samples from cells treated with combination pathway inhibitors clustered separately

from samples from cells treated with the various single agents with the samples from cells treated with combined MEK1/2 plus class PI3'-kinase showing the greatest separation.

The RPPA analysis generated predictions with regards to the consequences of inhibition of BRAF^{V600E} or PIK3CA^{H1047R} signaling on regulators of cell proliferation, some of which were then tested by conventional immunoblotting using an entirely independent set of validation samples generated from appropriately treated BPT cells (Fig. 1-7E and Supp. Fig. 1-S8). As predicted by the RPPA data and confirmed by immunoblotting, inhibition of MEK1/2→ERK1/2 signaling led to increased expression of the pro-apoptotic BCL-2 family protein BIM and decreased expression of the c-MYC transcription factor as well as cyclins D1 and A. Inhibition of PIK3CA^{H1047R}, but not AKT, signaling also promoted BIM expression and inhibited c-MYC, cyclins D1 and A and also led to elevated p27^{KIP1} expression and suppression of pRP-S6. Consistent with the lack of effect of MK-2206 against the proliferation of cultured BPT cell, we noted that inhibition of AKT had no effect single-agent effect on BIM, c-MYC, cyclins D1 or A, p4E-BP1 or pRP-S6 but largely extinguished phosphorylation of PRAS40, a known AKT substrate. Finally, combined inhibition of both MEK and PI3'-kinases displayed additive effects on the expression of c-MYC, cyclins D1 and A as well as BIM expression, the latter correlating with the strongest increases in cleaved Caspase 3 (CC3) and Caspase 7 (CC7) that were also predicted by RPPA analysis. Although these experiments do not unequivocally identify one single mechanism by which BRAF^{V600E} and PIK3CA^{H1047R} cooperate for accelerated lung carcinogenesis, they indicate that both pathways may regulate apoptosis through suppression of BIM and enhance proliferation and tumor

progression through activation of mTOR1. These processes in turn influence tumor latency burden and malignant progression, which is evident when comparing tumors expressing both mutated PIK3CA^{H1047R} and BRAF^{V600E} to BRAF^{V600E} or KRAS^{G12D} alone (Fig 1-7F). These experiments highlight the complexity of mechanisms by which these pathways cooperate to promote lung cancer cell growth *in vivo* and *in vitro* and suggest numerous areas of future investigation.

DISCUSSION

The mechanism(s) by which mutationally activated KRAS^{G12D} promotes the aberrant behavior of human lung cancer and elicits lung cancer in GEM models remain incompletely understood. However, this research suggests that two of the best-credentialed KRAS.GTP effectors, BRAF and PIK3CA, cooperate with one another to mimic the effects of oncogenic KRAS^{G12D} in GEM models of lung cancer. Expression of BRAF^{V600E} is sufficient to elicit benign lung tumorigenesis but, unlike similarly initiated KRAS^{G12D} expressing tumors, lung tumors initiated by BRAF^{V600E} rarely progress to lung cancer (Fig. 1-7F). Unexpectedly, we noted that mutationally activated PIK3CA^{H1047R} was insufficient to induce lung tumors, even when combined with PTEN silencing, a result at-odds with a previous report [43] (Fig. 1-7F). We tested whether observed differences in lung tumorigenesis may reflect differences in the magnitude of PI3'-kinase signaling between our conditional chromosomal knockin *Pik3ca^{lat}* allele and the tetracycline inducible transgene employed by Engelman et al. by generating mice with every possible combination of heterozygous or homozygous *Pik3ca^{lat}* and *Pten^{lox}* expecting that at least one combination would recapitulate the effects of the tetracycline-inducible *PIK3CA^{H1047R}*. However, even one year after initiation, we

obtained no evidence that PI3'-kinase signaling could initiate lung tumorigenesis although we detected occasional hyperplasias and even rarer adenomas with high levels of pAKT in the lungs of such mice. It remains possible that strength of pathway activation, genetic background or the promoter system may influence these disparate results as suggested by similar observations in pancreatic cancer [61, 68]. However, the lack of PIK3CA^{H1047R} effects in mouse lung is consistent with the modest effects of PIK3CA^{H1047R} in ovarian epithelial cells [13]. Furthermore, others have demonstrated that PI3'-kinase activation through PTEN silencing failed to elicit lung tumorigenesis [31]. It remains to be seen whether the inability of PIK3CA^{H1047R} to initiate lung tumorigenesis, either alone or in conjunction with PTEN silencing, will be predictive of anti-tumor effects of pharmacological inhibition targeting of PI3'-kinase in the clinic [43].

Despite its inability to initiate lung tumorigenesis, PIK3CA^{H1047R} cooperated with BRAF^{V600E} in dramatic fashion to promote lethal lung tumorigenesis, which occurred with short latency and complete penetrance (Fig. 1-7F). That PTEN silencing also cooperated with BRAF^{V600E}, albeit less strikingly, confirmed these observations and suggests that the effects of PTEN silencing are mediated by PI3'-kinase signaling. Although at early time points, BRAF^{V600E}/PIK3CA^{H1047R}-induced tumors displayed benign characteristics, six months after initiation there was clear evidence of cancer progression in ~3-8% of tumors in a manner reminiscent of KRAS^{G12D}. Finally, when TP53 was silenced in conjunction with combined BRAF^{V600E}/PIK3CA^{H1047R} expression, mouse lungs were replete with lung cancer within four weeks some of which showed signs of de-differentiation and epithelial-to-mesenchymal transition, frequent hallmarks of advanced lung cancer [69, 70] [71].

Taken in conjunction with previous reports of the MEK1/2 and PI3'-kinase dependency of KRAS^{G12D}-induced lung tumors [72], the simplest explanation is that combined activation of RAF→MEK→ERK and PI3'-kinase→AKT signaling cooperates to accelerate benign tumorigenesis and to promote malignant lung cancer progression. Although activation of BRAF and PI3'-kinase signaling can account for much of the phenotype associated with KRAS^{G12D} expression, a role for other effectors of RAS.GTP signaling in malignant progression remains possible since ~10% of KRAS^{G12D} expressing tumors display malignant progression whereas only ~3-8% of BRAF^{V600E}/PIK3CA^{H1047R} tumors do so [16]. Indeed, since only a minority of KRAS^{G12D} or combined BRAF^{V600E}/PIK3CA^{H1047R} expressing lung tumors progress to cancer, there remain unaccounted for stochastic genetic/epigenetic changes in the developing tumor cells that promote malignant progression. This is further illuminated by that fact that TP53 silencing further enhances cancer progression in response to KRAS^{G12D} or BRAF^{V600E}/PIK3CA^{H1047R} expression.

The failure of BRAF^{V600E}-initiated lung tumors to progress to cancer has been ascribed to the engagement of a senescence-like proliferative arrest [17]. Others have proposed that sustained RAF→MEK→ERK signaling can elicit inhibitory feedback on PI3'-lipid production, which serves as the trigger for such arrest [17]. Data presented here supports this hypothesis since expression of PIK3CA^{H1047R} clearly enhanced the proliferative capacity of clonally derived tumors initiated by BRAF^{V600E} expression. However, it remains unclear how PI3'-kinase signaling sustains the proliferation of BRAF^{V600E}-initiated lung tumors. Previous data suggest that these pathways converge to elevate D-type cyclin expression and suppress cyclin-dependent kinase inhibitor

expression [73]. Our analysis of BPT cells suggests that the cell division cycle is indeed under the coordinate control of both BRAF^{V600E} and PIK3CA^{H1047R} activity. However, future experiments are required to determine which of the many possible nodes of cell cycle regulation are essential to the observed cooperation *in vitro* and *in vivo*.

BPT lung cancer cells were sensitive to the combined effects of BRAF^{V600E} or PIK3CA^{H1047R} pathway-targeted inhibition. Single agent inhibition of either pathway had potent inhibitory effects on the cell division cycle without promoting apoptosis. By contrast, combined pathway inhibition had even stronger inhibitory effects on the cell cycle and also promoted cell death. These data are consistent with the anti-tumor effects of combined BRAF^{V600E} and PI3'-kinase inhibition *in vivo*. It was noteworthy that AKT inhibition was largely without effect against lung tumors initiated by BRAF^{V600E} expression but potently suppressed the cooperation between BRAF^{V600E} and PIK3CA^{H1047R}. Hence, there appears to be a genotype-drug response phenotype with regards to the effects of AKT inhibition in GEM models. It remains to be seen how these data will translate into the clinical utility of single or combined pathway-targeted interventions in humans with *BRAF* mutated lung cancer. Overall, expression of BRAF^{V600E} or PIK3CA^{H1047R} accounts for a small percentage of patients with NSCLC [38]. By contrast, mutational activation of *KRAS* is frequent in lung adenocarcinomas. Since mutationally activated *KRAS* has proven an intractable pharmacological target and, given the availability of specific and selective inhibitors of various KRAS^{G12D} effectors, it will be interesting to determine the extent to which combined pathway-targeted inhibition of RAF or PI3'-kinase signaling will promote regression of *KRAS* mutated lung cancers.

REFERENCES FOR CHAPTER 1

1. Herbst, R.S., J.V. Heymach, and S.M. Lippman, *Lung cancer*. N Engl J Med, 2008. **359**(13): p. 1367-80.
2. Heist, R.S. and J.A. Engelman, *SnapShot: non-small cell lung cancer*. Cancer Cell. **21**(3): p. 448 e2.
3. Network, T.C.G.A.R., *Diversity of Lung Adenocarcinoma Revealed by Integrative Molecular Profiling*. Nature, 2013. **Under Review**.
4. Chaff, J.E., et al., *Coexistence of PIK3CA and other oncogene mutations in lung adenocarcinoma-rationale for comprehensive mutation profiling*. Mol Cancer Ther, 2011. **11**(2): p. 485-91.
5. Altomare, D.A. and J.R. Testa, *Perturbations of the AKT signaling pathway in human cancer*. Oncogene, 2005. **24**(50): p. 7455-64.
6. Dankort, D., et al., *A new mouse model to explore the initiation, progression, and therapy of BRAFV600E-induced lung tumors*. Genes Dev, 2007. **21**(4): p. 379-84.
7. Trejo, C.L., et al., *MEK1/2 inhibition elicits regression of autochthonous lung tumors induced by KRASG12D or BRAFV600E*. Cancer Res, 2012. **72**(12): p. 3048-59.
8. Ji, H., et al., *Mutations in BRAF and KRAS converge on activation of the mitogen-activated protein kinase pathway in lung cancer mouse models*. Cancer Res, 2007. **67**(10): p. 4933-9.
9. Engelman, J.A., et al., *Effective use of PI3K and MEK inhibitors to treat mutant Kras G12D and PIK3CA H1047R murine lung cancers*. Nat Med, 2008. **14**(12): p. 1351-6.
10. Courtois-Cox, S., et al., *A negative feedback signaling network underlies oncogene-induced senescence*. Cancer Cell, 2006. **10**(6): p. 459-72.
11. Kinross, K.M., et al., *An activating Pik3ca mutation coupled with Pten loss is sufficient to initiate ovarian tumorigenesis in mice*. J Clin Invest, 2012. **122**(2): p. 553-7.
12. Jackson, E.L., et al., *Analysis of lung tumor initiation and progression using conditional expression of oncogenic K-ras*. Genes Dev, 2001. **15**(24): p. 3243-8.
13. Jonkers, J., et al., *Synergistic tumor suppressor activity of BRCA2 and p53 in a conditional mouse model for breast cancer*. Nat Genet, 2001. **29**(4): p. 418-25.
14. Trotman, L.C., et al., *Pten dose dictates cancer progression in the prostate*. PLoS Biol, 2003. **1**(3): p. E59.
15. Sutherland, K.D., et al., *Cell of origin of small cell lung cancer: inactivation of Trp53 and Rb1 in distinct cell types of adult mouse lung*. Cancer Cell, 2011. **19**(6): p. 754-64.
16. Fasbender, A., et al., *Incorporation of adenovirus in calcium phosphate precipitates enhances gene transfer to airway epithelia in vitro and in vivo*. J Clin Invest, 1998. **102**(1): p. 184-93.
17. Ullman-Cullere, M.H. and C.J. Foltz, *Body condition scoring: a rapid and accurate method for assessing health status in mice*. Lab Anim Sci, 1999. **49**(3): p. 319-23.
18. Capper, D., et al., *Assessment of BRAF V600E mutation status by immunohistochemistry with a mutation-specific monoclonal antibody*. Acta Neuropathol, 2011. **122**(1): p. 11-9.
19. Morita, S., T. Kojima, and T. Kitamura, *Plat-E: an efficient and stable system for transient packaging of retroviruses*. Gene Ther, 2000. **7**(12): p. 1063-6.
20. Zhu, J., et al., *Senescence of human fibroblasts induced by oncogenic Raf*. Genes Dev, 1998. **12**(19): p. 2997-3007.
21. Gopal, Y.N., et al., *Basal and treatment-induced activation of AKT mediates resistance to cell death by AZD6244 (ARRY-142886) in Braf-mutant human cutaneous melanoma cells*. Cancer Res, 2010. **70**(21): p. 8736-47.

22. Deng, W., et al., *Role and therapeutic potential of PI3K-mTOR signaling in de novo resistance to BRAF inhibition*. *Pigment Cell Melanoma Res*, 2011. **25**(2): p. 248-58.
23. Iwanaga, K., et al., *Pten inactivation accelerates oncogenic K-ras-initiated tumorigenesis in a mouse model of lung cancer*. *Cancer Res*, 2008. **68**(4): p. 1119-27.
24. Dankort, D., et al., *Braf(V600E) cooperates with Pten loss to induce metastatic melanoma*. *Nat Genet*, 2009. **41**(5): p. 544-52.
25. Ohren, J.F., et al., *Structures of human MAP kinase kinase 1 (MEK1) and MEK2 describe novel noncompetitive kinase inhibition*. *Nat Struct Mol Biol*, 2004. **11**(12): p. 1192-7.
26. Hirai, H., et al., *MK-2206, an allosteric Akt inhibitor, enhances antitumor efficacy by standard chemotherapeutic agents or molecular targeted drugs in vitro and in vivo*. *Mol Cancer Ther*, 2010. **9**(7): p. 1956-67.
27. Halilovic, E., et al., *PIK3CA mutation uncouples tumor growth and cyclin D1 regulation from MEK/ERK and mutant KRAS signaling*. *Cancer Res*. **70**(17): p. 6804-14.
28. Wee, S., et al., *PI3K pathway activation mediates resistance to MEK inhibitors in KRAS mutant cancers*. *Cancer Res*, 2009. **69**(10): p. 4286-93.
29. Drahl, C., *LGX818, Made To Fight Melanoma*. *Chemical & Engineering News*, 2013. **91**(16): p. 14.
30. Koul, D., et al., *Antitumor activity of NVP-BKM120--a selective pan class I PI3 kinase inhibitor showed differential forms of cell death based on p53 status of glioma cells*. *Clin Cancer Res*, 2011. **18**(1): p. 184-95.
31. Hofmann, I., et al., *K-RAS mutant pancreatic tumors show higher sensitivity to MEK than to PI3K inhibition in vivo*. *PLoS One*, 2012. **7**(8): p. e44146.
32. Collisson, E.A., et al., *A central role for RAF-->MEK-->ERK signaling in the genesis of pancreatic ductal adenocarcinoma*. *Cancer Discov*, 2012. **2**(8): p. 685-93.
33. Kissil, J.L., et al., *Requirement for Rac1 in a K-ras induced lung cancer in the mouse*. *Cancer Res*, 2007. **67**(17): p. 8089-94.
34. Meylan, E., et al., *Requirement for NF-kappaB signalling in a mouse model of lung adenocarcinoma*. *Nature*, 2009. **462**(7269): p. 104-7.
35. Nikitin, A.Y., et al., *Classification of proliferative pulmonary lesions of the mouse: recommendations of the mouse models of human cancers consortium*. *Cancer Res*, 2004. **64**(7): p. 2307-16.
36. Livet, J., et al., *Transgenic strategies for combinatorial expression of fluorescent proteins in the nervous system*. *Nature*, 2007. **450**(7166): p. 56-62.
37. Xu, X., et al., *Evidence for type II cells as cells of origin of K-Ras-induced distal lung adenocarcinoma*. *Proc Natl Acad Sci U S A*, 2012. **109**(13): p. 4910-5.
38. Raynaud, F.I., et al., *Biological properties of potent inhibitors of class I phosphatidylinositide 3-kinases: from PI-103 through PI-540, PI-620 to the oral agent GDC-0941*. *Mol Cancer Ther*, 2009. **8**(7): p. 1725-38.
39. Morris, E.J., et al., *Discovery of a novel ERK inhibitor with activity in models of acquired resistance to BRAF and MEK inhibitors*. *Cancer Discov*, 2013.
40. Eser, S., et al., *Selective requirement of PI3K/PDK1 signaling for Kras oncogene-driven pancreatic cell plasticity and cancer*. *Cancer Cell*, 2013. **23**(3): p. 406-20.
41. Snyder, E.L., et al., *Nkx2-1 represses a latent gastric differentiation program in lung adenocarcinoma*. *Mol Cell*, 2013. **50**(2): p. 185-99.
42. Winslow, M.M., et al., *Suppression of lung adenocarcinoma progression by Nkx2-1*. *Nature*, 2011. **473**(7345): p. 101-4.
43. Thiery, J.P., et al., *Epithelial-mesenchymal transitions in development and disease*. *Cell*, 2009. **139**(5): p. 871-90.
44. Gupta, S., et al., *Binding of ras to phosphoinositide 3-kinase p110alpha is required for ras-driven tumorigenesis in mice*. *Cell*, 2007. **129**(5): p. 957-68.

45. Mirza, A.M., et al., *Cooperative regulation of the cell division cycle by the protein kinases RAF and AKT*. Mol Cell Biol, 2004. **24**(24): p. 10868-81.

FIGURE LEGENDS

Figure 1-1. PI3'-kinase pathway activation is insufficient to initiate tumorigenesis in the mouse lung.

A: Mice of the indicated *Pik3ca*^{lat}, *Pten*^{lox} or *BRaf*^{CA} genotypes were infected with 10⁷ pfu of Ad-Cre by intranasal instillation and monitored for three or ≥12 months as indicated at which time they were euthanized and their lungs processed for H&E staining. Representative H&E-stained tissue sections from *Pik3ca*^{lat/lat} (left) or *Pik3ca*^{lat/lat};*Pten*^{lox/lox} (middle) animals euthanized at 6 months after infection indicate that these mice are free of lung tumors. However, small areas of apparent airway hyperplasia, particularly were detected the compound homozygous *Pik3ca*^{lat/lat};*Pten*^{lox/lox} mice as indicated in higher magnification in the middle panel inset. *BRaf*^{CA} mice analyzed 12 weeks following Ad-Cre initiation are presented as a positive control for successful infection (right).

B-U: Tissue sections of mouse lung sections from control (uninfected) mice or mice of the indicated *Pik3ca*^{lat} or *Pten*^{lox} genotypes treated as described in A were stained with DAPI, antisera against phospho-(p)-AKT or Ki67 as indicated. Insets in panels N-U indicate higher magnification of regions of airway hyperplasia found within the lower magnification fields.

Figure 1-2. PIK3CA^{H1047R} accelerates lung tumorigenesis initiated by BRAF^{V600E}

A: *BRaf*^{CA} and *BRaf*^{CA}; *Pik3ca*^{lat} mice were infected with 5x10⁶ pfu Ad-Cre and monitored prospectively for their health status over ~120 days. Mice were euthanized when they developed end-stage disease as defined by a body conditioning score per UCSF IACUC regulations. The percentage of animals alive was determined each day after infection until all animals had reached end-stage and been euthanized.

B: *BRaf*^{CA} and *BRaf*^{CA}; *Pik3ca*^{lat} mice were infected with 10⁷ pfu Ad-Cre to initiate expression of BRAF^{V600E} either alone or in combination with PIK3CA^{H1047R} as indicated. Mice were euthanized

three weeks later, prior to the onset of end-stage disease. Lungs were processed for H&E staining with both low and high power fields presented. Scale bar represents 100 μ m.

C: Tumor number, size and burden were calculated as described in Materials and Methods in mice carrying either BRAF^{V600E} or BRAF^{V600E}/PIK3CA^{H1047R} expressing tumors as indicated.

Figure 1-3. PTEN silencing accelerates BRAF^{V600E}-initiated lung tumorigenesis

A: Mice of the indicated *BRAF^{CA}*, *Pik3ca^{lat}* or *Pten^{lox}* genotypes were infected with 10⁶ pfu Ad-Cre and euthanized four weeks later for analysis of tumor burden by H&E staining, which was quantified as described previously. Scale bars represent 100 μ M.

B: Lung tumors arising in *BRAF^{CA}* (BRAF^{V600E}) or *BRAF^{CA}; Pten^{lox/lox}* (BRAF^{V600E}/PTEN^{null}) mice were stained with antisera against PTEN to test for loss of PTEN expression in tumors in mice of the appropriate genotype.

Figure 1-4. Pharmacological inhibition of PI3'K/AKT and MAPK signaling inhibits growth of BRAF^{V600E}/PIK3CA^{H1047R} tumors

A: BRAF^{V600E} or BRAF^{V600E}/PIK3CA^{H1047R} expressing lung tumors were initiated in mice of the appropriate genotype by intranasal instillation of 10⁶ pfu Ad-Cre. Two weeks after tumor initiation mice were dosed for a further four weeks with vehicle control, MK-2206 or PD325901 as described in Materials and Methods at which time mice were euthanized and lungs prepared for H&E staining. Scale bar represents 500 μ M.

B: The effects of AKT (MK-2206) or MEK1/2 (PD325901) inhibition on lung tumor number, size and overall burden in mice bearing BRAF^{V600E} or BRAF^{V600E}/PIK3CA^{H1047R} expressing lung tumors was estimated as described in Materials and Methods. ** represents *p* values less than or equal to 0.005.

C&D: Lung tumors were initiated in *BRaf^{CA}; Pik3ca^{lat}* mice and five weeks later, when the mice were close to end-point, they were either untreated or treated with inhibitors of BRAF^{V600E} (LGX-818) or class 1 PI3'-kinases (BKM-120) either alone or in combination as indicated. Mice were euthanized when they developed end-stage disease and this was used to calculate a Kaplan-Meier survival curve (C). In addition, the weight of every mouse in each group was measured and normalized to its starting weight which was set at 100%, and the average normalized weight of all mice in a treatment group was used to assess their response to that treatment (D).

E&F: Lung tumor burden in *BRaf^{CA}; Pik3ca^{lat}* treated as described in C&D was assessed by H&E staining of lung tumor sections. The lung tumor specimens from untreated or BKM-120 treated mice came from mice with end-stage disease whereas the specimens from the LGX-818 or combined LGX-818 plus BKM-120 treatments were derived from mice at the end of the 4 week dosing schedule when the mice were not at end-stage. *** represents a *p* value of 0.0003, **** represents a *p* value of less than 0.0001.

Figure 1-5. PIK3CA^{H1047R} promotes malignant progression of BRAF^{V600E}-initiated lung tumors

A: BRAF^{V600E} or BRAF^{V600E}/PIK3CA^{H1047R} expressing lung tumors were initiated in mice of the appropriate genotype by intranasal instillation of 5x10⁵ pfu Ad-Cre with mice monitored for 25 weeks at which time they were euthanized and their lungs processed for H&E staining. Scale bar represents 50µM. Lung tumor number, size and overall burden was assessed as described in Materials and Methods.

B: The grade of BRAF^{V600E} or BRAF^{V600E}/PIK3CA^{H1047R} expressing lung tumors was assessed on a 4 point scale using the grading criteria described in Supplemental Figure S3. In brief, Grade 1 is epithelial hyperplasia, Grade 2 is low-grade adenoma, Grade 3 is high-grade adenoma, Grade 4a is adeno-squamous carcinoma and Grade 4b is adenocarcinoma.

Figure 1-6. Ectopic expression of either activated PIK3CA or AKT1 promotes anchorage independent growth to BRAF^{V600E}; TP53^{null} lung cancer derived cells

A: BRAF^{V600E}/TP53^{null} lung cancer derived cells were infected with pBabePuro retrovirus vectors encoding mCherry, PIK3CA^{H1047R} or HA- tagged, myristoylated AKT (M+AKT1) as indicated. Cell extracts prepared from puromycin resistant cells were probed by immunoblotting with either protein backbone or phospho-specific antisera as indicated. The quantification of blots against loading control (β -actin) is included as Supp. Fig. 8A.

B: BRAF^{V600E}/TP53^{null} lung cancer derived cells engineered to express mCherry, PIK3CA^{H1047R} or M+AKT1 as indicated were plated in soft agar and cultured for three weeks. The growth of anchorage-independent colonies was quantified.

C: BRAF^{V600E}/PIK3CA^{H1047R}/TP53^{null} lung cancer derived cells were plated in soft agar in the absence (vehicle) or presence of inhibitors of MEK1/2 (1 μ M PD325901), class 1 PI3'-kinase (5 μ M GDC-0941) or AKT (5 μ M MK-2206). The growth of anchorage-independent colonies was assessed over three weeks.

Figure 1-7. Cooperative effects of combined pharmacological blockade BRAF^{V600E} and PIK3CA^{H1047R} signaling on BRAF^{V600E}/PIK3CA^{H1047R}/TP53^{null} lung cancer derived cells

A&B: BRAF^{V600E}/PIK3CA^{H1047R}/TP53^{null} lung cancer derived cells were treated with a range of concentrations of MEKi (PD325901), PI3'Ki (GDC-0941), ERKi (SCH772984) or AKTi (MK-2206) either alone or in the indicated combinations 72 hours at which time cell viability was measured by luminescence using the Cell-Titre-Glo assay (Promega) and normalized to zero concentration values.

C: BRAF^{V600E}/PIK3CA^{H1047R}/TP53^{null} lung cancer derived cells were treated with the indicated pathway-targeted inhibitors of MEK1/2, ERK1/2, AKT1-3 or class 1 PI3'-kinases either alone or

in the indicated combinations for 24 hours at concentrations listed in Table S1. 3 hours prior to analysis BrdU was added to the cells to allow estimation of the percentage of cells transiting through the S phase of the cell division cycle. Cells were fixed, permeabilized and then stained with anti-BrdU-FITC and Propidium Iodide for FACS analysis. Cells were gated according to their staining characteristics into sub-G1, G1, S, or G2/M DNA content with cells of each characteristic counted (represented in the bar graph as percent of total cells).

D: Unsupervised clustering of RPPA analysis of cell extracts derived from cells treated in biological triplicates with inhibitors of MEK1/2 (PD), ERK1/2 (SCH), AKT1-3 (MK) or class 1 PI3'-kinases (GDC) either alone or in the indicated combinations for 24 hours as described above. The full dataset is included as Supp. Fig. 7 and both the raw and normalized data is provided as an Excel file.

E: A validation set of cell extracts was prepared from BPT lung cancer cells treated with inhibitors of MEK1/2 (PD), ERK1/2 (SCH), AKT1-3 (MK) or class 1 PI3'-kinases (GDC) either alone or in the indicated combinations for 24 hours and then analyzed by immunoblotting with phospho- or backbone specific antisera against the indicated proteins. The quantification of blots against loading control (β -actin) is included as Supp. Fig. 8B.

F: Expression of mutationally activated KRAS^{G12D} in the lung epithelium leads initially to hyperplasia (H) then to benign adenomas (BA), some of which have the propensity to progress to non-small cell lung cancers (NSCLC) over the course of six months. Although similarly initiated expression of BRAF^{V600E} leads to more rapid and numerous hyperplasia and benign adenomas, such lesions rarely progress to NSCLC, most likely due to a senescence-like arrest of the tumor cell division cycle. Although expression of PIK3CA^{H1047R} fails to initiate any obvious pathology in the lung, when combined with BRAF^{V600E}, PIK3CA^{H1047R} promotes even more rapid emergence of hyperplasias and benign adenomas, some of which progress to NSCLC over the

course of six months in a manner reminiscent of, but not identical to, KRAS^{G12D}. At the molecular level, BRAF^{V600E} cooperates with PIK3CA^{H1047R} signaling to regulate expression of proteins involved in promoting the cell division cycle and suppressing apoptosis.

SUPPLEMENTARY FIGURE LEGENDS

Figure 1-S1. Pharmacological inhibition of AKT does not inhibit BRAF^{V600E}-initiated lung tumorigenesis

A: *BRaf^{CA}* mice were infected with 10⁶ pfu Ad-Cre to initiate BRAF^{V600E}-driven lung tumorigenesis. Five weeks later mice were dosed with either vehicle or 120 mg/kg of MK-2206 (as indicated) for a further five weeks at which time mice were euthanized and lungs prepared for H&E staining. Scale bar represents 500µM.

B: Overall lung tumor burden in vehicle or MK-2206 treated mice from the experiment described above was quantified as described in Materials and Methods.

C: Mice bearing BRAF^{V600E}-initiated lung tumors were treated with vehicle or MK-2206 two hours prior to euthanasia at which time tumor lysates were prepared for immunoblot analysis with the indicated protein backbone or phosphospecific antisera.

D: Six mice bearing BRAF^{V600E}/PIK3CA^{H1047R} expressing lung tumors were treated with vehicle, MEK1/2 inhibitor (PD901) or AKT1-3 inhibitor (MK-2206) in duplicate for two hours prior to euthanasia at which time tumor lysates were prepared from a single lobe of the lungs of each mouse for immunoblot analysis with the indicated protein backbone or phosphospecific antisera.

Figure 1-S2. BRAF^{V600E}/PIK3CA^{H1047R} expressing lung tumors are clonally derived

BRaf^{CA}; *Pik3ca^{lat}*; *R26^{Confetti}* mice were infected with 10⁷ pfu Ad-Cre and euthanized nine weeks post infection for analysis of frozen tumor spectral properties by fluorescence microscopy.

Individual tumors displayed either membrane-targeted YFP (faint green), membrane-targeted RFP or nuclear EGFP.

Figure 1-S3. Pathology grading system used to determine progression of lung tumors.

A: Tumor bearing lungs from mice of the appropriate genotype were isolated and sectioned for H&E staining as indicated in the Materials & Methods. Scale bar represents 50 μ M. Grading of lung tumors was performed using the criteria described below:

Grade 1: Hyperplasia - Thickening of the alveoli or airway walls, nuclei and cells are uniform.

Grade 2: Low-grade adenoma - Tumors comprised of well-differentiated cells with regular nuclei.

Grade 3: High-grade adenoma - Tumors contain moderately to poorly differentiated cells. Nuclei show pleomorphism, prominent nucleoli, inclusions, frequent mitotic figures and occasional multi-nucleated cells

Grade 4a: Mixed adeno-squamous lung cancers - Large tumors exhibiting the features of Grade 3 in addition to regions of squamous appearance and necrosis. These tumors lack expression of lung epithelial markers (TTF1, SPC) and express p63 (a basal stem cell transcription factor).

Grade 4b: Adenocarcinoma - Large tumors containing all the features of Grade 3 in addition to regions of desmoplasia indicating invasion of stromal cells.

B: Immunofluorescence analysis of sections of mouse lung from a *BRaf^{CA}; Pik3ca^{lat}* mouse 25 weeks after tumor initiation displaying adjacent areas of Grade 4a and Grade 2 tumors at high magnification (40x). Grade 2 tumors are positive for the lung epithelial markers SPC and TTF-1

while Grade 4a tumors are negative for both SPC and TTF-1 but positive for nuclear p63, a basal stem cell transcription factor.

Figure 1-S4. Ad-SPC-Cre initiation of $BRAF^{CA}$; $Pik3ca^{lat}$ mice leads to malignant lung cancer

A: $BRAF^{CA}$ or $BRAF^{CA}$; $Pik3ca^{lat}$ mice were infected with 10^7 pfu Ad-SPC-Cre and then monitored for 22 weeks at which time the mice were euthanized with their lungs processed for H & E staining. Low and high power images of representative lung lobes/tumors expressing either $BRAF^{V600E}$ or $BRAF^{V600E}$ and $PIK3CA^{H1047R}$ are presented.

B: The grade of lung tumors in mice of the genotypes described above was assessed using the grading criteria defined in Figure S3 and in the Materials and Methods.

Figure 1-S5. $PIK3CA^{H1047R}$ promotes rapid development of adenocarcinoma

A: $BRAF^{CA/+}$; $Trp53^{lox/lox}$ and $BRAF^{CA/CA}$; $Pik3ca^{lat}$; $Trp53^{lox/lox}$ mice were infected with 10^7 pfu Ad-Cre and monitored for a further four weeks. Whereas the $BRAF^{CA/+}$; $Trp53^{lox/lox}$ remained healthy, the $BRAF^{CA/CA}$; $Pik3ca^{lat}$; $Trp53^{lox/lox}$ required euthanasia. Sections of lung from mice of both genotypes was stained with H & E staining as described previously with representative sections presented in low or high power. Scale bar in top panel bars represents 1mm and in the bottom panel represents 100 μ M.

B: Immunohistochemical staining of a high-grade $BRAF^{V600E}$; $PIK3CA^{H1047R}$; $TP53^{null}$ lung cancer assessing expression of TTF-1, Ki67 or Vimentin.

Figure 1-S6. Cooperative effects of combined pharmacological blockade $BRAF^{V600E}$ and $PIK3CA^{H1047R}$ signaling on $BRAF^{V600E}/PIK3CA^{H1047R}/TP53^{null}$ lung cancer derived cells assessed by Crystal Violet staining and validation of the effects of inhibitors in cell lysates analyzed by RPPA

A: BRAF^{V600E}/PIK3CA^{H1047R}/TP53^{null} lung cancer derived cells were treated with inhibitors or MEK1/2 (MEKi), ERK1/2 (ERKi), AKT1-3 (AKTi) or class 1 PI3'-kinases (PI3Ki) either alone or in the indicated combinations for 48 hours at which time cells were fixed and stained with Crystal Violet. Drug concentrations are listed in Table S1.

B: BRAF^{V600E}/PIK3CA^{H1047R}/TP53^{null} (BPT) lung cancer derived cells were treated in biological triplicates with inhibitors of MEK1/2 (PD), ERK1/2 (SCH), AKT1-3 (MK) or class 1 PI3'-kinases (GDC) either alone or in the indicated combinations for 24 hours at which time cell extracts were probed by immunoglotting with either protein backbone or phospho-specific antisera as indicated (Drug concentrations listed in Table S1). These cell extracts were then analyzed in biological triplicates by RPPA as described in the Materials & Methods.

Figure 1-S7. RPPA analysis of drug treated BPT cells

Unsupervised hierarchical clustering of RPPA analysis of extracts derived from BPT cells treated in biological triplicates with inhibitors of MEK1/2 (PD), ERK1/2 (SCH), AKT1-3 (MK) or class 1 PI3'-kinases (GDC) either alone or in the indicated combinations for 24 hours as described above.

Figure 1-S8. Quantification of Western Blots

A&B: Blots corresponding to Figure 1-6A (A) and 1-7F (B) were quantified against the loading control for each blot (β -actin) using the Odyssey FC system (Li-Cor) and Image Studio software.

Figure 1-1

A

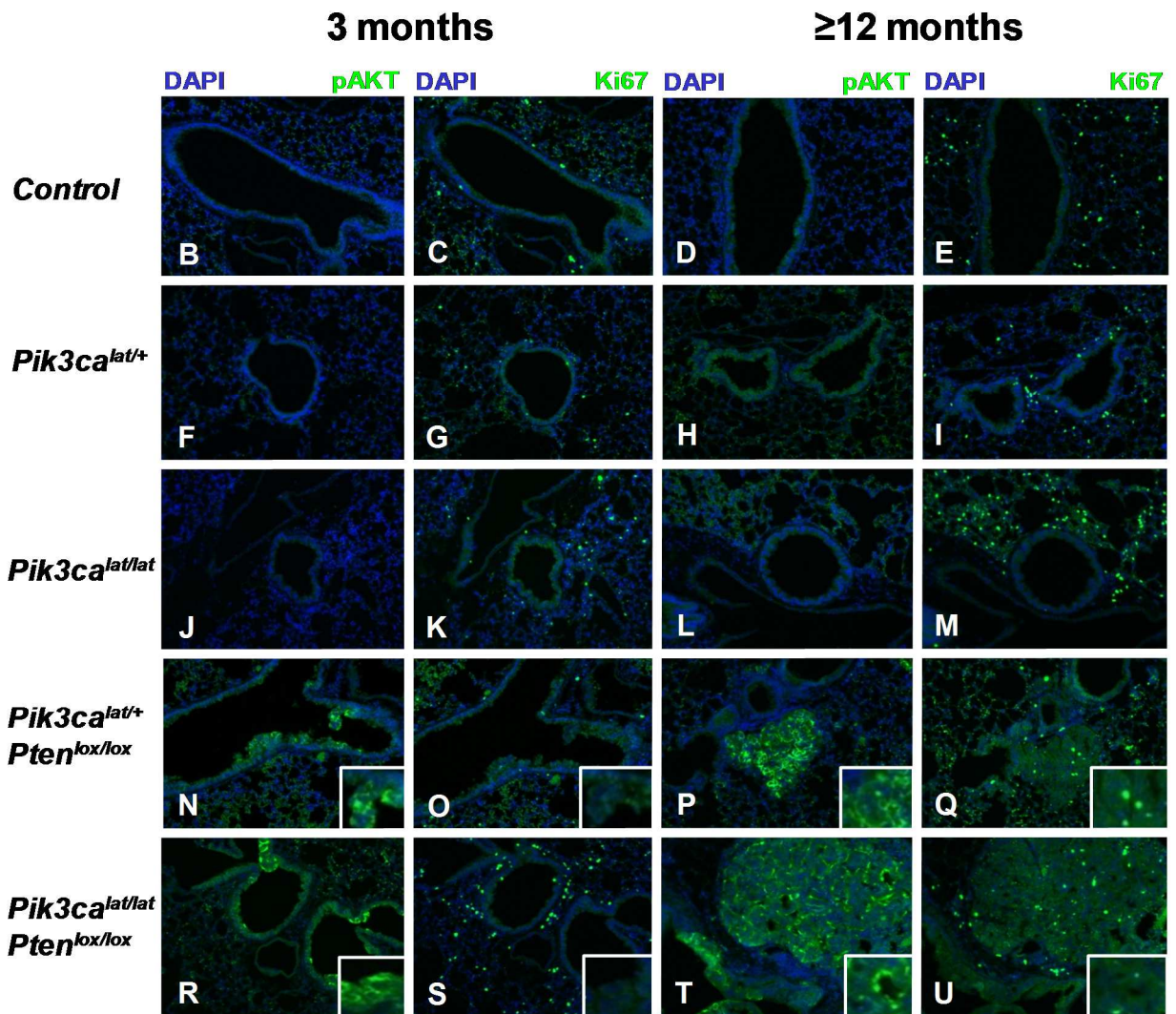
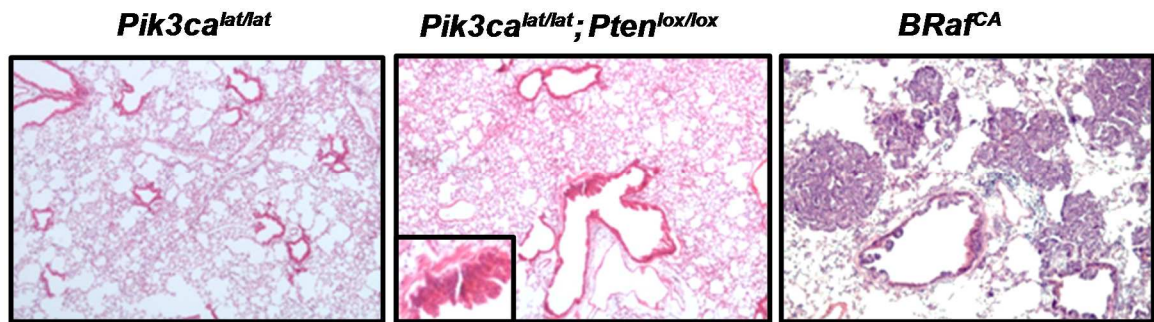


Figure 1-2

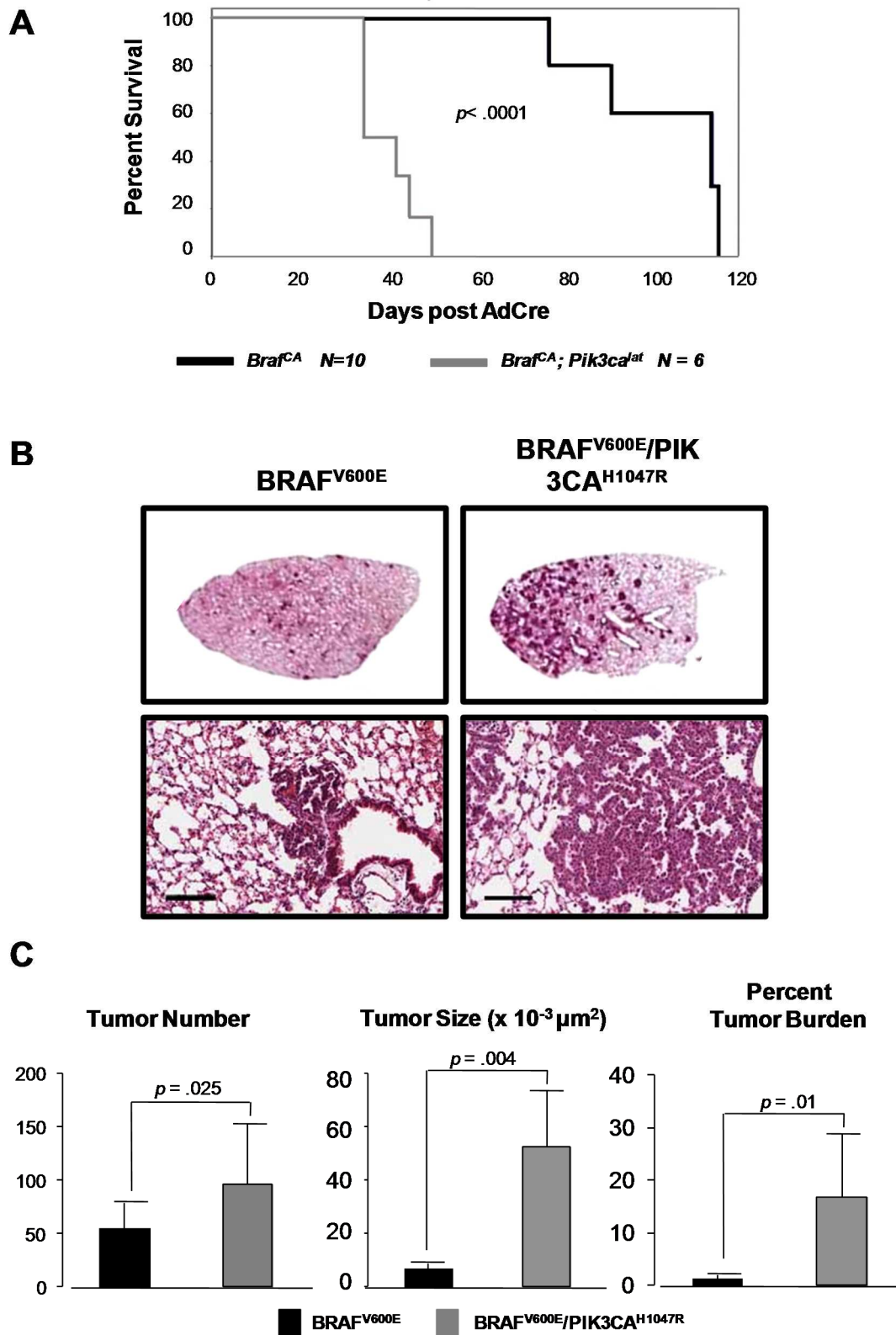
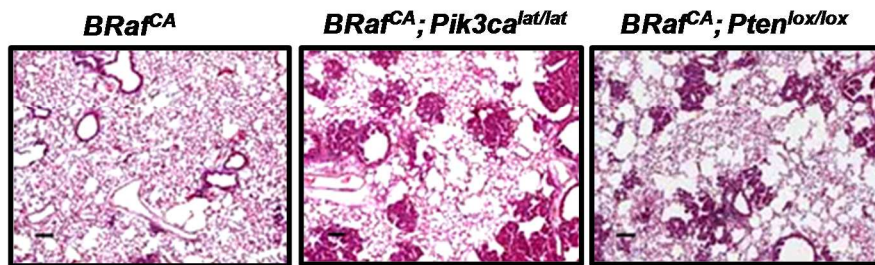
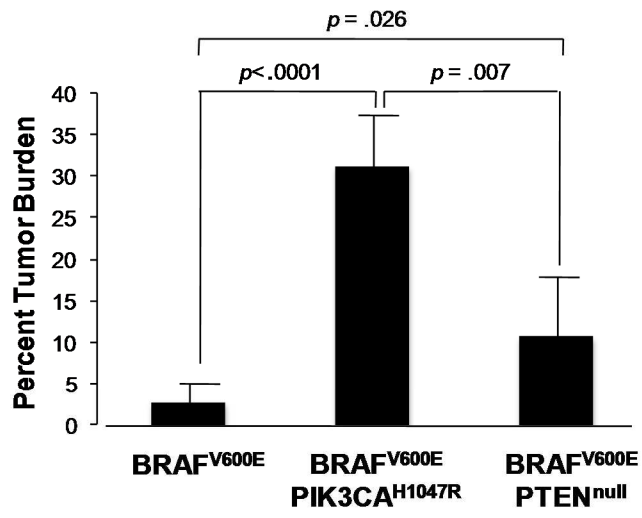


Figure 1-3

A



B



C

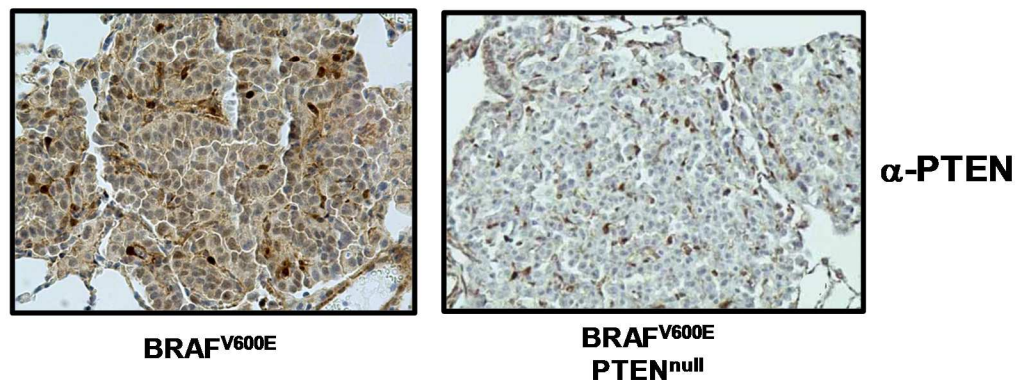


Figure 1-4

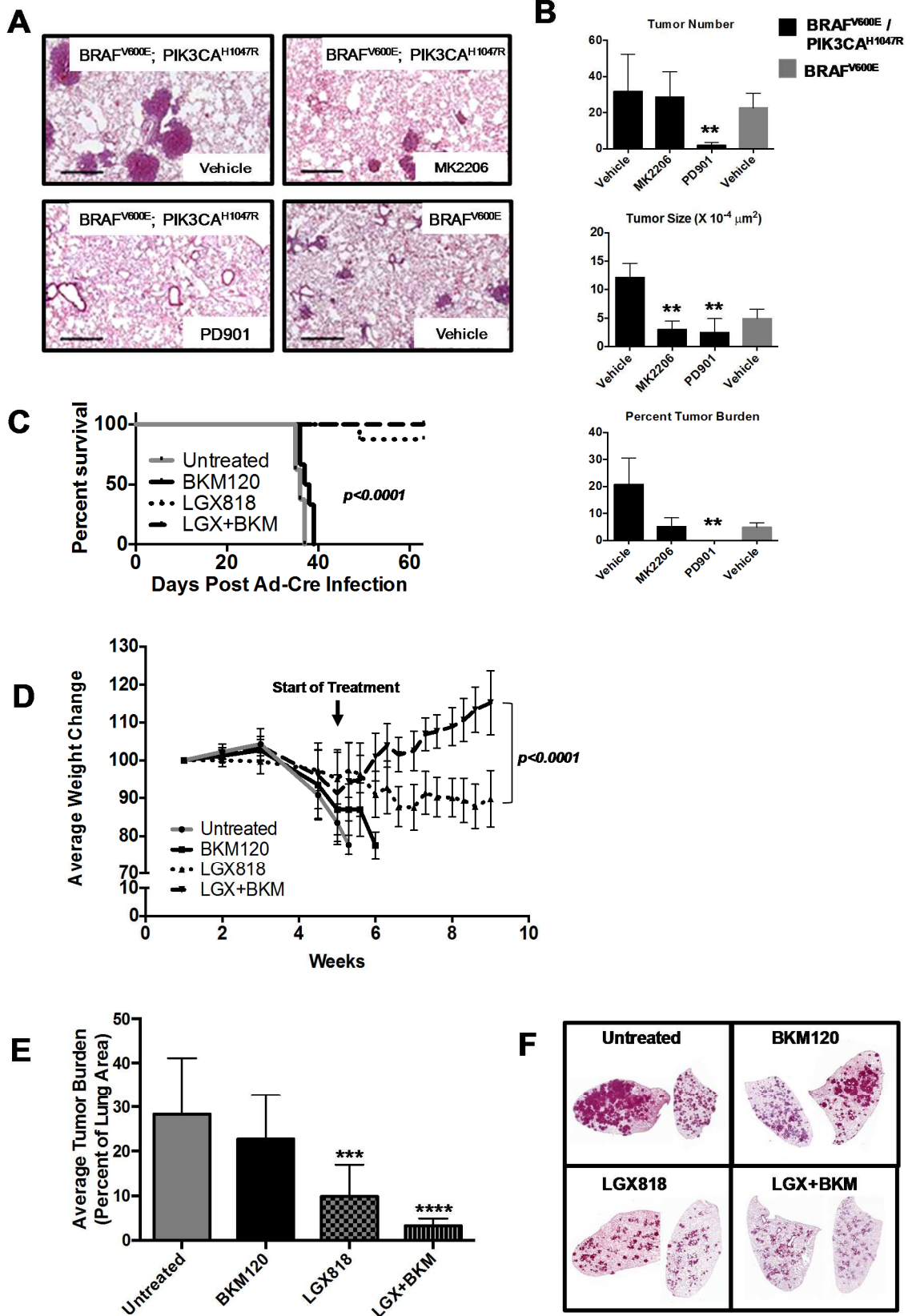


Figure 1-5

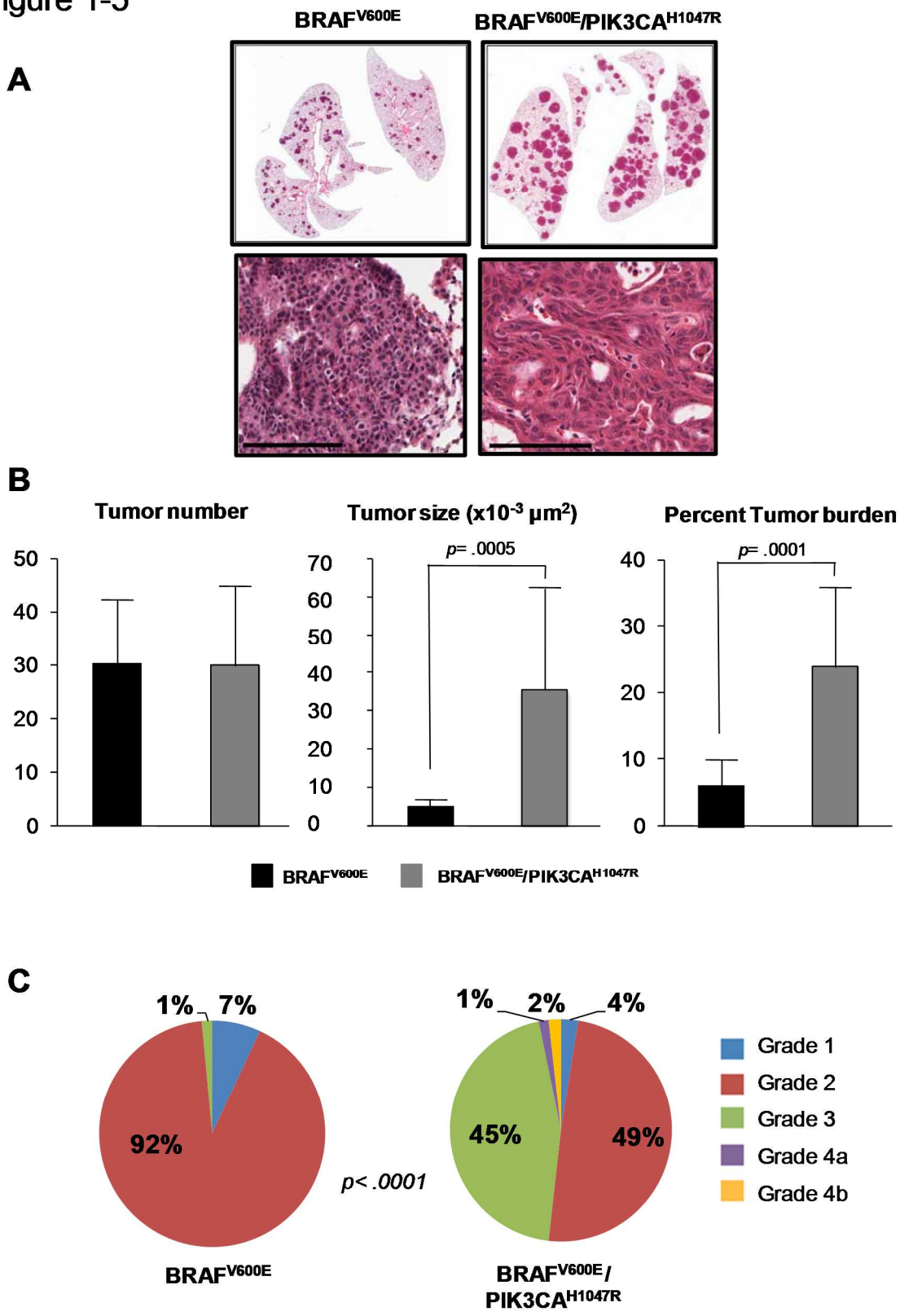


Figure 1-6

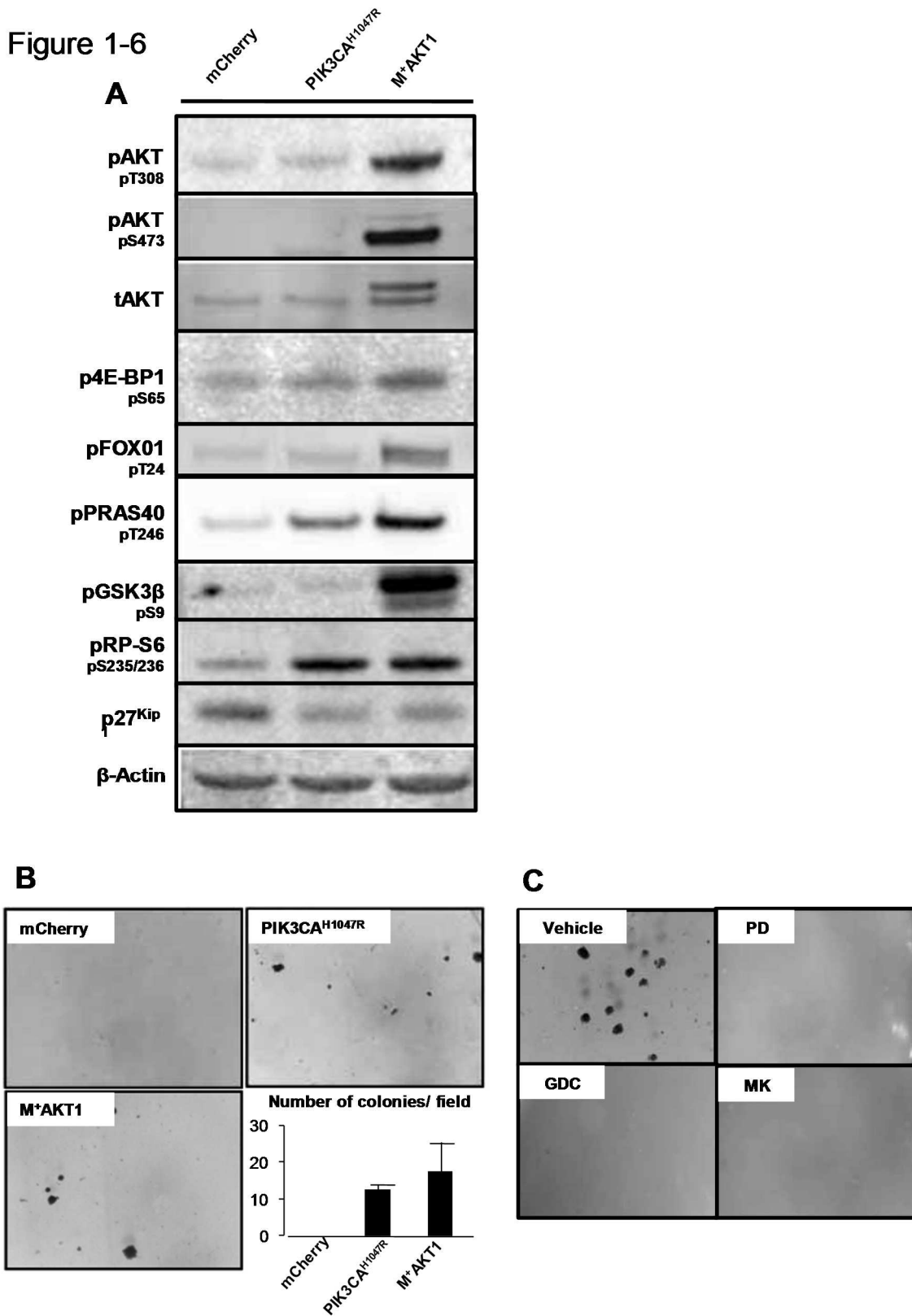
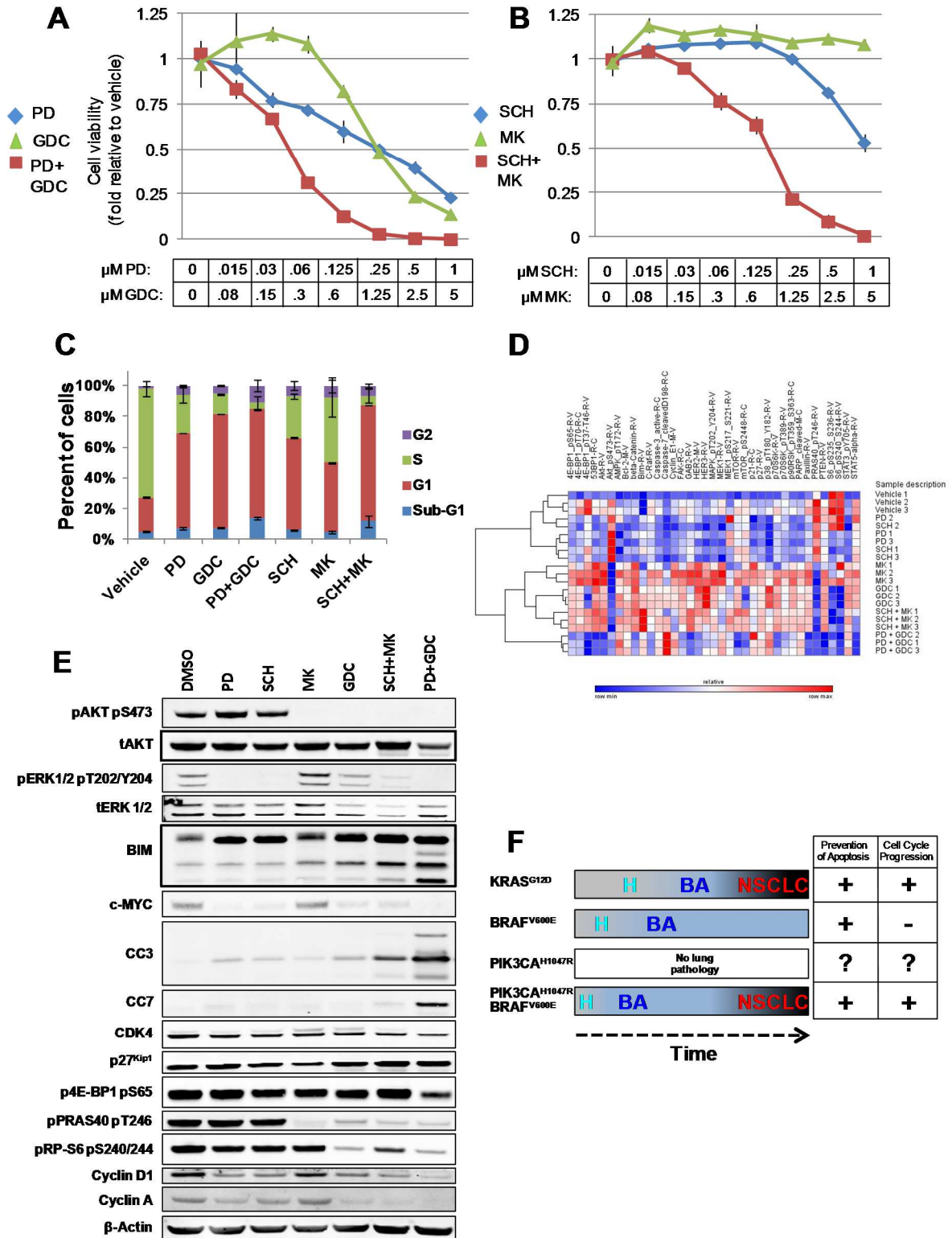
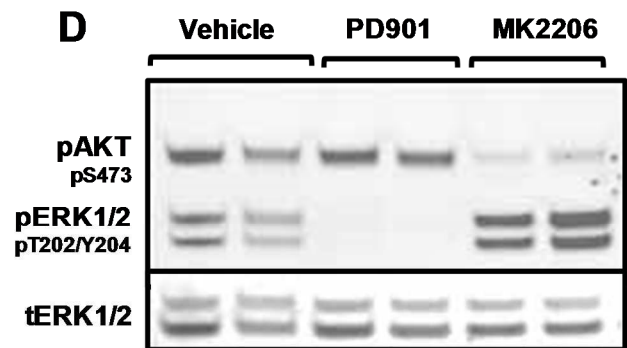
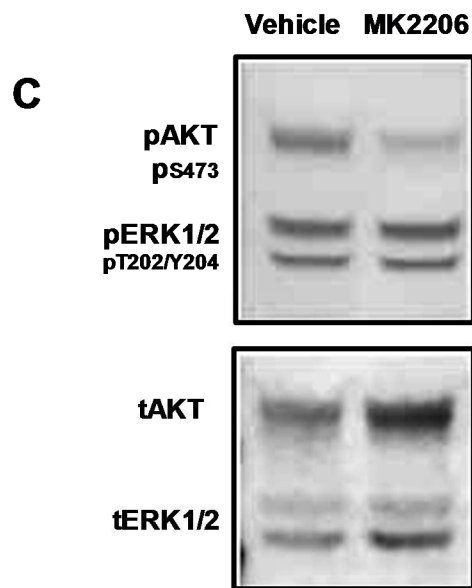
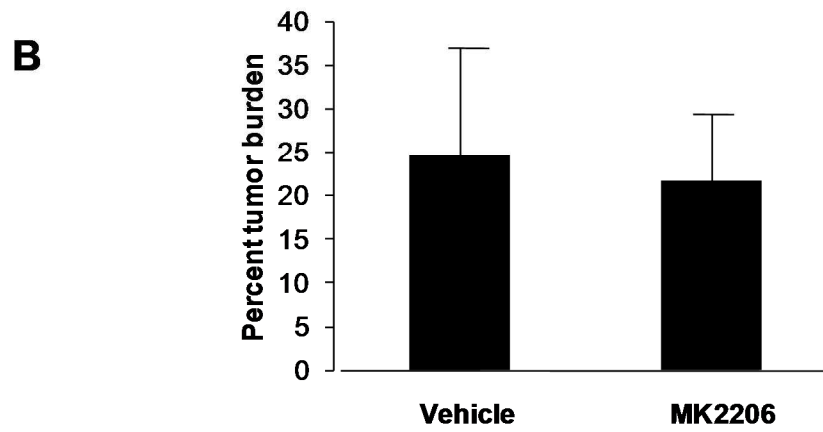
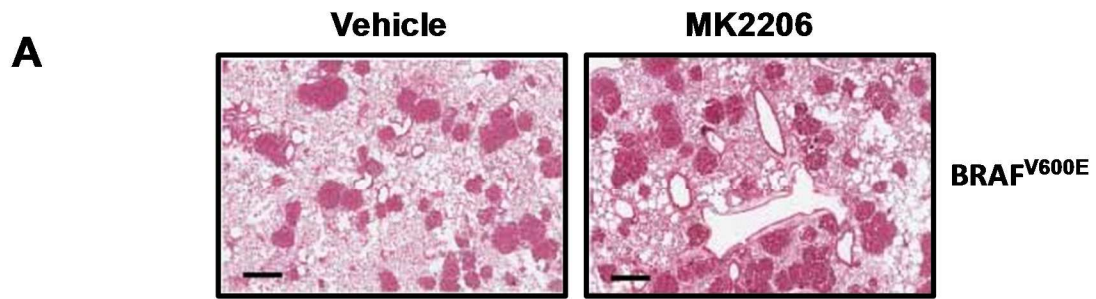


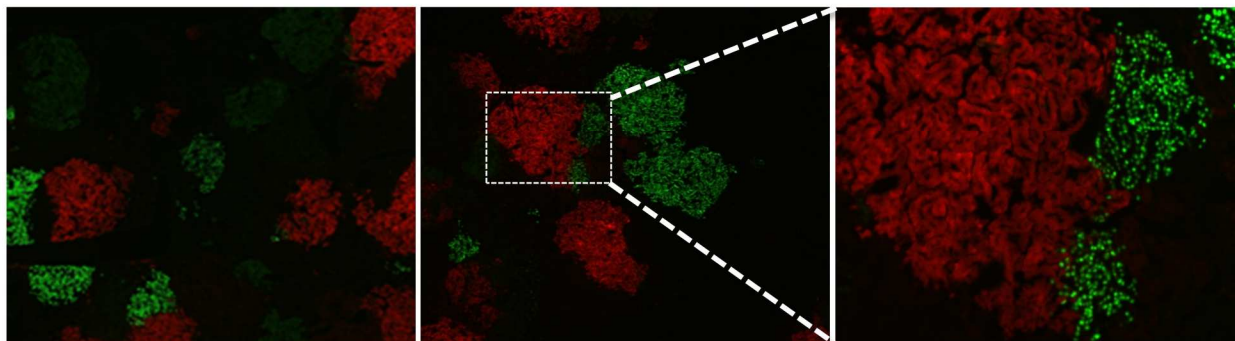
Figure 1-7



Supplementary Figure 1-S1

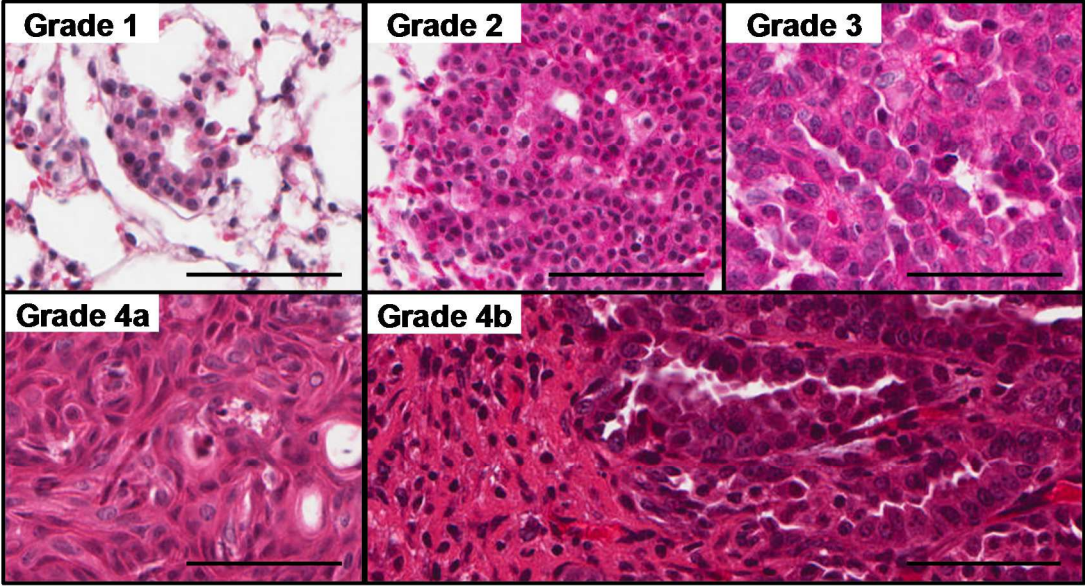


Supplementary Figure 1-S2

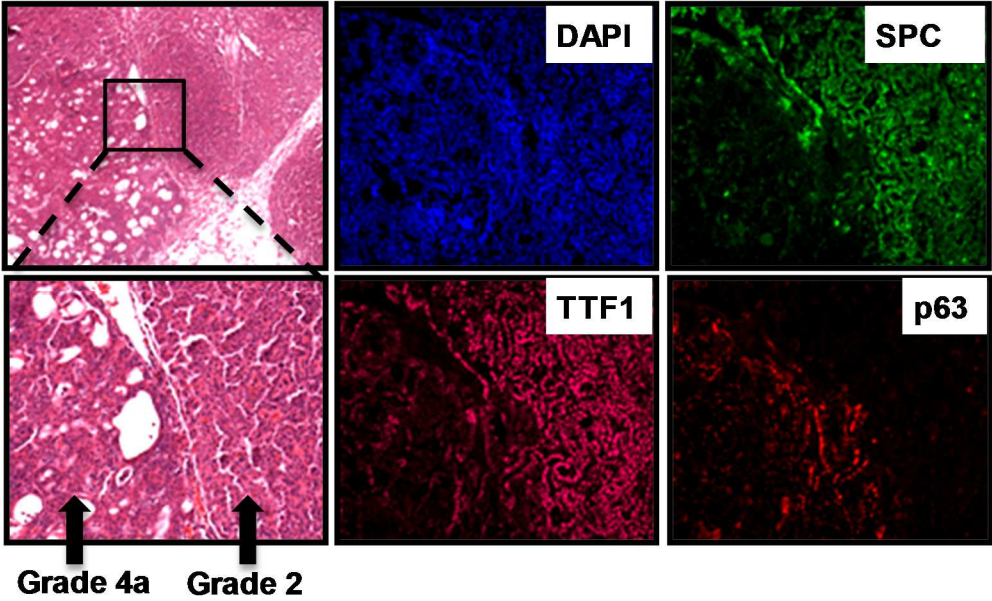


Supplementary Figure 1-S3

A

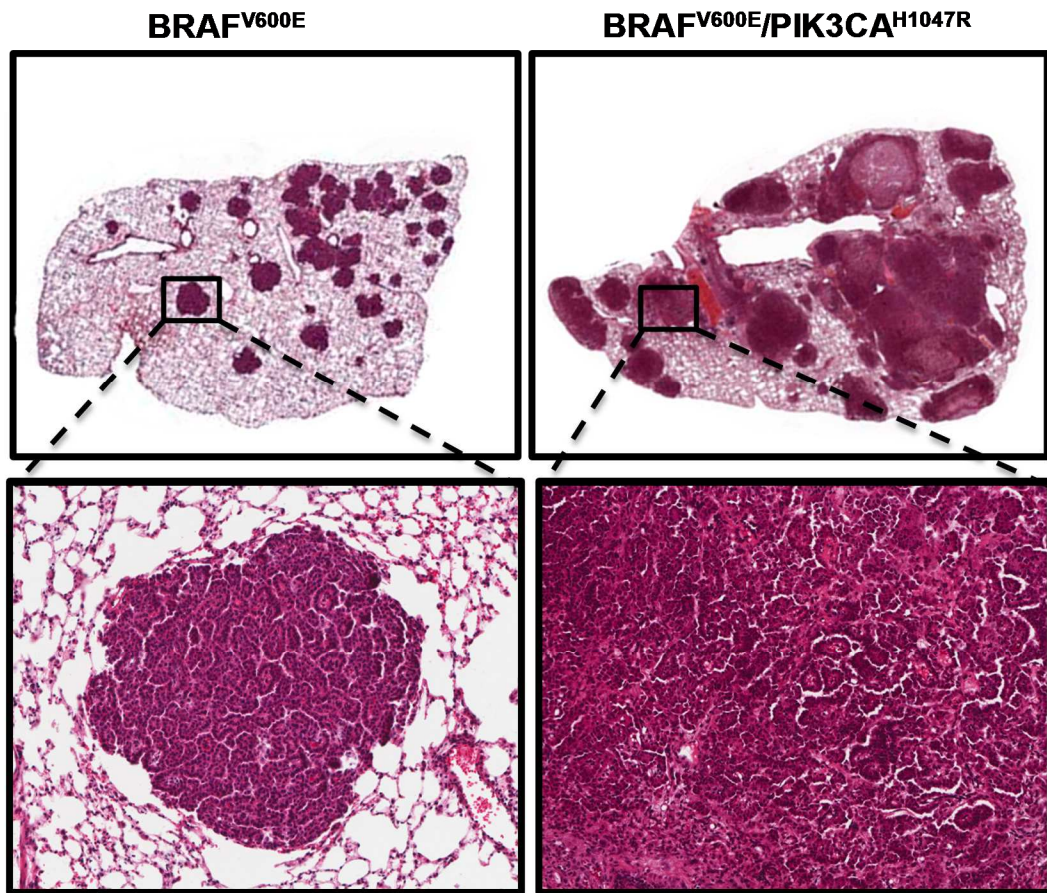


B

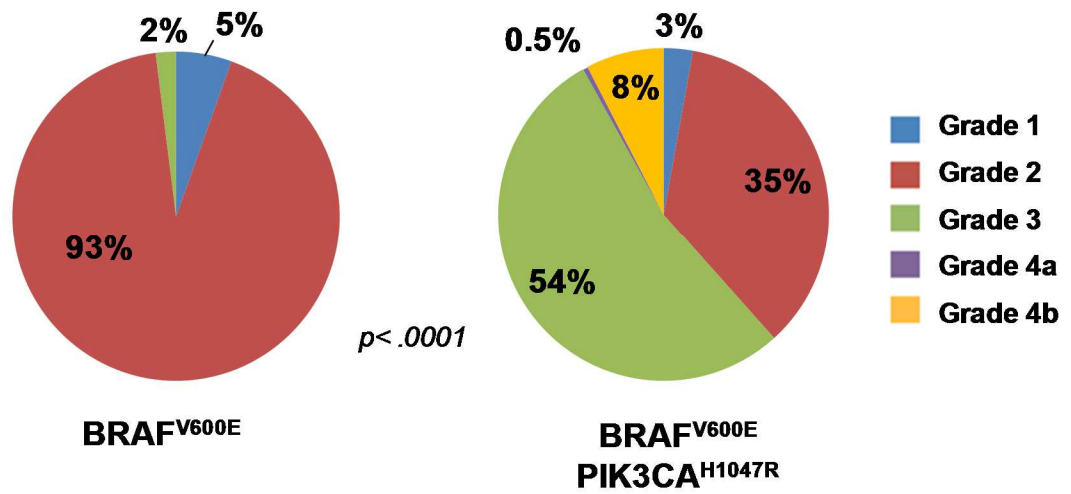


Supplementary Figure 1-S4

A

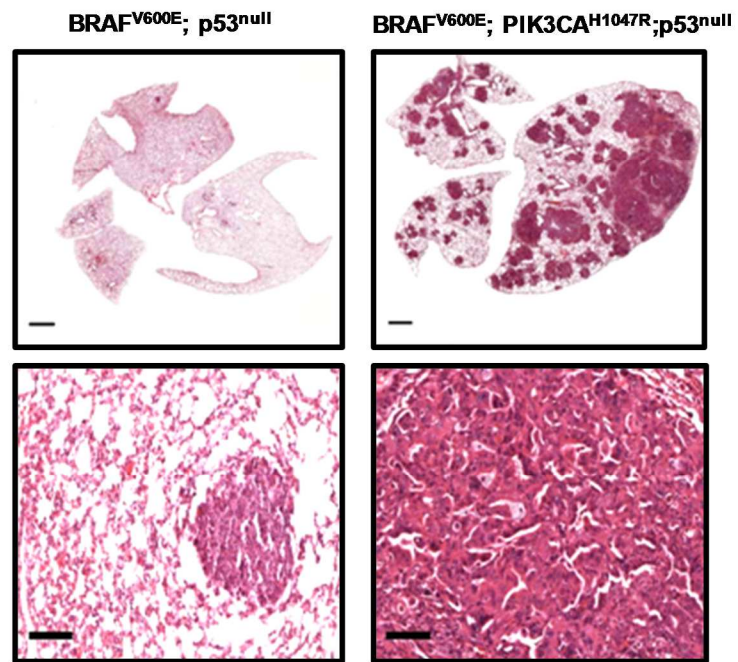


B

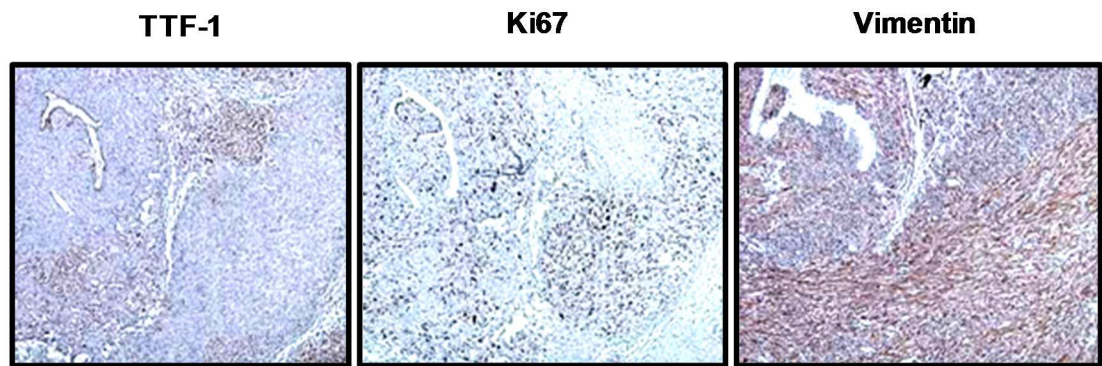


Supplementary Figure 1-S5

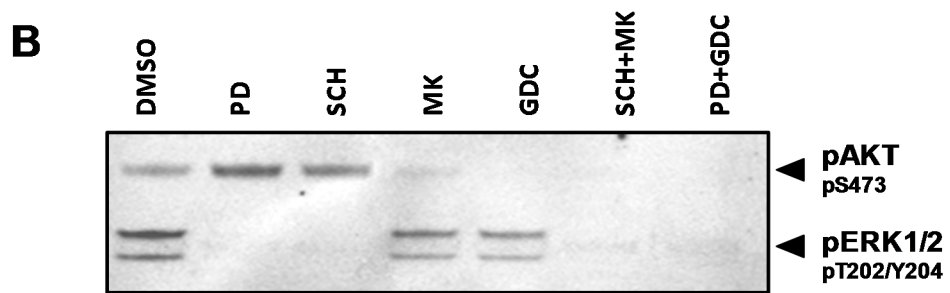
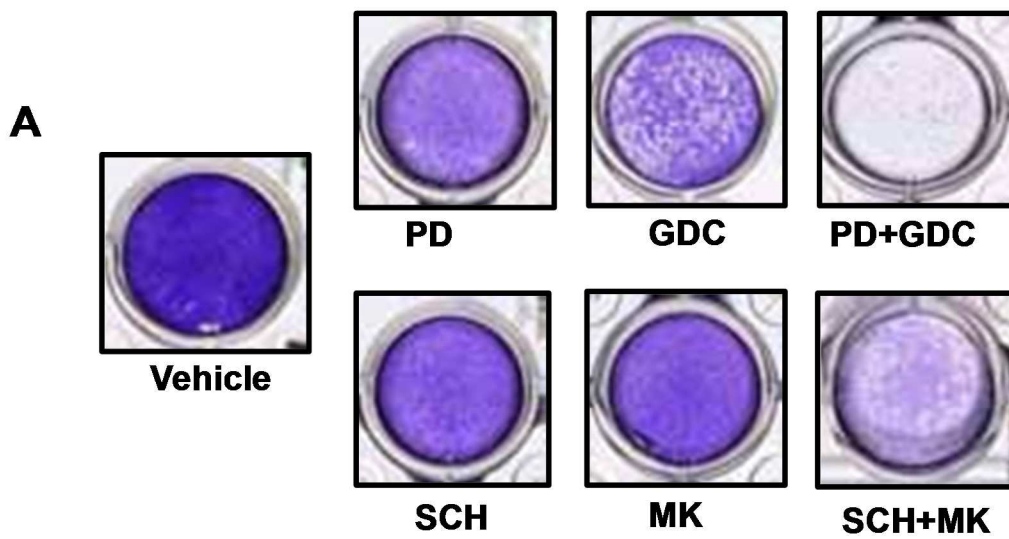
A



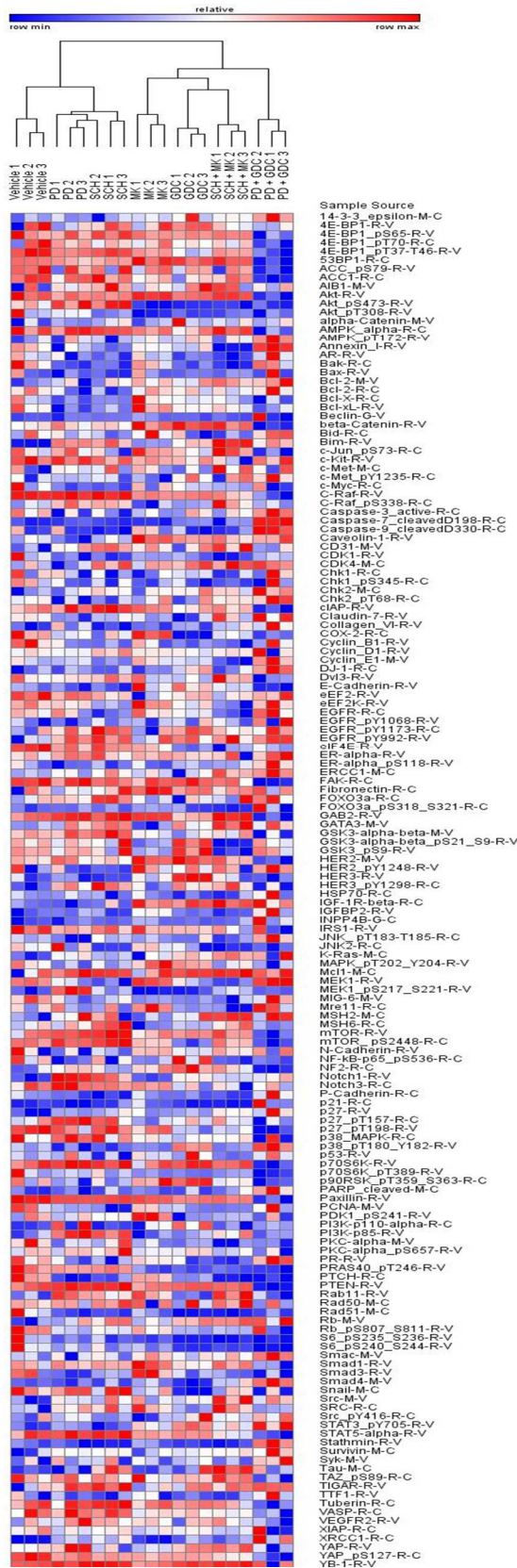
B



Supplementary Figure 1-S6

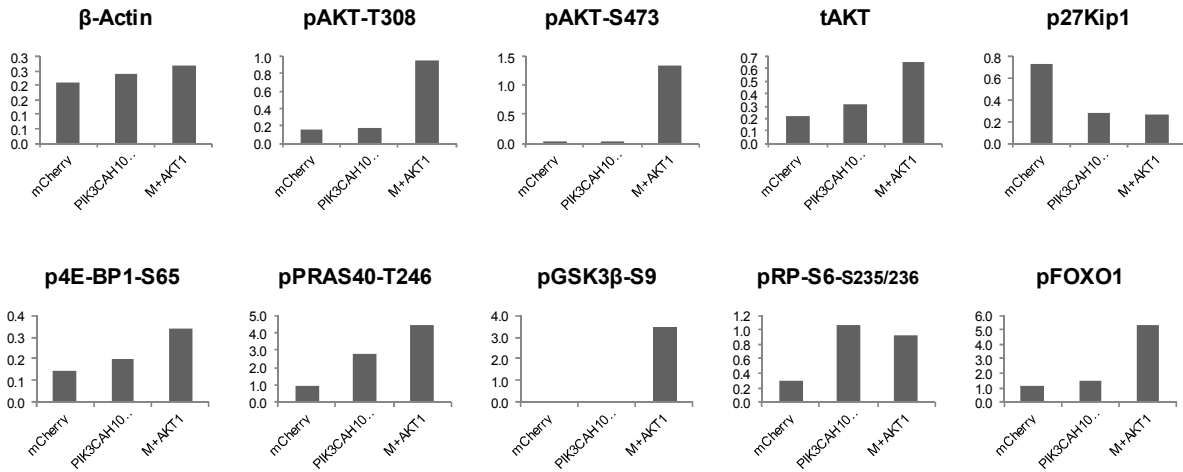


Supplementary Figure 1-S7

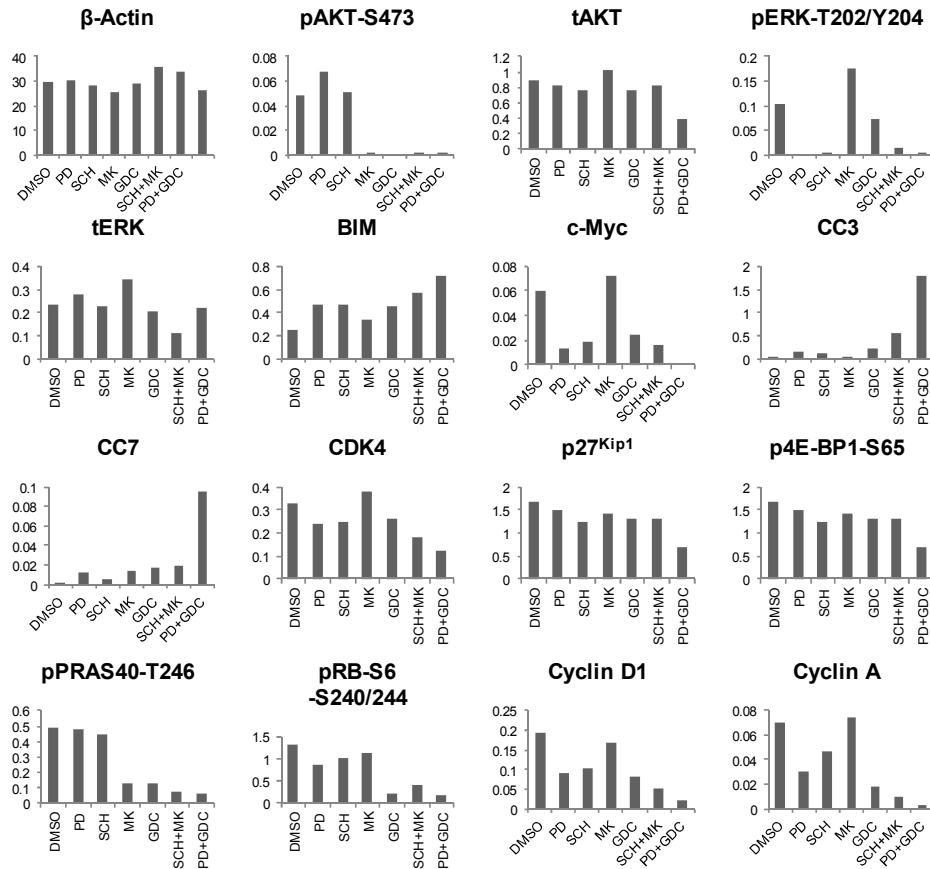


Supplementary Figure 1-S8

A



B



Supplementary Table 1-S1. Inhibitor identities, molecule targeted, and concentrations used for in vitro cell studies.

Inhibitor ID	Shorthand Name	Target	Concentration
PD325901	PD	MEK	1 μ M
SCH772984	SCH	ERK	1 μ M
MK2206	MK	AKT	5 μ M
GDC0941	GDC	PI3'K	5 μ M

Supplementary Table 1-S2. Percentages of BRAF^{V600E}/PIK3CA^{H1047R}/TP53^{null} cells found to be in different stages of the cell division cycle following pathway-targeted pharmacological inhibition of cell signaling.

FACS-based Cell Cycle Analysis Results

Percent of gated (live) cells, average of 2 runs				
	Sub-G1	G1	S	G2
Vehicle	4.9	21.5	68.6	1.55
PD	6.7	58.75	23.85	5.3
GDC	7	70.45	12.35	5
PD+GDC	11.6	60.15	4.03	9.05
SCH	5.5	56.2	25.25	6.11
MK	4.3	41.175	39	6.6
SCH+MK	10.3	66.45	5.53	5.7

CHAPTER 2:

PI3'-kinase signaling is limiting for KRAS^{G12D}-driven lung tumorigenesis in mice

INTRODUCTION

Mutationally activated *KRas* is detected in ~30% of non-small cell lung cancers (NSCLC) [2]. Because of the difficulties in direct pharmacological targeting of KRAS oncoproteins, efforts have turned to defining and targeting RAS-regulated effector pathways required for cancer cell maintenance. Prominent amongst these are RAF protein kinases and PI3'-lipid kinase- α (PIK3CA), which have been credentialed both as key effectors of activated KRAS and as *bona fide* human oncogenes [18, 19, 43, 74]. GEM models of NSCLC based on the conditional expression of mutationally-activated KRAS^{G12D}, BRAF^{V600E} or PIK3CA^{H1047R} have been important tools in this endeavor [11-13]. Using such models, we previously demonstrated the ability of PIK3CA^{H1047R} to cooperate with BRAF^{V600E} in lung carcinogenesis in a manner similar to that initiated by KRAS^{G12D} [75]. However, it remains unclear whether RAF and PI3'-lipid signaling are coordinately activated in lung epithelial cells when KRAS^{G12D} is expressed at normal physiological levels.

Although KRAS is a potent oncogenic driver of NSCLC, healthy human lungs are reported to possess KRAS-mutated cells [23] and in mouse models only a small fraction of cells expressing oncogenic KRAS display tumorigenic potential [22]. Furthermore, KRAS^{G12D}-induced lung tumors in mice develop after an extended and variable latency period and only 10-20% of benign lung tumors progress to adenocarcinoma. These observations suggest that additional factors are required to promote the proliferation and malignant progression of KRAS^{G12D}-initiated lung tumors. Indeed, there are reports that elevated expression of RAS oncoproteins is required for their oncogenic effects [24-26], and that signals from the microenvironment are required to activate mutated KRAS

through upstream receptors [27]. In addition, various factors have been found to influence progression of KRAS^{G12D} expressing lung tumors, including alterations in TP53, CDKN2A, APC, LKB1 or PTEN tumor suppressors and WNT→ β -catenin signaling [28-33]. Interestingly, despite PIK3CA being a direct effector of KRAS, it is reported that additional activation of PIK3CA through IGF1R is required for KRAS-driven lung tumorigenesis [34]. The latter suggests that mutated KRAS does not activate PIK3CA to the full extent possible and may explain the co-mutation of *KRas* and *Pik3ca* in a number of cancer types, including lung [5, 35, 36]

Based on these observations, we tested the hypothesis that PI3'-lipid signaling may be rate-limiting for the clonal expansion of initiated KRAS^{G12D}-expressing lung epithelial cells. Indeed, co-expression of PIK3CA^{H1047R} and KRAS^{G12D} in the mouse lung led to a dramatic and rapid increase in tumor burden and enhanced malignant progression. Using cell culture models, we observed that KRAS and PIK3CA oncoproteins cooperatively regulate the cell cycle machinery to promote progression through the S-phase of the cell cycle. Moreover, PIK3CA mutated lung cancer cell lines were sensitive to selective PIK3CA inhibition both *in vitro* and *in vivo*. Disappointingly, selective PIK3CA blockade had largely cytostatic effects on tumor cells, which translated into slower tumor growth but not tumor regression. These results may have implications for the successful clinical deployment of PIK3CA inhibitors against lung cancer, even those expressing mutationally activated PIK3CA.

MATERIALS AND METHODS

Animal experiments

All animal experiments were conducted in accordance with protocols approved by the UCSF Institutional Animal Care and Use Committee (IACUC). *Kras^{LSL}*, *Pik3ca^{Lat}*, *Trp53^{lox}*, *R26^{mT-mG}* and *SPC^{CreER}* mice were previously described [11, 13, 14, 28, 76]. Stocks of Adenovirus encoding Cre recombinase (Ad-CMV-Cre) were purchased from Viraquest (North Liberty, IA) and instilled into the nasal passage of mice as previously described [47]. Tumor bearing mice were euthanized for analysis either at a pre-determined time point or when their body conditioning score (BCS) was ≤ 2 [48]. BrdU labeling was achieved by intraperitoneal (IP) injection of 1mg BrdU dissolved in PBS (BD) per mouse at 24 hours or 4 hours prior to euthanasia. Tamoxifen (sigma) was dissolved in peanut oil at 10mg/ml and administered by IP injection at 1mg/mouse daily for 5 consecutive days. Orthotopic lung cancer models were generated by tail vein injections of 10^4 to 10^6 cells in DMEM. In vivo bioluminescence was measured using a Xenogen IVIS Spectrum imaging system 15 minutes after injection of 150 mg/kg D-luciferin (GoldBio). BYL719 (Novartis) was formulated in 0.5% Methylcellulose (Sigma) and mice were dosed by oral gavage (p.o.) at 50 mg/kg either once (q.d.) or twice (b.i.d.) per day. Kaplan-Meier survival curves were plotted using Prism and statistical significance determined using the Log-rank (Mantel-Cox) test and the Gehan-Breslow-Wilcoxon test.

Histology and quantification of lung tumor burden

Lungs were removed and fixed in zinc buffered formalin prior to paraffin-embedding. 6 μ m sections were cut and slides were stained with Hematoxylin and Eosin (H&E) and then scanned with an Aperio ScanScope. Quantification was performed using Aperio Spectrum ImageScope viewing software. Tumor burden was calculated as the percent

area of a lung section occupied by tumors. Tumor number per lung cross section and tumor size (μm^2) were calculated using ImageScope software. Grading of lung tumors was performed based on a previously published classification scheme [64, 75]

Immunostaining of mouse lung tissue and immunoblotting of cell extracts

6 μm paraffin-embedded lung tissue sections were deparaffinized prior to antigen retrieval with 10mM sodium citrate (pH 6) and blocking with 5%(v/v) goat serum. The following antibodies were used for detection: anti-phospho-AKT (pS473) and anti-phospho-ERK1/2 (pT202/pY204) (Cell signaling technology), anti-BrdU (Roche) and anti-GFP (Santa Cruz).

50 μg aliquots of cell or lung/tumor lysates were probed with antisera against phospho-AKT (pS473), phospho-ERK1/2 (pT202/pY204), total ERK1/2, total AKT, Cyclin D1, Cleaved Caspase 3, survivin, phospho-4E-BP1 (pS65), phospho-RP-S6 (pS240/244), phospho-PRAS40 (pT246), phospho-p70S6K (T389), p27^{KIP1}, phospho-RB (S780 or S807/811), phospho-CDK2 (T160), PUMA (rodent or human specific), BCL-X_L and BCL-2 (Cell Signaling technology), BIM, c-MYC (Epitomics), Cyclin A, CDK4 and MCL1 (Santa Cruz) and α -actin (Sigma). Immunoblots were visualized using the Odyssey FC system (Li-Cor) and Odyssey application software v3.0.30.

Lung tumor cell isolation, culture and analysis

Individual lung lobes from tumor bearing mice were minced and incubated with 2mg/ml dispase/collagenase (Roche). Cell suspensions were then filtered and plated directly into culture in Hams-F12/Glutamax media supplemented with 10%(v/v) fetal bovine serum. Following the outgrowth of a mixed population of lung cancer-derived cells, a series of single cell-derived clones were isolated by limiting dilution and then

expanded. Recombination of the *Kras*^{L^{SL}} and *Pik3ca*^{L^{at}} alleles was verified by PCR [11, 13]. H460 cells were cultured in RPMI 460 media supplemented with 10%(v/v) fetal bovine serum. Cells were engineered to express luciferase using the lentiviral vector pLV430G-oFL-T2A-eGFP which expresses EGFP and Luciferase [77]. Lentivirus infected cells were sorted based on EGFP expression using a FACS Aria III (BD).

Cell proliferation was assessed in triplicate by plating 2000 cells/well in 96-well plates. Cells were treated with a range of concentrations of the following inhibitors: DMSO control, MEK1/2 inhibitor (PD0325901), class 1 PI3'-kinase inhibitor (GDC-0941), selective PIK3CA inhibitor (BYL719), AKT1-3 inhibitor (MK2206) or combinations as indicated. 72 hours after drug addition, a Cell Titer Glo viability assay was performed with luminescence detected using a Glo-Max microplate reader (Promega). S phase transit was assessed by incubating control versus drug treated cells (24 hours) with 10µM BrdU (BD) for the final 3 hours of drug treatment. Adherent cells were collected, fixed and stained with anti-BrdU-FITC (BD) and propidium iodide (Sigma). Quantification was performed by flow cytometry using a FACS-Calibur (BD).

3D culturing experiments were performed by plating 10 or 100 cells/well in 96-well Ultra Low Attachment plates (Sigma) and culturing them for 4 weeks, after which spheres were imaged and counted using a bright-field microscope. Spheres were then transferred to 24-well plates and cultured for an additional week, then stained with Crystal Violet.

Ex-vivo lung culturing and tumorigenesis system

A previously described *ex vivo* lung culture system [78] was modified to increase the ease of imaging. Lungs of mice in which tumors had been initiated were inflated with

2%(w/v) low melting temperature agarose (Sigma) at 42°C, then rapidly extracted from the mouse and chilled in cold tissue culture media. The agarose was allowed to solidify for 20 minutes at which time 150µm-thick sections were generated using a vibratome. Lung slices were cultured in DMEM F12 Glutamax supplemented with 1%(v/v) PenStrep, 1%(v/v) Fungizone, 0.1 µg/ml insulin and 0.1µg/ml hydrocortisone. Sections were cultured in glass-bottom 6-well plates (MatTek) and imaged using a high-speed wide-field inverted fluorescence microscope (Nikon)

RESULTS

PIK3CA^{H1047R} dramatically accelerates lung tumorigenesis initiated by KRAS^{G12D} in a GEM model

Despite the demonstrated ability of oncogenic KRAS^{G12D} to activate PI3Kα by direct biochemical means [20], phospho(p)-AKT was not readily detectable in early-stage KRAS^{G12D}-initiated lung epithelial cells in which pERK was readily detected (Supp. Fig. 2-S1A). However, once initiated epithelial cells commenced tumorigenic growth, pAKT was more readily detected, indicating a correlation between PI3'-lipid signaling and proliferative expansion of tumors (Supp. Fig. 2-S1A).

To test the effects of elevated PI3'-lipid signaling on KRAS^{G12D}-initiated lung tumorigenesis, we generated compound *KRas^{LSL}*, *Pik3ca^{Lat-H1047R}* (*Pik3ca^{Lat}*) heterozygous mice (*KPi* mice) and appropriate controls heterozygous for either allele alone [11, 13]. As reported previously, Ad-Cre mediated expression of PIK3CA^{H1047R} in the lungs of *Pik3ca^{Lat}* mice failed to elicit any overt lung pathology even up to one year post-initiation (p.i.) [75]. As extensively reported by others, similarly initiated expression

of KRAS^{G12D} led to the onset of lung tumorigenesis that required euthanasia by ~6 months p.i. [11]. Remarkably, *KPi* compound heterozygous mice rapidly developed end-stage disease that required euthanasia by 5-7 weeks p.i. (Fig. 2-1A).

Histopathological analysis of the lungs of *KPi* mice demonstrated a dramatic increase in tumor number and overall burden compared to similarly initiated *KRas^{LSL}* mice. Quantification of tumor number, size and overall burden at one week intervals indicated that, even at 2 weeks p.i., a time when *KRas^{LSL}* mice display no overt lung pathology, *KPi* mice had fully formed lung tumors (Fig. 2-1B & C). Furthermore, pAKT and pERK were both readily detected at high levels in early-stage initiated lesions from *KPi* mice (Supp. Fig. 2-1B). Tumor number increased steadily in *KPi* mice between 1 and 3 weeks p.i., after which it remained constant, indicating that the proliferative expansion of lung tumors is more synchronous than in *KRas^{LSL}* mice. Tumor size and overall burden increased continuously between 1-5 weeks p.i. in *KPi* mice, the majority of which displayed end-stage confluent lung tumorigenesis at that point (Fig. 2-1B & C). By contrast, only atypical alveolar hyperplasias (AAH) and rare small tumors were detected in *KRas^{LSL}* mice at 5 weeks p.i. (Fig. 2-1B & C). The rapid and synchronous growth of tumors observed in *KPi* mice emphasizes the striking ability of PIK3CA^{H1047R} to promote the early-stage proliferative expansion of KRAS^{G12D}-initiated lung tumors.

To more accurately assess events in the earliest stages of tumor development we utilized a *Rosa26^{mT-mG}* knock-in allele (*R26^{mT-mG}*) that expresses tdTomato in all cells prior to Cre-mediated recombination after which cells express EGFP [76]. Imaging of Cre-mediated recombination in the lung was combined with assessment of cells transiting through S phase by administering BrdU to initiated mice 24 hours prior to

euthanasia. Small clusters of EGFP⁺/BrdU⁺ double positive cells were detectable in lung sections from *KRas*^{LSL}; *Pik3ca*^{Lat}; *R26*^{mT-mG} (*KPiR*) mice as soon as one week p.i. (Fig. 2-1D & E). By contrast, few clusters but many single EGFP⁺/BrdU⁻ cells were detected in the lungs of initiated *Kras*^{LSL}; *R26*^{mT-mG} (*KR*) mice. At 1 or 2 weeks p.i., the percentage of EGFP⁺ cells that were also BrdU⁺ was <10% in lung sections from *KR* mice, while it was 25%-30% in identically treated *KPiR* mice (Fig. 2-1E). This analysis suggests that PI3'-lipid signaling enhances the entry/transit of KRAS^{G12D}-initiated lung tumors cells through the S phase of the cell cycle.

To monitor growth of early-stage lung lesions in *KR* versus *KPiR* mice in real time, we adapted a lung slice culture system [78] in which tumor growth can be assessed *ex vivo*. The lungs of Ad-Cre initiated *KR* or *KPiR* mice were inflated with agarose and sectioned using a vibratome into 150µm slices. Lung slices were cultured and imaged with a fluorescence microscope over a period of 3 weeks. These experiments confirmed that KRAS^{G12D}/PIK3CA^{H1047R} expressing lung tumors expanded more rapidly compared to similarly initiated KRAS^{G12D} expressing lung tumors consistent with our *in vivo* observations (Supp. Fig. 2-S2).

PIK3CA^{H1047R} promotes malignant progression and growth of established KRAS^{G12D}-initiated lung tumors

Given the dramatic effects of PIK3CA^{H1047R} on early-stage lung tumor growth, we assessed its effects on malignant progression of KRAS^{G12D}-initiated lung tumors. Initial experiments indicated that five weeks p.i., lung tumors in *KPi* mice remained histologically benign. Hence, although the mice were at end-stage and their lung

tumors rapidly proliferating, they have not acquired characteristics of lung cancer. To test if PIK3CA^{H1047R} potentiates malignant progression of KRAS^{G12D}-initiated lung tumors, *KRas^{LSL}* and *KPi* mice were initiated with 5x10⁶ or 5x10⁵ pfu of Ad-Cre respectively. In this experiment *KPi* mice survived 4-5 months p.i. and were compared to *KRas^{LSL}* mice analyzed at 6 months p.i. Lung tumors were graded on a scale from benign to malignant according to a previously published classification scheme [64, 75].

At 6 months p.i., we noted that lung tumor number and overall burden in the *KRas^{LSL}* mice was highly variable from mouse-to-mouse and lobe-to-lobe, emphasizing the stochastic nature of this model (Fig. 2-2A & B). Consistent with previous reports, ~20% of KRAS^{G12D}-initiated tumors displayed malignant characteristics (Fig. 2-2C). By contrast, *KPi* mice initiated with 10-fold less Ad-Cre had a substantially larger number of tumors distributed evenly throughout their lungs, a significantly higher tumor burden (~40% vs. ~20%, $p=0.0063$) and a larger fraction of tumors (>50%) that were malignant (Figs. 2-2A-C). KRAS^{G12D}/PIK3CA^{H1047R} co-expressing lung cancers also displayed histopathological characteristics of malignancy not observed in the KRAS^{G12D}-driven lung cancers. These included signet ring morphology, elevated levels of immune cell infiltration and areas of necrosis often indicative of fast-growing, aggressive cancers (Fig. 2-2D). However both KRAS^{G12D}/PIK3CA^{H1047R} and KRAS^{G12D}-driven tumors expressed NKX2.1 and surfactant protein C (SP-C), markers of alveolar type 2 (AT2) pneumocytes. In addition, these lesions were generally negative for expression of TP63 (a basal cell marker) and Club cell antigen (CCA/CC10), as previously demonstrated by others (data not shown) [16, 79].

Our data thus far suggested that increased PI3'-lipid signaling provides KRAS^{G12D}-initiated lung cells with a strong proliferative advantage and promotes development of malignant characteristics. To test if expression of PIK3CA^{H1047R} could also accelerate the proliferation/progression of established KRAS^{G12D}-driven lung tumors, we employed mice carrying a Flp-regulated allele of *KRas* (*Kras*^{FSF-G12D}), which allows for temporal dissociation of oncoprotein expression [80]. Compound heterozygous *KRas*^{FSF}; *SPC*^{CreER}; *Pik3ca*^{Lat}; *R26*^{mT-mG} (*KSPiR*) and *KRas*^{FSF}; *SPC*^{CreER}; *R26*^{mT-mG} (*KSR*) mice were bred. Since benign KRAS^{G12D}-driven lung tumors express SPC uniformly, temporal dissociation of PIK3CA^{H1047R} expression in established KRAS^{G12D} tumors can be achieved by intraperitoneal administration of tamoxifen (TAM) at any time p.i. The *R26*^{mT-mG} allele allows assessment of the efficiency of CreER mediated recombination. KRAS^{G12D}-driven lung tumors were initiated in *KSPiR* and in *KSR* mice using Ad-Flp (2x10⁷ pfu) and 14 weeks p.i., a time when such tumors are benign and display signs of a senescence-like proliferative arrest, mice were treated with control solvent or TAM (daily injections of 2mg/mouse for 5 days) and aged for a further 10 weeks at which time they were euthanized for analysis.

Both PCR and immunohistochemical analysis of EGFP expression confirmed the TAM-dependent, CreER-mediated recombination of the *R26*^{mT-mG} allele and the *Pik3ca*^{Lat} allele within KRAS^{G12D}-driven lung tumors (data not shown). Notably, lung tumor number and overall tumor burden were significantly increased in TAM treated *KSPiR* mice compared to control *KSR* mice or *KSPiR* mice that received solvent (~150 tumors/lung section vs. ~50, *p*=0.0068 and ~18% tumor burden vs. ~5%, *p*=0.0025) (Fig. 2-2E). These data indicate that induced expression of PIK3CA^{H1047R} in established

KRAS^{G12D}-driven tumors can promote their proliferative expansion (Fig. 2-2E). The larger number of tumors observed in TAM treated mice also suggest that expression of PIK3CA^{H1047R} might induce proliferation in dormant KRAS^{G12D}-expressing cells that have not yet formed tumors.

To complement this experiment, some *KSPiR* mice were first treated with TAM to initiate expression of PIK3CA^{H1047R} in AT2 cells prior to activation of KRAS^{G12D} expression with Ad-Flp. Consistent with the experiment described above, TAM treated *KSPiR* mice analyzed at 14 weeks p.i. displayed significantly higher tumor numbers and overall tumor burden compared to controls (Supp. Fig. 2-3A). Immunofluorescence analysis of lung sections confirmed that the increased tumor burden in TAM treated mice is largely comprised of EGFP⁺ cells, a marker of Cre-mediated recombination (Supp. Fig. 2-3B). These observations suggest that the order in which KRAS^{G12D} and PIK3CA^{H1047R} are expressed does not substantially influence the tumorigenic process in these GEM models. Furthermore, these data are consistent with the hypothesis that the AT2 cell is the cell of origin for KRAS^{G12D}-initiated tumors [15].

Selective PIK3CA blockade inhibits KRAS^{G12D}/PIK3CA^{H1047R} lung tumor growth

Previous studies have indicated that KRAS^{G12D}-initiated lung epithelial cells are dependent upon signaling through PIK3CA for tumorigenesis [20, 43]. Hence, we examined the consequences of pharmacological blockade of PIK3CA on the growth and maintenance of KRAS^{G12D}/PIK3CA^{H1047R} mutant lung tumors, reasoning that these tumors might display enhanced sensitivity to PI3K α blockade. KRAS^{G12D}/PIK3CA^{H1047R} lung tumors were initiated in *KPi* mice and at either 2 days or 4 weeks p.i. mice were

randomized for treatment with vehicle or the selective PIK3CA inhibitor BYL719 (50mg/kg, p.o., b.i.d.) [81] to test if blockade of PIK3CA^{H1047R} would prevent tumor formation, or promote regression of established tumors, respectively. This dosing schedule was selected based on a pharmacodynamic study in which a single 50mg/kg dose of BYL719 suppressed pAKT levels in lung tumors for at least 8 hours (Supp. Fig. 2-4A). We did not test BYL719 against KRAS^{G12D}-driven lung tumors since this has previously been described [20].

Four weeks of BYL719 treatment of *KPi* mice starting 2 days p.i. significantly inhibited tumor growth compared to vehicle treated mice (tumor burden ~3% vs. ~15%, $p < 0.0016$) (Fig. 2-3A). Indeed, tumor burden in BYL719-treated mice was similar to that detected in control *KRas^{LSL}* mice initiated at the same time (Fig. 2-3A). Thus BYL719 sufficiently inhibits PIK3CA^{H1047R} signaling to reverse its cooperation with KRAS^{G12D} for lung tumorigenesis. In the therapy setting, we similarly observed that BYL719-treated *KPi* mice displayed significantly reduced tumor burden compared to vehicle treated mice (~9% vs. ~40%, $p = 0.0003$). Indeed, the overall tumor burden of BYL719 treated mice was modestly, but significantly, lower than that observed in mice analyzed prior to the start of treatment (~9% vs. ~15%, $p = 0.0338$) (Fig. 2-3B). Immunoblot analysis of pS473-AKT in lung lysates from control versus BYL719 treated mice confirmed inhibition of PI3'-lipid signaling, although residual pAKT remained (Fig. 2-3C). Immunohistochemical analysis of lung sections revealed that BYL719 reduced the level of BrdU incorporation and also the level of both pAKT and pERK in KRAS^{G12D}/PIK3CA^{H1047R}-driven lung tumors (Fig. 2-3D). As expected, these data indicate that PIK3CA^{H1047R} signaling promotes the proliferative expansion of KRAS^{G12D}-

initiated lung tumors and is required for continued proliferation of established tumors. However, the lack of substantial BYL719-induced regression of KRAS^{G12D}/PIK3CA^{H1047R}-driven lung tumors suggests that blockade of this pathway fails to elicit substantial death of tumor cells.

PIK3CA inhibition has modest growth-inhibitory effects in orthotopically engrafted KRAS^{G12D}/TP53^{Null} and KRAS^{G12D}/PIK3CA^{H1047R}/TP53^{Null} lung cancers

KRAS^{G12D}/PIK3CA^{H1047R} tumors at four weeks p.i. are almost uniformly benign, as are the majority KRAS^{G12D} tumors even at end-stage disease. We therefore wanted to test the effects of PI3K α inhibition against *bona fide* lung cancers, which would more accurately represent the aggressive nature of the human disease. To do so, we initiated lung cancers in *KRas^{LSL}; Trp53^{lox/lox}* and *KRas^{LSL}; Pik3ca^{Lat}, Trp53^{lox/lox}* mice. When these mice developed end-stage lung cancer, KRAS^{G12D}/TP53^{Null} (KP) and KRAS^{G12D}/PIK3CA^{H1047R}/TP53^{Null} (KPiP) lung cancer cell lines were clonally generated by standard techniques (Materials and Methods). These cells were then engineered to express luciferase (KPL and KPiPL cells) to allow bioluminescent imaging of tumor growth and response to therapy in real-time in individual mice.

When KPiPL or KPL cell lines were injected into the tail vein of immunocompromised (Hsd Athymic Nude-Foxn1) mice, both lines elicited large lung adenocarcinomas, although tumor number and growth rates varied substantially between the lines. KPiPL cells rapidly formed numerous lung tumors following injection of as few as 10⁵ cells, resulting in confluent lung cancerization that required the mice be euthanized within ~2 weeks post-injection (Supp. Fig. 2-S5A & B). By contrast, mice injected with 10⁶ KPL

cells developed end-stage disease at ~5 weeks post-injection and these mice died with smaller numbers of lung tumors compared to that observed with KPiPL cells (Supp. Fig. 2-S5A & B). Hence, consistent with our observations, expression of PIK3CA^{H1047R} correlates with more rapid lung tumor formation even in cells lacking TP53 expression.

To test the effects of selective PIK3CA blockade on KPiPL tumors, nude mice were injected with 5×10^4 KPiPL cells and lung tumor growth was assessed by bioluminescent imaging. One week post-injection, mice displayed an approximate 100-fold increase in bioluminescence from their lungs and a tumor burden encompassing ~5% of lung area. At this time the mice were divided into two groups for treatment with either vehicle (n=7) or BYL719 (n=12). Initially, BYL719 was administered twice daily, but this dosing regimen was toxic, requiring reduction to 50mg/kg once daily. Under these conditions, we noted that vehicle treated mice developed end-stage disease by ~4 weeks post injection whereas BYL719-treated mice survived ~10 additional days ($p=0.0003$) (Fig. 2-4A). BYL719-treated mice that were euthanized for comparison to vehicle-treated mice at matching time points had a significantly reduced tumor burden (~8% vs. ~35%, $p=0.0002$), though it was higher than observed at the start of treatment (~5%, $p=0.0413$) (Fig. 2-4B & C), indicating that blockade of PIK3CA^{H1047R} was largely cytostatic. Indeed, all BYL719-treated mice eventually progressed, as evidenced by increased lung bioluminescence (Fig. 2-4D & Supp. Fig. 2-S6A) and, at end-stage, their overall tumor burden was only modestly decreased compared to vehicle-treated mice (data not shown). The fact that BYL719 treated mice required euthanasia despite lower overall tumor burden suggests that the combination of drug toxicity and their lung tumor burden may be contributing to their decreased survival. Immunoblot analysis confirmed target

modulation by BYL719, however, at 50mg/kg once daily, blockade of pAKT was incomplete (Supp. Fig. 2-S6B), which may account for the modest anti-tumor efficacy of BYL719 in this model.

Next we tested the anti-tumor effects of BYL719 on KPL cells orthotopically transplanted into nude mice. In this setting, 5×10^5 KPL cells were injected into the tail vein of mice, and lung tumors allowed to develop until the bioluminescence signal was ~100 fold above background, at which point drug treatment was initiated. Similar to KPiPL-injected mice, BYL719 delayed the onset of end-stage disease, providing a significant survival benefit ($p < 0.0002$) (Fig. 2-4E). However, upon euthanasia, both vehicle-treated and drug-treated mice had similar levels of lung tumor burden (~8% vs. ~6%, n.s.) and both were higher than at the start of treatment (~3%) (Fig. 2-4F & G). Interestingly, we observed KPL cell-derived tumors in the lymph nodes, chest cavity, heart and other distant locations in the bodies of vehicle-treated mice, but not in 11/12 BYL719-treated mice (Fig. 2-4H). These tumors largely account for the high luciferase signal observed in the chest area of vehicle-treated mice (Supp. Fig. 2-S6C). We confirmed target modulation by BYL719 by immunoblotting for pS473-AKT and downstream effectors in lung lysates (Supp. Fig. 2-S6D). Thus, BYL719 treatment did not significantly influence the growth of lung tumors seeded by KPL cells, however it prevented or slowed the growth of tumors in other sites in the body to the extent that they were undetectable. The latter likely accounts for the significant increase in survival enjoyed by BYL719-treated KPL tumor-bearing mice.

PIK3CA^{H1047R} enhances the tumorigenic potential of KRAS mutated lung cancer cells in culture

To analyze the signaling networks downstream of KRAS^{G12D} and PIK3CA^{H1047R} that might explain how these oncoproteins cooperate to drive lung tumorigenesis, we employed the KP and KPiP mouse lung cancer derived cell lines. KPiP cells proliferated at significantly higher rates than KP cells (doubling time ~15 hours vs. ~30 hours, $p < 0.0001$) and proliferated in the absence of fetal calf serum (FCS) whereas KP cells became growth arrested in the absence of FCS (Fig. 2-5A). When cultured in low attachment plates, KPiP cells formed sizable 3-dimensional spheroids that grew into large colonies when re-plated onto normal tissue culture dishes (Fig. 2-5B). Such anchorage-independent growth is considered a hallmark of cancer cells because of its correlation with tumorigenic potential of cells *in vivo*, and is commonly utilized as a marker for *in vitro* transformation [82]. By contrast, KP cells did not survive well in low attachment conditions and generated only small spheroids that failed to form viable colonies when re-plated (Fig. 2-5B). KP cells were also observed to have a diminished ability to form colonies in soft agar or on normal tissue culture plates at low plating density (data not shown). These data suggest that PI3'-lipid signaling renders KPiP cells less dependent on exogenous growth factors such as the mitogens in FCS (lysophosphatidic acid and sphingosine-1-phosphate) and less dependent on attachment. In addition, KPiP cells have a heightened capability to embed and proliferate in the lungs of immunocompromised mice, as discussed above (Supp. Fig. 2-S5). Taken together, these characteristics further confirm the ability of PI3'-lipid

signaling to enhance the tumorigenic potential of lung epithelial cells transformed by oncogenic KRAS.

To begin to define the contributions of downstream signaling pathways to the proliferative capacity of KPiP and KP cells we used immunoblotting to examine baseline signaling levels and assess the consequences of selective pathway-targeted blockade of PIK3CA or RAF→MEK→ERK signaling in these cells. RAF→MEK→ERK signaling was inhibited with the MEK1/2 inhibitor PD0325901 (PD901, 1μM) and PI3'-kinase signaling was inhibited using: 1. the pan-class 1 PI3K inhibitor GDC-0941 (5μM); 2. the selective PIK3CA inhibitor BYL719 (5μM) or 3. The AKT1-3 inhibitor MK2206 (5μM) [81, 83-85]. The consequences of combined blockade of both PIK3CA and RAF→MEK→ERK signaling were assessed using the combination of PD901 and BYL719.

Control KPiP and KP cells had similar levels of pERK1/2 but KPiP cells displayed elevated pAKT, pPRAS40, p70^{S6K}, pRPS6 and p4E-BP1 levels compared to KP cells, consistent with PIK3CA^{H1047R} expression (Fig. 2-5C). Treatment of KPiP cells with GDC-0941 or BYL719, either alone or in combination with PD901, led to striking inhibition of pAKT, pPRAS40, p70^{S6K}, pRPS6 and p4E-BP1 (Fig. 2-5C). Although pAKT was barely detectable in KP cells, treatment of these cells with GDC-0941 or BYL719 led to a reduction of pPRAS40 consistent with there being flux through the PI3'-kinase pathway in these cells. It was noted that KP cells expressed substantially less PTEN than KPiP cells, although this observation is of uncertain significance (Fig. 2-5C). Inhibition of MEK1/2 in both KPiP and KP cells led to reduced pERK, elevated expression of BIM and decreased expression of the known RAF→MEK→ERK target

DUSP6. In both KP and KPiP cells, the expression of cyclin D1 was inhibited by PD901 and GDC-0941 but was largely resistant to BYL719 and MK2206. Finally, cleaved caspase 3 (CC3, marker of apoptosis) was most strongly elevated in KP cells by PD901 as a single agent or in combination with BYL719. In contrast, only the combination of PD901 plus BYL719 led to substantial induction of CC3 in KPiP cells (Fig. 2-5C).

We next determined the effects of 72 hours of treatment with the various inhibitors on cell viability using a range of drug concentrations in conjunction with a Cell Titer Glo assay (Fig. 2-5D). In agreement with the effects we observed on signaling, KP cells were more sensitive to MEK1/2 inhibition with PD901 (GI_{50} ~40nM vs ~150nM, Fig 2-5D & E). However KPiP cells were more sensitive to PIK3CA→AKT pathway inhibitors compared to KP cells (GDC-0941, KP GI_{50} = 2.5 μ M, KPiP GI_{50} = 0.5 μ M; BYL719, KP GI_{50} >5 μ M, KPiP GI_{50} = 1.25 μ M; MK2206, KP GI_{50} >5 μ M, KPiP GI_{50} = 1.5 μ M). It was striking that the only PI3K pathway agent that inhibited the growth of KP cells was the pan-class 1 inhibitor GDC-0941 (Fig. 2-5E), which may reflect this agent's ability to directly inhibit mTORC1/2 signaling [86]. Hence, despite somewhat similar sensitivity to MEK1/2 inhibition, KP and KPiP cells displayed substantially different sensitivity to inhibitors of PI3K→AKT signaling. These data indicate that PIK3CA^{H1047R} contributes substantially to the regulation of proliferation in KRAS^{G12D}/PIK3CA^{H1047R} mutant cells which demonstrate a genotype-drug response phenotype to PI3K pathway inhibitors.

Cooperative regulation of the cell division cycle by RAF and PIK3CA signaling in KRAS^{G12D}/PIK3CA^{H1047R}/TP53^{Null} cells

To test the hypothesis that PIK3CA^{H1047R} may promote the cell division cycle, KP and KPiP cells were treated with: 1. PD901; 2. GDC-0941; 3. BYL719 or combinations of: 4. PD901 plus GDC-0941 and; 5. PD901 plus BYL719 for 24 hours. Cells were labeled with BrdU for the last 3 hours of treatment and then stained with anti-BrdU and analyzed by flow cytometry (Fig. 2-6A & B). Approximately 17% of vehicle-treated KP cells incorporated BrdU over the labeling period. Inhibition of MEK reduced this by 75%. Inhibition of either class 1 PI3Ks or PIK3CA inhibited S phase progression by ~60% and ~40% respectively (Fig. 2-6A). By contrast, and in agreement with the cell proliferation rates assessed in Fig 2-5A, approximately 35% of vehicle-treated KPiP cells incorporated BrdU over the labeling period. Inhibition of MEK reduced this by 60% whereas blockade of either class 1 PI3Ks or PIK3CA inhibited S phase progression by 90% and 75% respectively (Fig. 2-6B). Hence, S phase progression is similarly sensitive to MEK1/2 inhibition but is more sensitive to PI3K inhibition in KPiP compared to KP cells. However, in both cell lines, combined inhibition of both MEK1/2 plus PI3K (either all class 1 or PI3K α) reduced S phase progression by >95% (Fig. 2-6A & B).

To assess signaling changes that might account for these observations, KP or KPiP cells were treated with inhibitors for 24 hours and then analyzed by immunoblotting for changes in protein modification/expression. Expression of c-MYC, a transcription factor essential for lung tumorigenesis and a key cell-cycle regulator [87, 88], was potently suppressed by PD901 in both KP and KPiP cells (Fig. 2-6C & D). However, while c-MYC expression was largely resistant to GDC-0941 or BYL719 in KP cells, it was potently suppressed by these agents in KPiP cells (Fig. 2-6C & D). Reciprocally, the low level of p27^{KIP1} expression in KP cells was largely unaffected by MEK or PI3K

inhibitors, either as single agents or in combination. By contrast, p27^{KIP1} was modestly elevated in response to PD901 and robustly elevated by either GDC-0941 or BYL719 in KPiP cells (Fig. 2-6C & D). These data clearly indicate that two proteins known to play a role in lung tumorigenesis are regulated downstream of PIK3CA in KPiP but not in KP cells [87, 89]

PIK3CA^{H1047R}-mediated regulation of c-MYC and p27^{KIP1} is predicted to increase the activity of cyclin/CDK complexes that promote entry into and transit through S-phase [87, 89]. Indeed, we noted that expression of cyclin A (CCNA), phosphorylation of CDK2 at pT160 (producing the active form of CDK2) and phosphorylation of RB (pS780 and pS807/S811) were more susceptible to inhibition of PI3K signaling in KPiP cells compared to similarly treated KP cells (Fig. 2-6C & D). In addition, cyclin D1 (CCND1) and CDK4 were found to be under the dual control of both RAF→MEK→ERK and PI3K signaling in both KP and KPiP cells (Fig. 2-6C & D). We also noted that survivin, an inhibitor of apoptosis protein (IAP) that has key roles in promoting cell cycle progression and preventing apoptosis [90], was under PIK3CA^{H1047R} control in KPiP cells. Survivin is not widely expressed in adult tissues but it is highly expressed in the majority of cancers [90, 91]. In our models, we found that baseline levels of survivin were higher in KPiP cells and while survivin was potently suppressed by MEK inhibition in both cell lines, its expression was suppressed by selective PI3Kα blockade only in KPiP cells (Fig. 2-6C & D).

Since KPiP cells were more resistant to apoptosis induction by either single or combined pathway inhibition, as assessed by CC3 and by the observation that fewer cells detached or stained with Trypan Blue after 24 hours of treatment (data not shown),

we examined pro- and anti-apoptotic proteins that might be regulated by PIK3CA^{H1047R} that could explain this diminished apoptotic response. We noted that expression of the pro-survival protein MCL-1 was largely unchanged under all conditions in both cell lines. However, it was detected at higher levels in KPiP cells (Fig. 2-6C & D). Expression of the pro-survival BCL-2 and BCL-X_L proteins was sensitive to both MEK1/2 and PI3K inhibition in KPiP cells, showing modestly decreased expression upon inhibition of either pathway, which was enhanced by combined inhibition of both pathways (Fig. 2-6C & D). Reciprocally, we observed that the pro-apoptotic BH3-domain-only proteins BIM and PUMA were induced upon inhibition of either MEK1/2 or PI3K signaling in KPiP cells, which was enhanced by combined inhibition of both pathways (Fig. 2-6C & D). Thus PI3K signaling contributes to upregulation of pro-survival BCL-2 and BCL-X_L and suppression of pro-apoptotic BIM and PUMA. In contrast, only BCL-2 appeared to be regulated by dual RAF→MEK→ERK and PI3K signaling in KP cells (Figs. 2-6C & D). BIM expression was also lower in untreated KPiP compared to KP cells (Fig. 2-5C & 6C-D), which may contribute to the apparent resistance of KPiP cells to apoptosis. These results shed light on the pleiotropic mechanisms by which RAF→MEK→ERK and PI3K signaling may cooperate to promote proliferation and suppress apoptosis in lung cancer cells. They also may help to explain how PIK3CA^{H1047R} accelerates the proliferation of KRAS^{G12D}-initiated lung tumors *in vivo*.

Human H460 KRAS^{Q61H}/PIK3CA^{E545K} mutated NSCLC cells are sensitive to selective blockade of PIK3CA

Genetic analysis of lung cancer specimens reveals that mutational activation of *KRas* and *Pik3ca* occurs in a small percentage of human lung adenocarcinomas [5]. We therefore obtained H460 NSCLC cells that express mutationally activated KRAS^{Q61H} and PIK3CA^{E545K} [92]. In parallel, we conducted analysis of A549 NSCLC cells that express KRAS^{G12S} but do not carry any genetic alterations in the PI3K pathway [92]. Although both cell lines were equally sensitive to inhibition of MEK1/2 (PD901) or pan-class 1 PI3K (GDC-0941), H460 cells were ~3-fold and 2-fold more sensitive to the PIK3CA selective inhibitor (BYL719) and the pan-AKT inhibitor (MK2206) respectively (Fig. 2-7A & B). Analysis of BrdU incorporation over a 3-hour labeling period following 24 hours of drug treatment revealed that 47% of vehicle treated H460 cells transited through S phase during the labeling period. Inhibition of MEK1/2 led to a ~60% reduction in BrdU incorporation (Fig. 2-7C). Strikingly, inhibition of all class 1 PI3Ks or selective inhibition of PIK3CA led to a ~80% reduction in BrdU incorporation. Finally, combined inhibition of MEK1/2 plus PI3'-lipid signaling (PD901 plus GDC-0941 or PD901 plus BYL719) led to a >95% reduction in BrdU incorporation as seen in the KPiP cells. Hence, H460 cells appear highly dependent on PI3'-lipid signaling for S phase progression and the combined inhibition of both PI3K α and MEK1/2 further promoted this anti-proliferative effect (Fig. 2-7C).

Immunoblot analysis of H460 cells treated with the inhibitors described above for 24 hours revealed them to have detectable levels of pERK and pAKT that were reduced in response to the appropriate treatment. We noted that MEK1/2 inhibition led to a modest increase in pS473-AKT, which has been reported in other situations [8]. Similar to KPiP cells, both MEK1/2 and PI3K signaling contributed to the expression of c-MYC. c-MYC

was partially suppressed by MEK1/2 inhibition as well as by selective PI3K α inhibition, while the pan class I PI3K inhibitor or combinations of MEK1/2 and PI3K pathway inhibitors caused a substantial decrease in c-MYC expression. MEK1/2 inhibition also led to a modest increase in p27^{KIP1} and modest decreases in cyclin A and phosphorylation of RB at S807/811 (Fig. 2-7D). However, consistent with the effects of PI3K inhibitors on BrdU incorporation, either pan-class 1 or PIK3CA selective inhibitors led to increased p27^{KIP1} combined with striking decreases in pCDK2, cyclin A and pRB (S780 and S807/811) (Fig. 2-7D). Finally, combined MEK1/2 plus PI3K inhibition more potently suppressed pCDK2 and pRB than single agent blockade of either target alone. Hence, analysis of the response of human KRAS^{Q61H}/PIK3CA^{E545K} mutated H460 NSCLC cells to pathway-targeted blockade of MEK1/2 or PI3K signaling revealed some striking similarities to the effects of the same agents against KRAS^{G12D}/PIK3CA^{H1047R} mutated mouse lung cancer cell lines. These results suggest that mutationally-activated KRAS mouse or human lung cancer cells expressing mutationally-activated PIK3CA are dependent on PI3'-lipid signaling for cell cycle progression and cell proliferation.

Next we tested the responsiveness of H460 cells engineered to express Luciferase (H460L) to pharmacological inhibition of PIK3CA^{E545K} *in vivo*. H460L cells (5x10⁵ cells/mouse) were injected into the tail vein of immunocompromised (NSG) mice. These mice were monitored until lung tumor-derived bioluminescence was ~100 fold above background and then randomized for treatment with either vehicle (n=7) or BYL719 (n=12). However, BYL719 (50mg/kg q.d.) was poorly tolerated in NSG mice; drug toxicity deteriorated their health, resulting in no survival benefit over vehicle-treated mice. Both groups reached end-stage (BCS_≤2) requiring euthanasia by ~4 weeks post

injection of cells (Fig. 2-7E), despite BYL719-treated mice having lower lung tumor derived bioluminescence (Supp. Fig. 2-S7A & B). Analysis of the lungs of end-stage mice indicated that BYL719-treated mice displayed a significantly lower tumor burden compared to vehicle treated controls (~25% vs. ~50%, $p < 0.0001$), though it was significantly higher than observed at the onset of treatment (~25% vs. ~5%, $p = 0.0011$) (Fig. 2-7F & G). In addition, they displayed diminished seeding of tumors at other locations in the body (e.g. the liver). Since analysis of lung tumor derived lysates indicate that this dose of BYL719 only partially inhibited pS473-AKT (Supp. Fig. 2-S7C), it is likely that differences in tumor burden would be more pronounced if more complete blockade of PI3'-lipid signaling could be achieved. Together with observations made with cultured cells, these results indicate that human NSCLC cells expressing mutationally-activated PIK3CA are sensitive to selective inhibition of PI3K α , but that this elicits predominantly a cell cycle arrest and not apoptosis.

DISCUSSION

Here we addressed the requirement for PI3'-lipid signaling in the promotion and maintenance of KRAS-driven lung tumorigenesis, and attempted to identify downstream effectors of mutationally activated PIK3CA in mouse and human lung cancer models. Our results suggest that, despite the reported ability of KRAS to activate PIK3CA in lung tumor cells by direct biochemical means [20], the PI3'-kinase pathway remains rate limiting for KRAS^{G12D}-initiated tumor growth in GEMs. Indeed, the number of tumors initiated by KRAS, their growth rate, and their malignant progression, is significantly

increased by additional activation of PI3'-lipid signaling through expression of mutationally activated PIK3CA^{H1047R}.

These observations suggest that, when expressed at normal physiological levels, oncogenic KRAS^{G12D} may be insufficient to activate downstream signaling pathways required for cell cycle entry in the majority of lung epithelial cells. This is consistent with the apparent latency and stochastic nature of lung tumorigenesis observed in the *Kras*^{LSL-G12D} GEM model [22], and the presence of KRAS mutated cells in healthy human lungs [23]. Hence a substantial fraction of KRAS mutated cells remain dormant until additional signals/events initiate the cell division cycle and promote the process of tumor growth. Our findings suggest that activation of PI3K signaling is sufficient to provide these required accessory signals.

PIK3CA is mutated in about 7% of lung adenocarcinomas and the PI3K→AKT→mTOR signaling pathway in ~25% of cases [2]. Despite being downstream of KRAS, *Pik3ca* mutations co-occur with *KRas* mutations at low frequency in NSCLC (6-10% of KRAS mutant tumors) [5, 35, 36], and at high frequency in colorectal cancers [5], pointing to non-redundant roles of these oncogenes. In the lung, elevated PI3'-kinase signaling is also associated with early stages of smoking-related disease. Analysis of normal versus lungs of smokers with bronchial dysplasia show increased PI3-kinase pathway activation [93, 94]. Thus it is possible that smoking-induced PI3'-lipid signaling in the lung epithelium acts as a promoter of early-stage KRAS mutated lung tumors.

Our analysis of downstream effectors that might explain this cooperation identified key components of the cell division machinery that control entry and transit through S

phase as being selectively regulated by mutationally-activated PIK3CA. In particular, PIK3CA-dependent regulation of c-MYC, p27^{KIP1}, survivin, and the RB pathway were observed. c-Myc, p27^{KIP1}, and the RB pathway have been shown to have important roles in KRAS mutated NSCLC [87, 95, 96]. Survivin is under clinical evaluation as a potential therapeutic target in several cancer types including NSCLC, where its inhibition exhibited modest single agent activity [91]. Our data supports a role for PI3'-lipid signaling in the regulation of these proteins.

PI3'-kinase inhibitors have been demonstrated to promote regression of KRAS^{G12D}-induced lung tumors in GEMs [20]. However an important caveat relates to the grade of the tumors at the time of treatment, which were largely adenomatous and most likely not malignant [20]. Data presented here suggests that selective inhibition of PIK3CA in aggressive KRAS and PIK3CA mutated lung cancers only modestly attenuated their growth and provided little or no survival benefit to cancer-bearing mice. These results are consistent with the low efficacy observed in clinical trials testing PIK3CA inhibitors in a wide range of malignancies including NSCLC [97]. *De novo* or acquired resistance to PI3'-kinase inhibitors is frequently observed in the clinic and several of the mechanisms proposed to explain this involve signals from other pathways that bypass a dependency on mutationally-activated PIK3CA to regulate key downstream effectors such as c-MYC [98]. Thus blocking signals downstream of PIK3CA, such as those identified here, might enhance the activity of PIK3CA inhibitors or forestall resistance to them. For example, agents that stabilize p27^{KIP1} by inhibiting SCF^{SKP2} [99], inhibitors of the cyclin D1-CDK4/6→RB pathway [100] and IAP inhibitors that suppress the anti-apoptotic effects of survivin [91] might be worthy of consideration.

Consistent with previous studies, we conclude that mutationally-activated PIK3CA^{H1047R} is not an initiator, but rather a powerful promoter of lung tumorigenesis initiated by other oncoproteins, particularly KRAS^{G12D} or BRAF^{V600E}. Indeed, the RAF→MEK→ERK and the PI3'-kinase→AKT pathways have been found to synergistically drive tumorigenesis in many cancer models including NSCLC, melanoma and thyroid cancer [9, 75, 101]. This work further illuminates nodes of dual regulation where these pathways converge to promote the entry of cells into the cell cycle and suppress apoptosis. Although the first step towards tumorigenesis is expression of mutationally-activated KRAS or BRAF, PI3'-lipid signaling may provide a crucial second step required to initiate the expansion of tumor cells either by activating the cell division cycle or preventing the senescence-like proliferative arrest observed in KRAS and BRAF mutant NSCLC models [12, 17]. However, it remains uncertain whether targeting PI3'-lipid signaling as a monotherapy will provide a fruitful avenue for treatment of KRAS or PIK3CA mutated lung cancer.

ACKNOWLEDGEMENTS

We thank all members of the McMahon Lab, especially Jillian Silva, Marian Deuker and Anny Shai for support and advice. SG thanks members of her thesis committee: Frank McCormick, Trever Bivona, Emmanuelle Passegue and Eric Collisson for advice and guidance throughout the project. We thank Wayne Phillips (Peter MacCallum Inst.), Tyler Jacks (MIT Cancer Center), Scott Seeley and Hal Chapman (UCSF) for access to various mouse strains. We acknowledge Gioia Iezza (UCSF Department of Pathology) for assistance in histopathological evaluation of mouse tumors. We thank Tina Yuan for

providing advice and reagents and Man-Tzu Wang for advice on the spheroid growth assay. We acknowledge Yunita Lim, Jane Gordon and Byron Hann in the HDFCCC Brain Tumor Research Center, Laboratory for Cell Analysis, and Preclinical Therapeutics cores, respectively for technical support. We thank Emmanuelle di Tomaso & Janet Lyle (Novartis) for access to BYL719, Lori Friedman (Genentech) for access to GDC-0941, Stephen M Townson (Merck) for access to MK2206 and Kurt Thorne and colleagues of the UCSF Nikon Imaging Center for microscopy equipment and support.

GRANT SUPPORT

S. Green was supported by the National Science Foundation Graduate Research Fellowship Program, Grant No. 1144247. MM by an R01 from the NCI (CA 131261) and by a grant from Uniting Against Lung Cancer.

FIGURE LEGENDS:

Figure 2-1. *PIK3CA^{H1047R}* accelerates lung tumorigenesis initiated by *KRAS^{G12D}*

A: Mice of the indicated genotypes were infected with 5×10^7 pfu Ad-Cre and euthanized when body conditioning score was <2 or at 6 months p.i. Overall survival of each mouse cohort is indicated by a Kaplan-Meier survival curve.

B: Representative Hematoxylin and Eosin (H&E) stained lung sections from mice of the indicated genotypes infected with 5×10^7 pfu Ad-Cre and euthanized for analysis at the indicated time points.

C: Lung tumor number (defined as lesions $\geq 10000 \mu\text{m}^2$ and quantified per lung cross section), tumor size (cross section area in μm^2) and overall lung tumor burden (defined as the area occupied by tumors divided by the total area of a lung section) were quantified for each time point. $n=3$ in each category.

D: Mice of the indicated genotypes that also carry the *R26^{mT-mG}* reporter allele were infected with 2×10^7 pfu Ad-Cre and euthanized at one or two weeks p.i. as indicated. Mice were administered BrdU 24-hours prior to euthanasia to label cells transiting through S-phase. Lung sections were stained for GFP expression and BrdU incorporation and imaged by fluorescence microscopy. Scale bar = $50 \mu\text{m}$.

E: Quantification of double EGFP⁺/BrdU⁺ cells. As a control, Ad-Cre infected *R26^{mT-mG}* mice were employed. $n=2$ in each category.

Figure 2-2. *PIK3CA^{H1047R}* promotes malignant progression and growth of established *KRAS^{G12D}*-initiated lung tumors

A: Representative H&E stained lung sections from *KRas^{LSL}* or *KRas^{LSL}; Pik3ca^{Lat}* mice infected with 5×10^6 or 5×10^5 pfu Ad-Cre respectively, which were euthanized for analysis when their body conditioning score was <2 or at 6 months p.i.

B: Quantification of lung tumor burden of mice described in 2A. Error bars indicate +SEM. Significance determined using Student's t test: * $p \leq 0.05$, ** $p \leq 0.01$, *** $p \leq 0.001$, **** $p \leq 0.0001$.

C: Classification of tumor grade from mice described in 2A using previously established criteria.

D: H&E stains of lung tumors from mice of the indicated genotypes. Arrowheads indicate tumor cells with signet ring morphology. Scale bar = 50 μ m.

E: Quantification of lung tumor burden with representative H&E stained lung sections from *KRas^{FSF}; SPC^{CreER}*; *Pik3ca^{Lat}*; *R26^{mT-mG}* (*KSPiR*) and *KRas^{FSF}; SPC^{CreER}*; *R26^{mT-mG}* (*KSR*) mice infected with 2×10^7 pfu Ad-FLP, allowed to develop tumors for 14 weeks, then treated with vehicle or tamoxifen as indicated. Mice were euthanized 10 weeks after tamoxifen treatment. Scale bar = 2mm. n=3 in each category.

Figure 2-3. Selective PIK3CA blockade inhibits KRAS^{G12D}/PIK3CA^{H1047R} lung tumor growth

A: Lung tumor burden and representative H&E stained lung sections from mice of the indicated genotypes infected with 2×10^7 pfu Ad-Cre and treated with vehicle or the selective PI3K α inhibitor BYL719 (50mg/kg, p.o., b.i.d) for 4 weeks, starting 2 days p.i. Scale bar = 2mm. n=4 in each category.

B: Lung tumor burden and representative H&E stained lung sections from *KRas^{LSL}*; *Pik3ca^{Lat}* mice infected with 2×10^7 pfu Ad-Cre and treated with vehicle or BYL719 for 4 weeks, starting 4 weeks p.i. Scale bar = 2mm. n=4 in each category.

C: Immunoblot analysis of lung lysates obtained from mice described in 3A & 3B, probed with antisera against the indicated backbone- or phosphorylation-specific sites.

D: Representative lung sections from mice described in 3B stained with antisera against AKT (pS473), ERK1/2 (pT202/Y204) or BrdU.

Figure 2-4. *PIK3CA* inhibition has modest growth-inhibitory effects in orthotopically engrafted *KRAS^{G12D}/TP53^{Null}* and *KRAS^{G12D}/PIK3CA^{H1047R}/TP53^{Null}* lung cancers

A: Kaplan-Meier survival analysis of mice with *KRAS^{G12D}/PIK3CA^{H1047R}/TP53^{Null}/LUC* (KPiPL) orthotopically engrafted lung tumors treated with vehicle or BYL719 as indicated, starting 7 days after tumor cell injection.

B: Quantification of lung tumor burden of mice described in 4A. For each vehicle-treated mouse that reached end-point, a BYL719-treated mouse was euthanized at the same time for comparison.

C: Representative H&E stained lung sections from mice described in 4A.

D: Representative images of tumor-derived bioluminescence of mice described in 4A, imaged at the indicated time point. Exposure = 10 seconds.

E: Kaplan-Meier survival analysis of mice with $\underline{K}RAS^{G12D}/\underline{T}P53^{Null}/\underline{L}UC$ (KPL) orthotopically engrafted lung tumors treated with vehicle or BYL719 as indicated, starting 10 days after tumor cell injection.

F: Quantification of lung tumor burden of mice described in 4E. For each vehicle-treated mouse that reached end-point, a BYL719-treated mouse was euthanized at the same time for comparison. All remaining BYL719-treated mice were euthanized when the last vehicle-treated mouse reached end point.

G: Representative H&E stained lung sections of mice described in 4E.

H: Representative images of tumor-derived bioluminescence of mice described in 4E, imaged at the indicated time point. Exposure = 10 secs.

Figure 2-5. *PIK3CA^{H1047R} enhances tumorigenic potential of KRAS mutated lung cancer cells in culture*

A: Relative cell count of indicated cell lines grown in the absence (ns) or presence of 10% fetal calf serum assessed using Cell Titer Glo. Each data point represents the average of 7 biological replicates.

B: Representative images of tumor cell spheres cultured in low attachment plates (top panels) and Crystal Violet stains of such spheres following re-plating on normal tissue culture dishes and culturing for 1 week (bottom panels). Scale bar = 100 μ M.

C: Immunoblot analysis of extracts from KP or KP*P* cells treated for 24 hours with the indicated pathway-targeted inhibitors. PD901 at 1 μ M, all others at 5 μ M.

D: Relative cell counts measured using Cell Titer Glo and normalized to DMSO-treated cells after 72 hours of treatment with the indicated drugs at the indicated range of concentrations.

E: GI₅₀ values (μM) for each single agent and cell line in 5D.

Figure 2-6. Cooperative regulation of the cell division cycle by RAF and PIK3CA signaling in KRAS^{G12D}/PIK3CA^{H1047R}/TP53^{Null} cells

A & B: KP and KP*i*P cells were treated with the indicated inhibitors (PD901 at 1μM, all others at 5μM) for 24 hours, then pulsed with 10μM BrdU for the final 3 hours. Transit through S-phase was assessed by staining with anti-BrdU-FITC and quantifying BrdU⁺ cells by flow cytometry. Data represents the average of two separate experiments.

C & D: Immunoblot analysis of lysates from KP or KP*i*P cells treated for 24 hours with the indicated inhibitors (PD901 at 1μM, all others at 5μM).

Figure 2-7. Human KRAS^{Q61L}/PIK3CA^{E545K} mutated H460 NSCLC cells are sensitive to selective blockade of PIK3CA in vitro and in orthotopic lung cancer models

A: Relative cell counts measured using Cell Titer Glo and normalized to DMSO-treated cells after 72 hours of treatment with indicated drugs at the indicated range of concentrations.

B: GI₅₀ values (μM) for each single agent and cell line in 7A.

C: H460 cells were treated with the indicated inhibitors (PD901 at 1μM, all others at 5μM) for 24 hours, then pulsed with 10μM BrdU for the final 3 hours. Transit through S-

phase was assessed by staining with anti-BrdU-FITC and quantifying BrdU⁺ cells by flow cytometry. Data represents the average of two separate experiments.

D: Immunoblot analysis of lysates from H460 cells treated for 24 hours with the indicated inhibitors (PD901 at 1 μ M, all others at 5 μ M).

E: Kaplan-Meier survival analysis of mice with H460L orthotopically engrafted lung tumors treated with vehicle or BYL719 as indicated, starting 7 days after tumor cell injection.

F: Quantification of lung tumor burden of mice described in 7E.

G: Representative H&E stained lung sections of mice described in 7E.

SUPPLEMENTARY FIGURE LEGENDS

Supplementary Figure 2-S1:

A & B: Lung sections from Ad-Cre initiated *KRas^{LSL}* or *KRas^{LSL}; Pik3ca^{Lat}* mice were stained with antisera against ERK (pT202/Y204) or AKT (pS473) at the time points indicated p.i.

Supplementary Figure 2-S2:

Native fluorescence of 150 μ m vibratome slices of mouse lung obtained from *KRas^{LSL}*; *R26^{mT-mG}* or *KRas^{LSL}; Pik3ca^{Lat}; R26^{mT-mG}* mice. Vibratome sections were prepared 2 days p.i. with 2×10^7 Ad-Cre and imaged at the indicated time points. Scale bar = 50 μ m.

Supplementary Figure 2-S3:

A: Quantification of tumor burden and representative H&E stained lung sections from *KRas^{LSL}*; *SPC^{CreER}*; *Pik3ca^{Lat}*; *R26^{mT-mG}* mice treated with tamoxifen for 5 consecutive days and then divided into two groups, one untreated and one infected with 2×10^7 pfu Ad-FLP to induce KRAS^{G12D} expression. Mice were euthanized 14 weeks p.i. Scale bar = 2mm.

B: Immunofluorescence analysis of lung sections from mice described in S3A using anti-GFP antisera. Scale bar = 50 μ m.

Supplementary Figure 2-S4:

Lung tumor-bearing *KPi* mice were treated with one dose of BYL719 (50mg/kg p.o.) and then euthanized at the indicated time points for immunoblot analysis with the indicated antisera.

Supplementary Figure 2-S5:

A: Tumor-derived bioluminescence (photons/second) from individual mice orthotopically engrafted with either 10^5 KP_iP or 10^6 KP cells and imaged over the indicated time period.

B: Representative H&E stained lung sections from KP- or KP_iP-driven orthotopic lung tumor models. Top panels show whole lungs, bottom panels show 20x images of tumors (Scale bar = 50 μ m).

Supplementary Figure 2-S6:

A: Average total luminescence counts (photons/second) from mice orthotopically engrafted with KPiPL lung cancers, treated with vehicle or BYL719, and imaged at the indicated time points.

B: Immunoblot analysis of lung lysates from mice described in 2-S6A, sacrificed 4 hours after the last dose.

C Average total luminescence counts (photons/second) from mice orthotopically engrafted with KPL lung cancers, treated with vehicle or BYL719, and imaged at the indicated time points.

D: Immunoblot analysis of lung lysates from mice described in 2-S6C, sacrificed 4 hours after the last dose.

Supplementary Figure 2-S7:

A: Representative images of tumor-derived bioluminescence from mice orthotopically engrafted with H460L lung cancers, treated with vehicle or BYL719, and imaged at the indicated time points. Exposure = 10 secs.

B: Average total luminescence counts (photons/second) from mice described in 2-S7A.

C: Immunoblot analysis of lung lysates from mice described in 2-S7A, sacrificed 4 hours after the last dose.

Figure 2-1

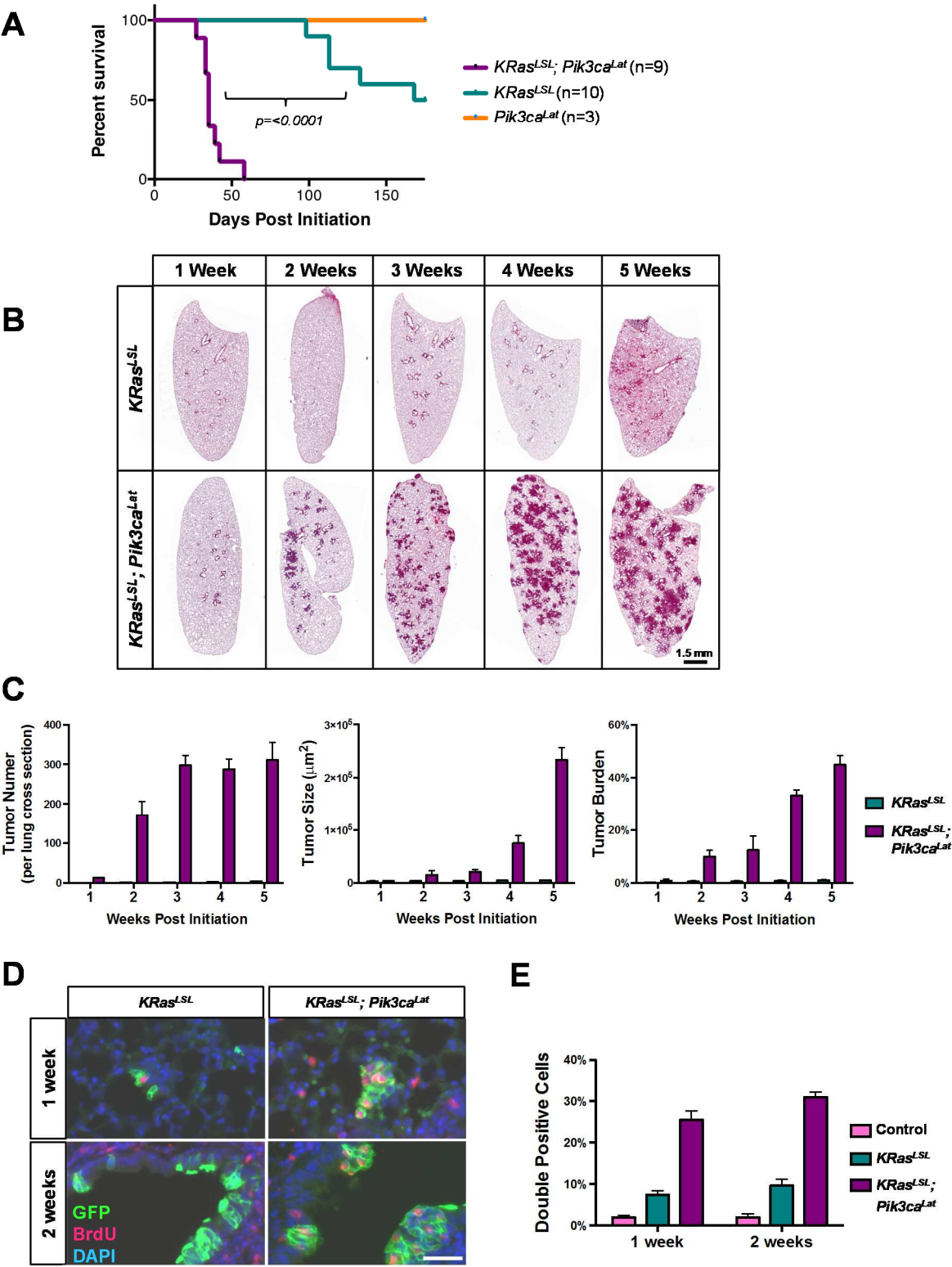


Figure 2-2

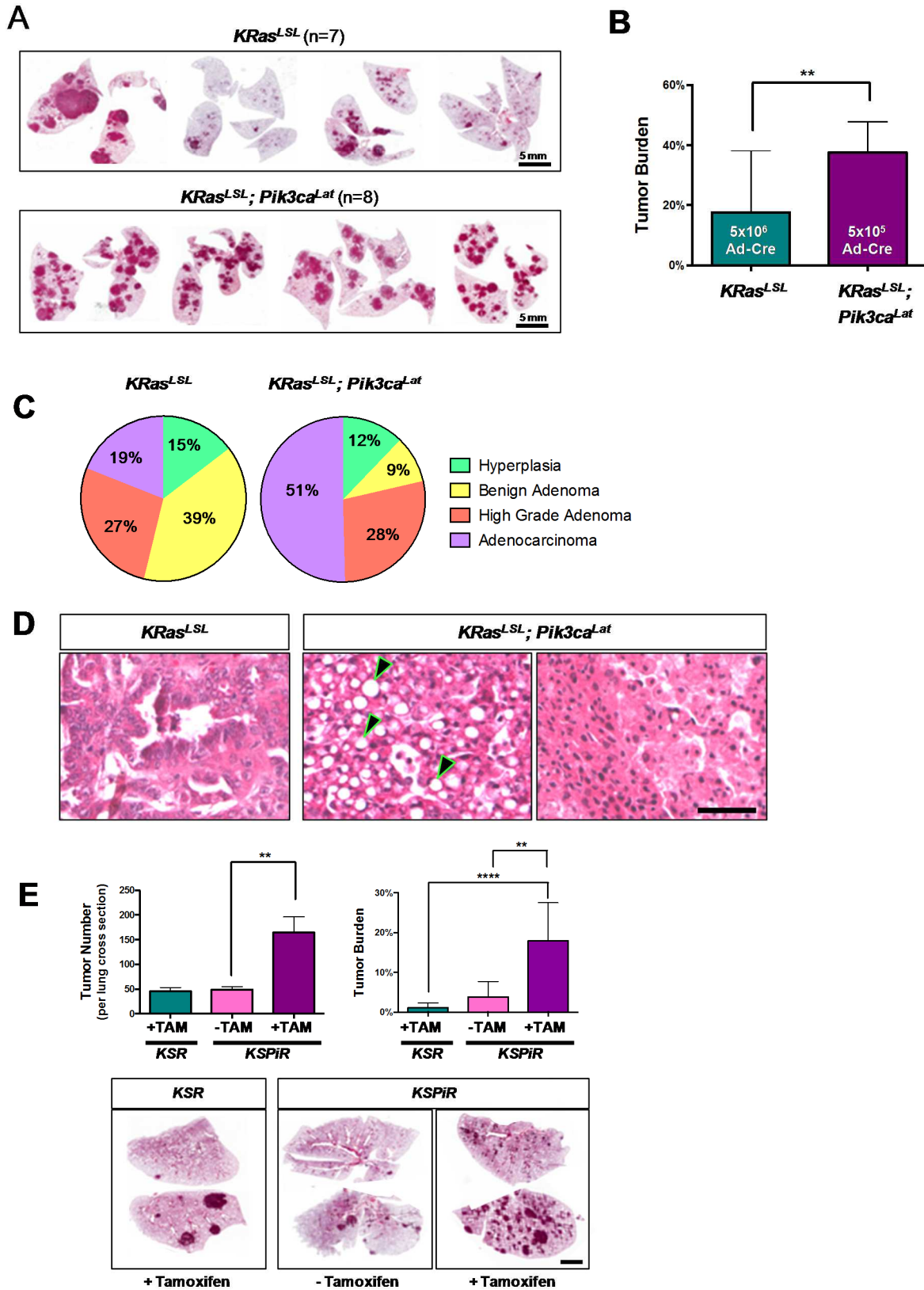


Figure 2-3

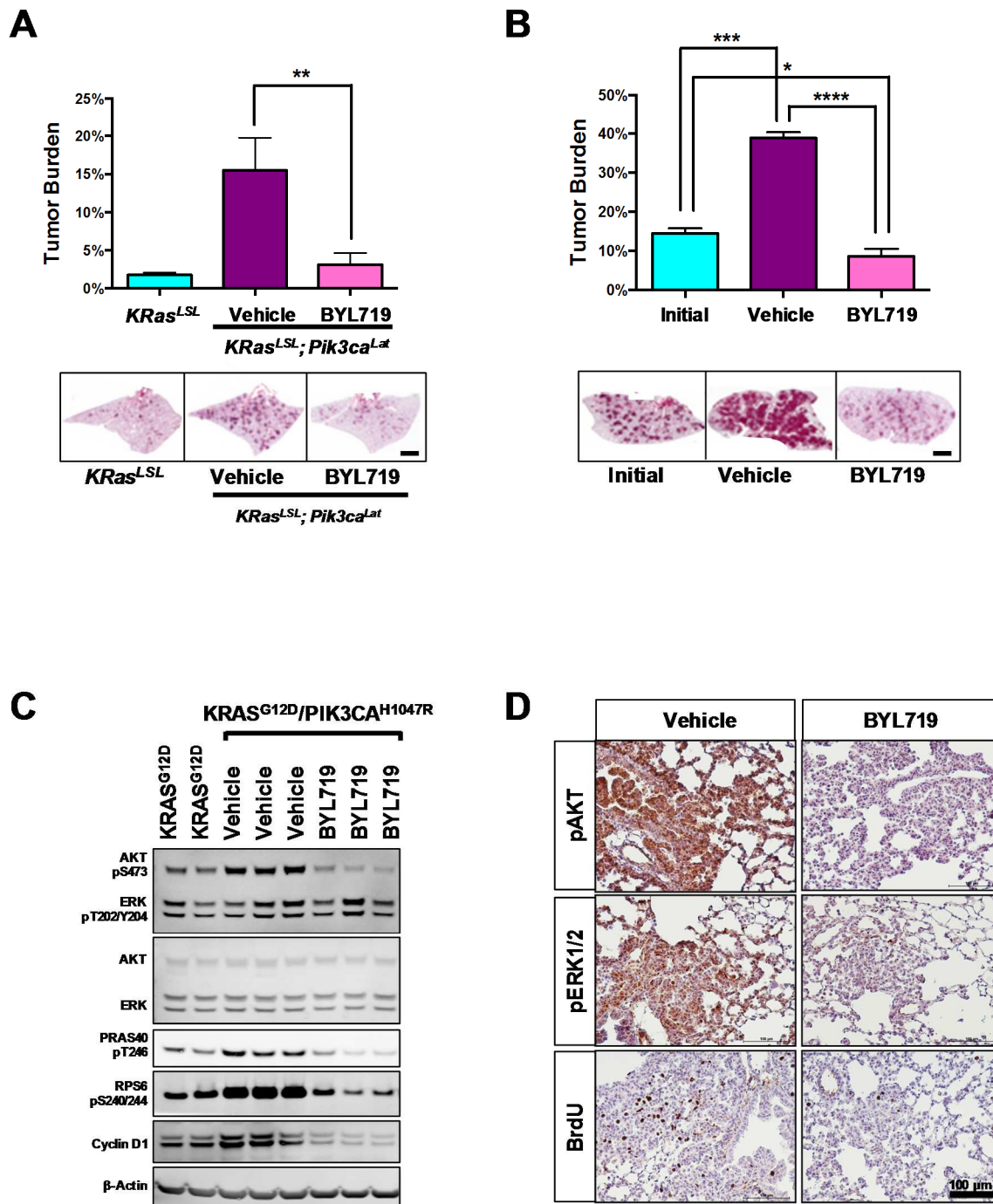


Figure 2-4

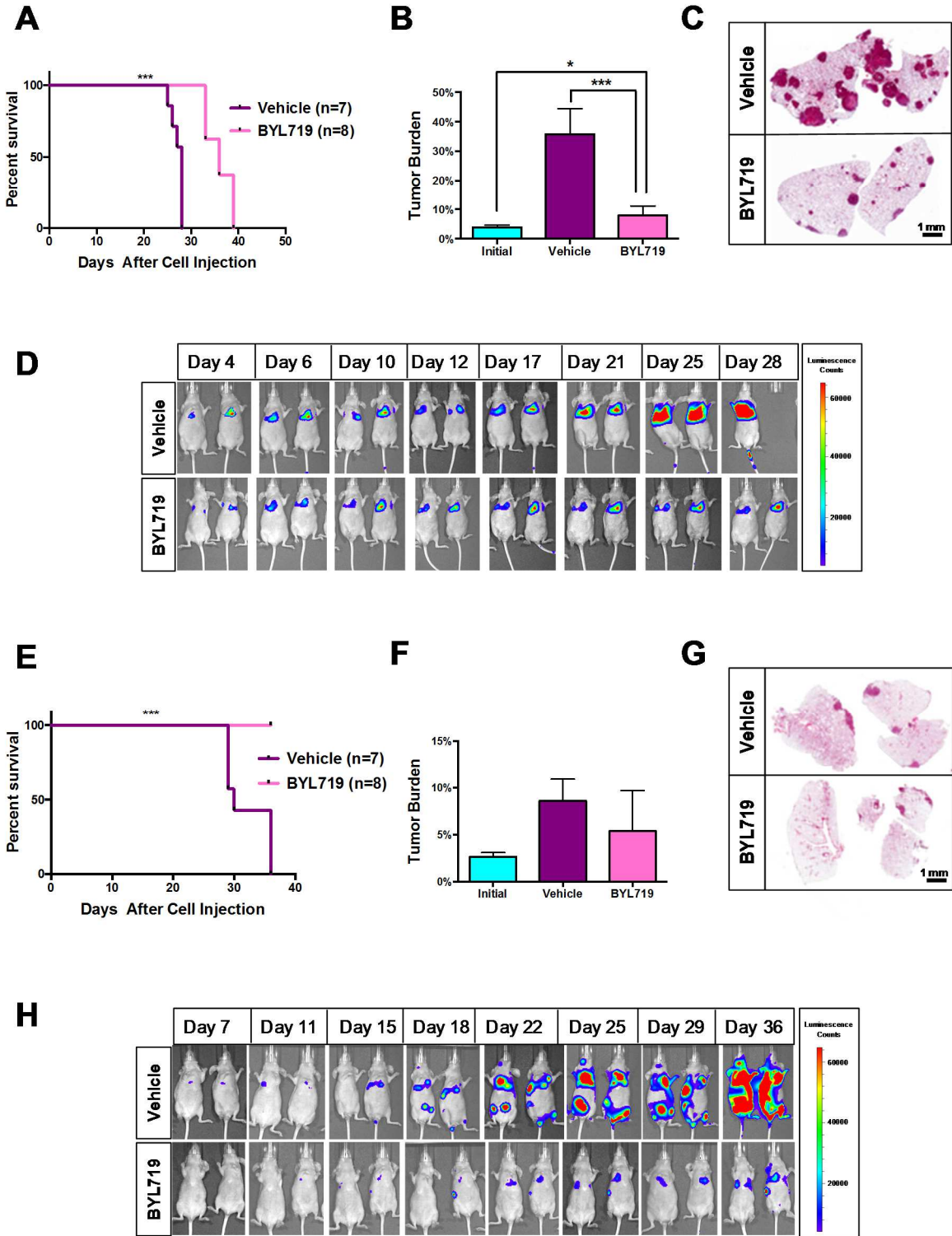


Figure 2-5

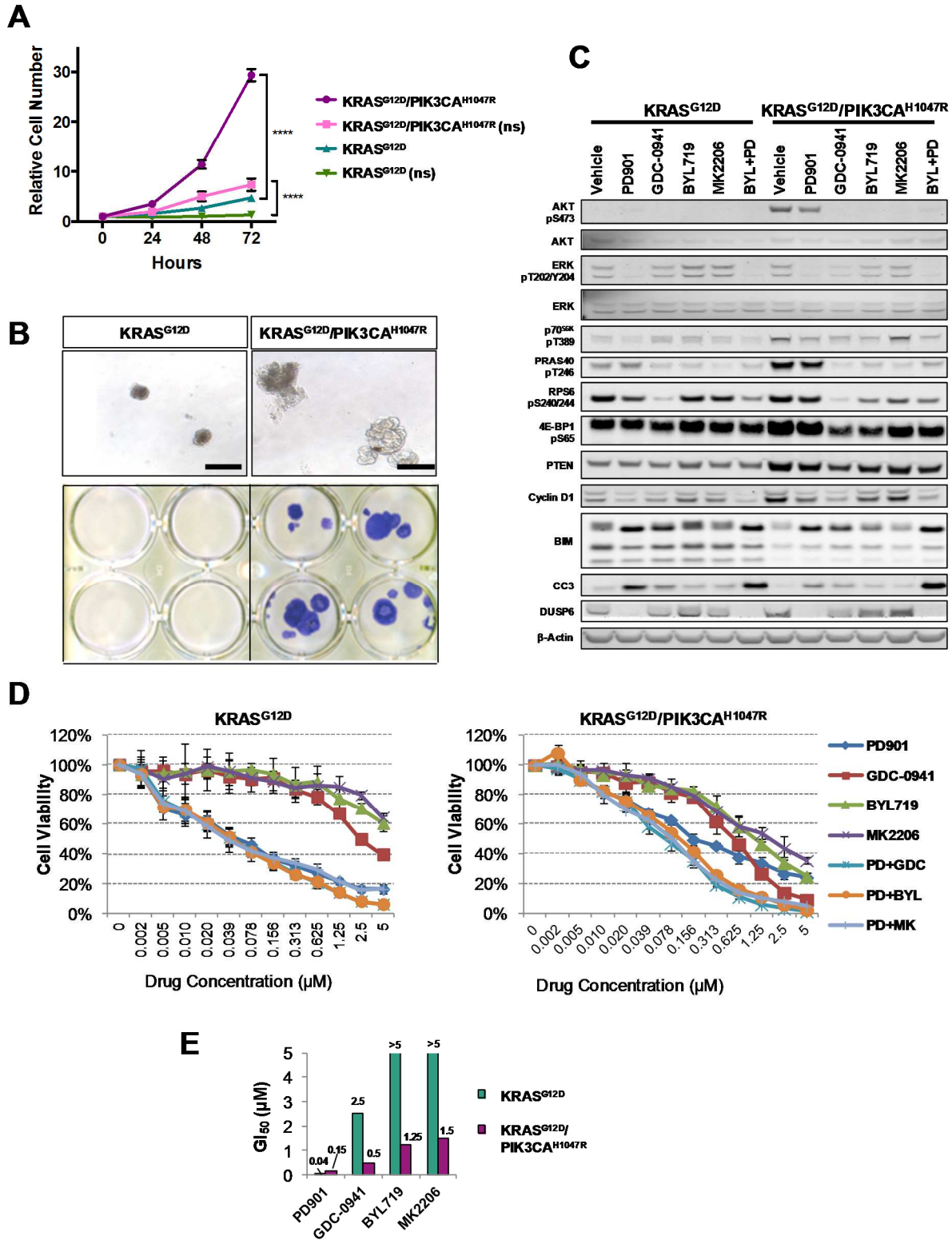


Figure 2-6

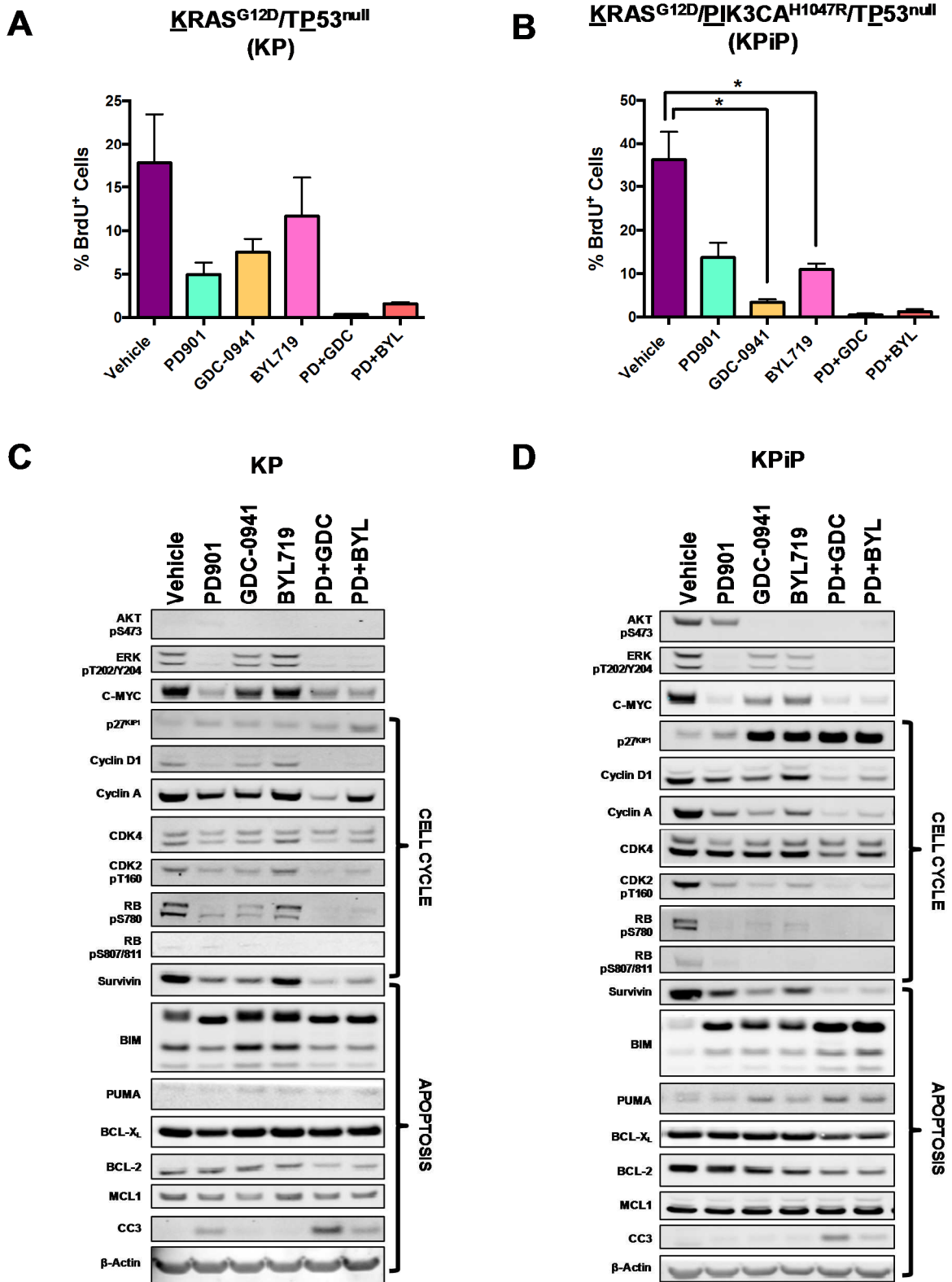
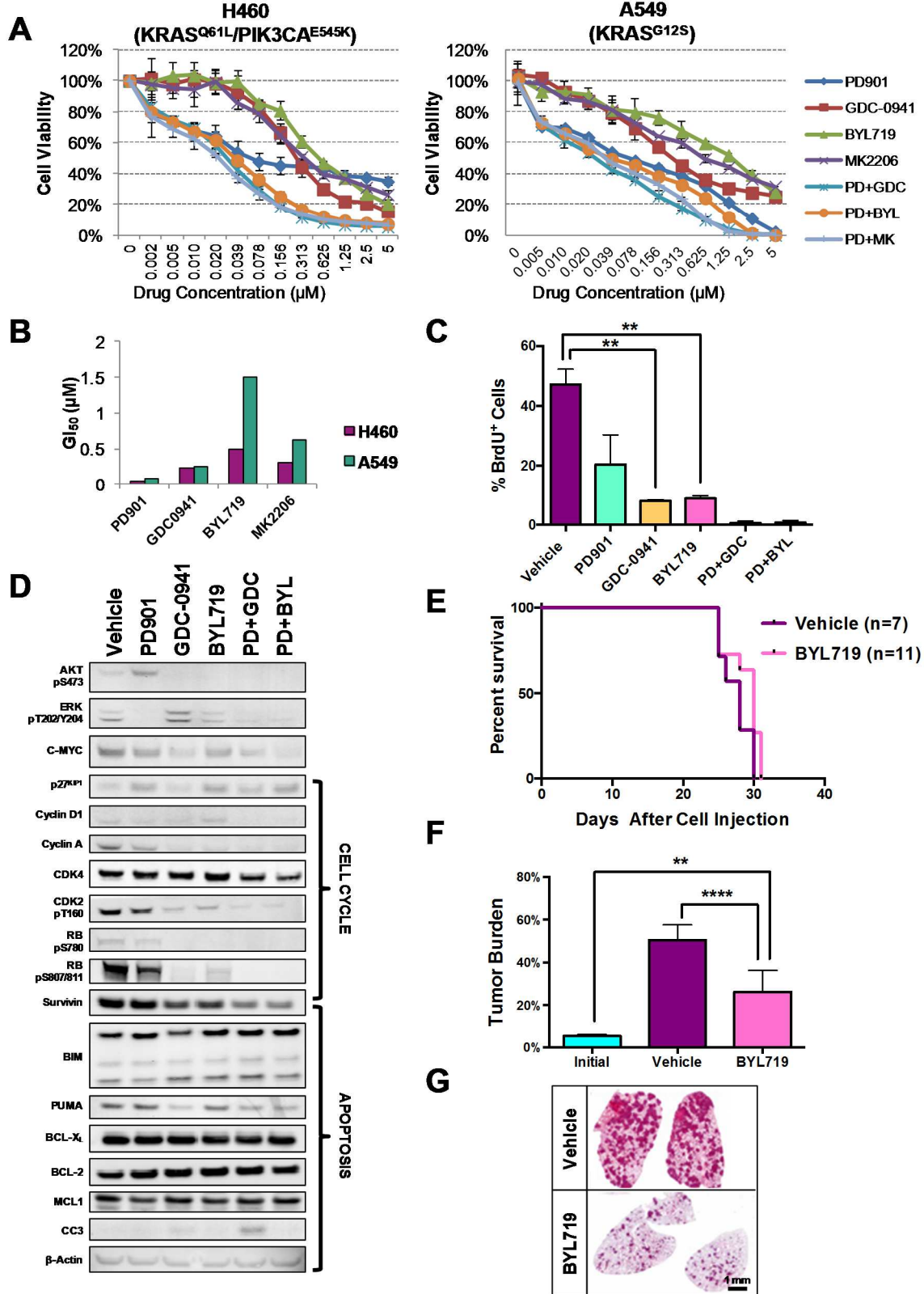
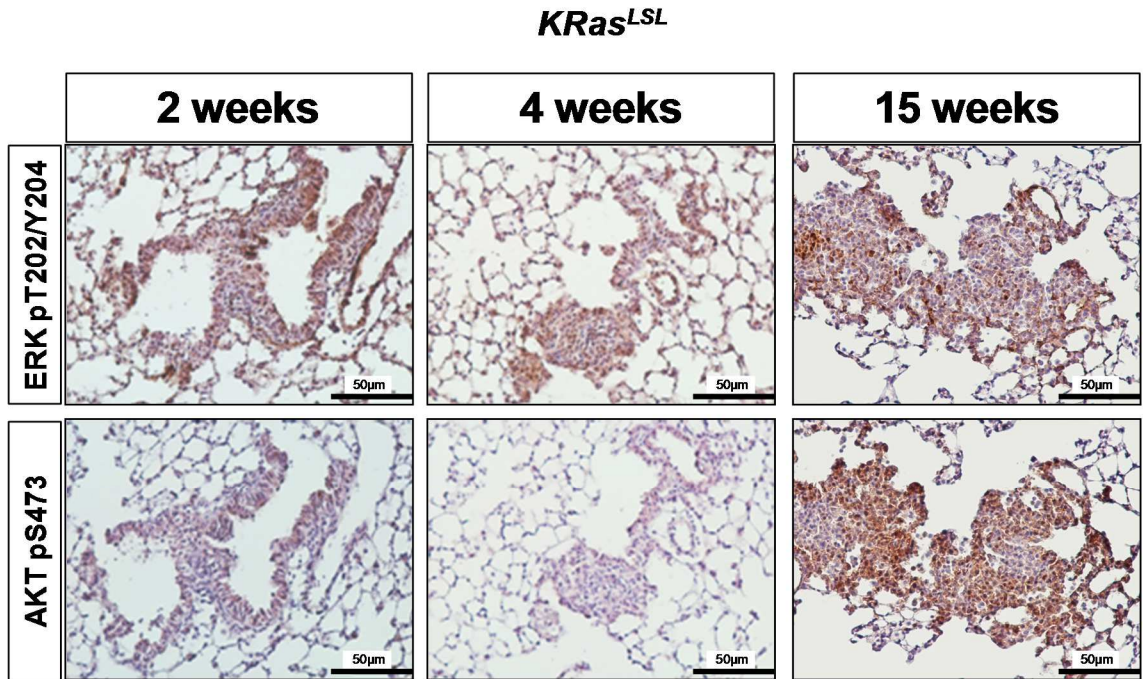


Figure 2-7

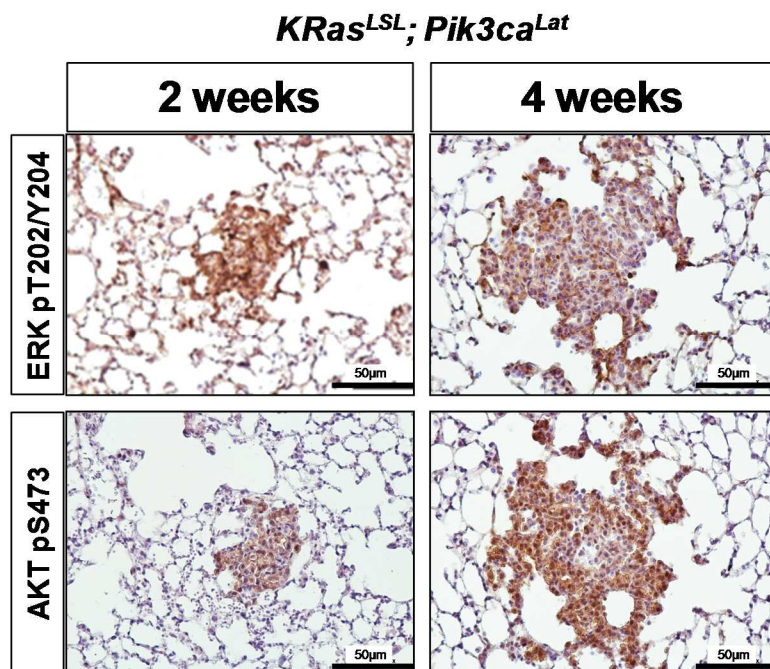


Supplementary Figure 2-S1

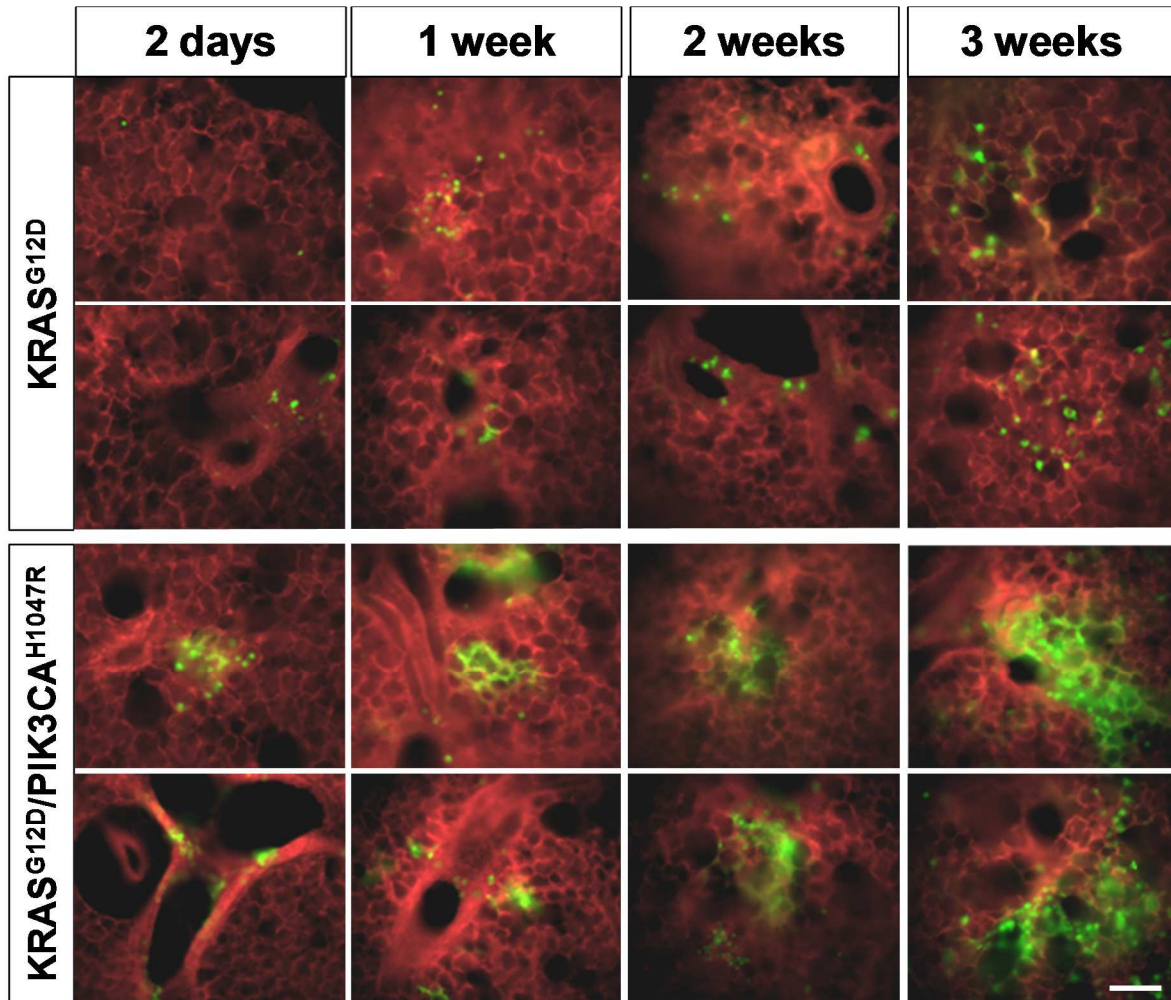
A



B

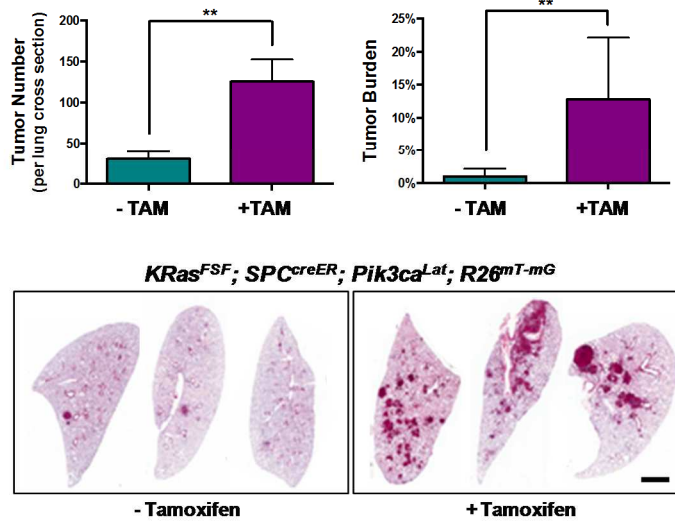


Supplementary Figure 2-S2

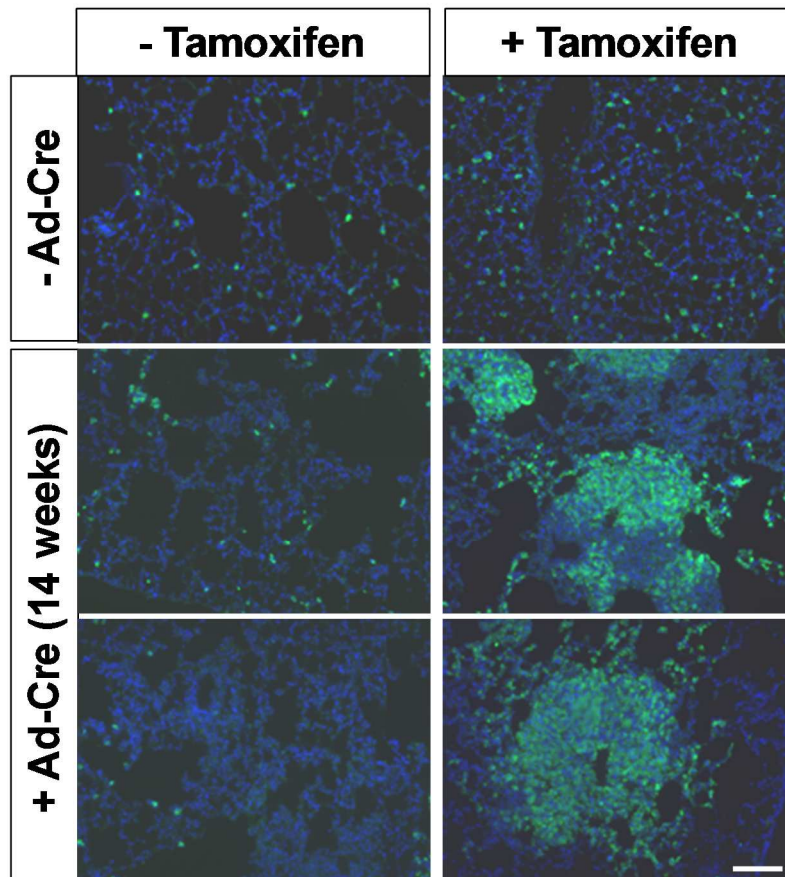


Supplementary Figure 2-S3

A

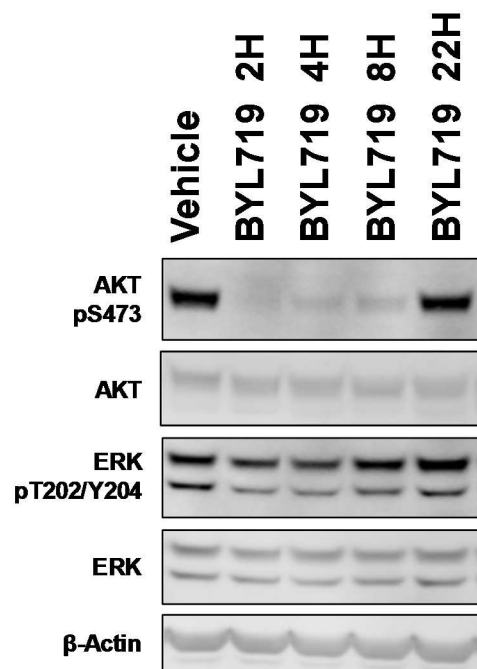


B



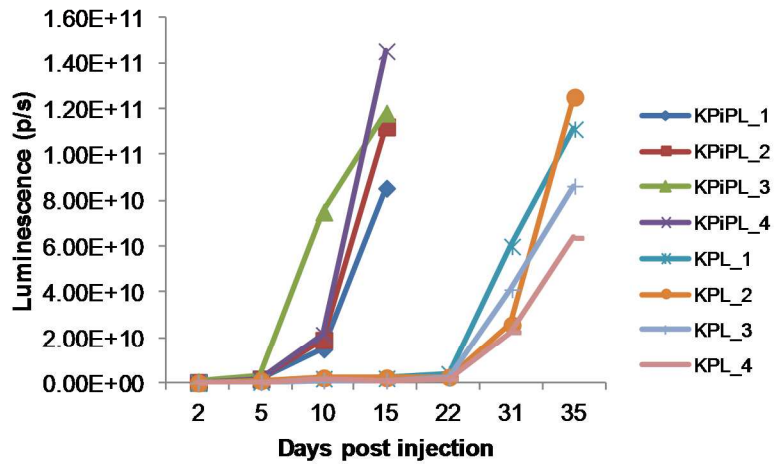
Supplementary Figure 2-S4

A

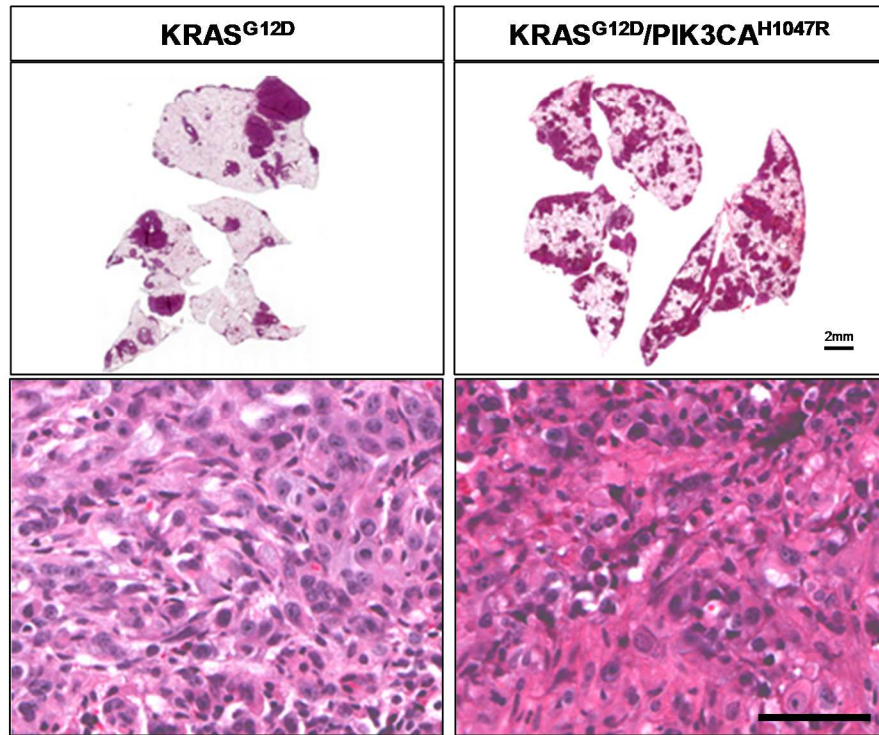


Supplementary Figure 2-S5

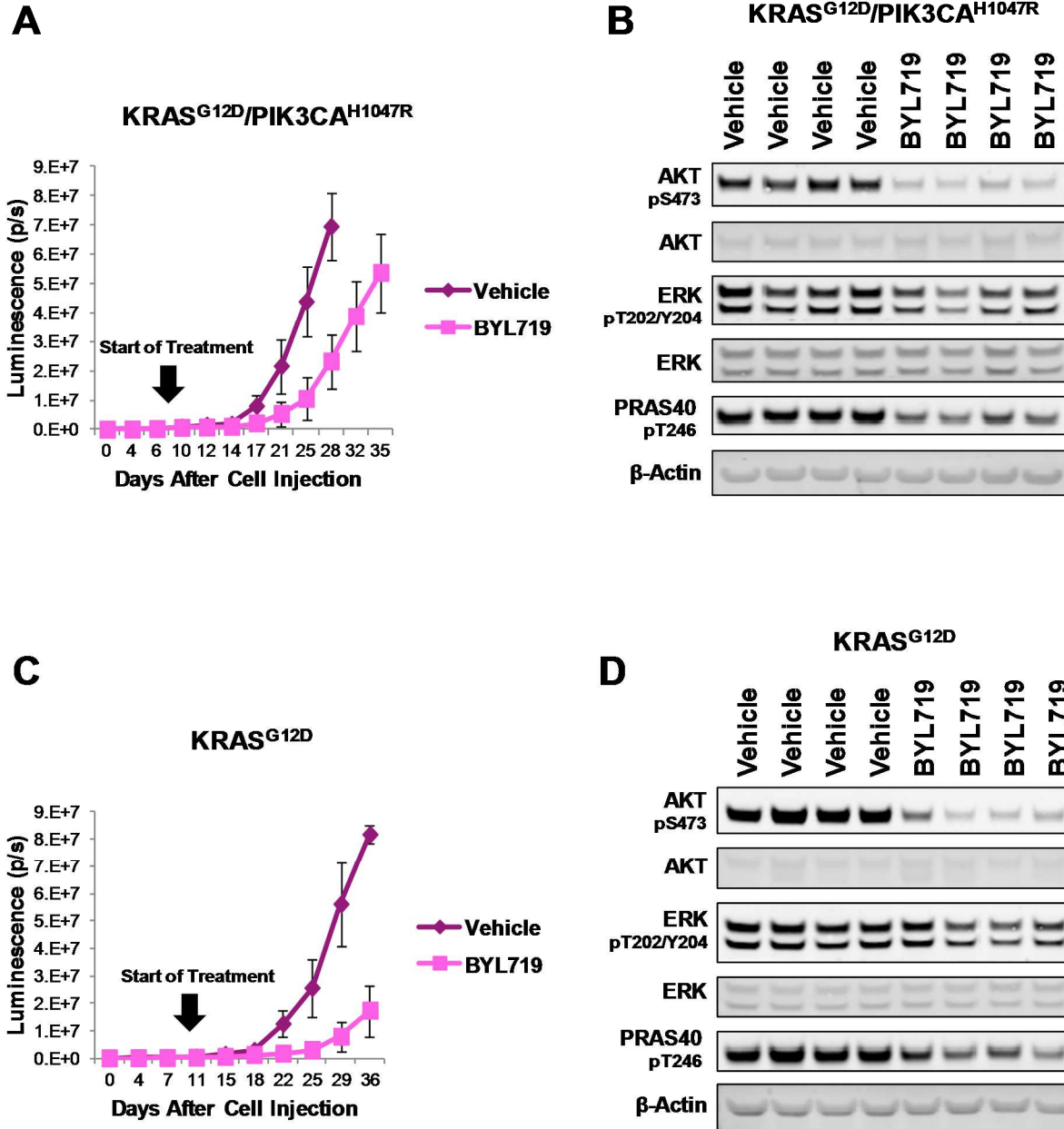
A



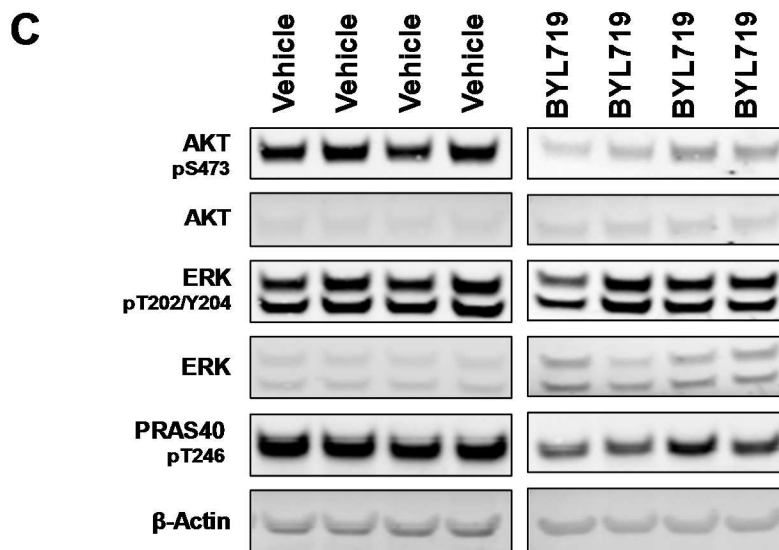
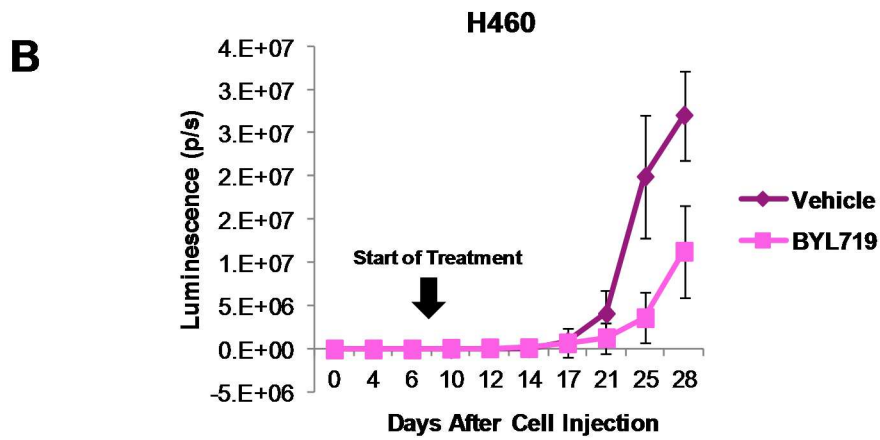
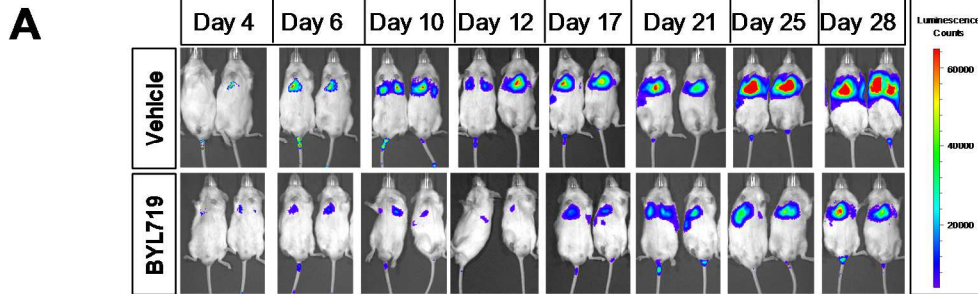
B



Supplementary Figure 2-S6



Supplementary Figure 2-S7



CONCLUSIONS

The mechanisms by which mutationally activated KRAS^{G12D} promotes the aberrant behavior of human lung cells and elicits lung cancer in GEM models remain incompletely understood. However, this research shows that two of the best-credentialed KRAS-GTP effectors, BRAF and PIK3CA, cooperate with one another to mimic the effects of oncogenic KRAS^{G12D}. While expression of BRAF^{V600E} is sufficient to elicit only benign lung tumors, and expression of PIK3CA^{H1047R} is not sufficient to drive any overt lung pathology, expression of both oncogenes results in lethal lung tumorigenesis and cancer that occurs with short latency and high multiplicity. Taken in conjunction with previous reports of the MEK1/2 and PI3K dependency of KRAS^{G12D}-induced lung tumors [43], these data indicate that combined activation of RAF→MEK→ERK and PI3Kα→AKT signaling is necessary and sufficient for lung cancer formation.

The cooperation of PIK3CA^{H1047R} with BRAF^{V600E} might be expected given that these are non-redundant pathways known to be highly mutated in cancers. However, since PIK3CA is a direct downstream effector of KRAS, the dramatic cooperation observed upon co-expression of PIK3CA^{H1047R} and KRAS^{G12D} in the mouse lung was surprising. In contrast to the long, variable latency and sporadic tumor growth observed in KRAS^{G12D}-expressing lungs, simultaneous expression of PIK3CA^{H1047R} and KRAS^{G12D} resulted in rapid growth and progression of malignant cancers with complete penetrance. These results indicate that despite the reported ability of KRAS to activate

PIK3CA in lung tumor cells by direct biochemical means [20], PI3-lipid signaling remains rate limiting for KRAS^{G12D}-initiated tumor growth in GEM models.

Examination of early events in KRAS^{G12D}-expressing mouse lungs shows that when expressed at normal physiological levels, oncogenic KRAS^{G12D} is insufficient to activate the signals required for cell cycle entry in the majority of cells. This is consistent with the apparent latency and stochastic nature of lung tumorigenesis observed in the *Kras*^{LSL-G12D} GEM model [22], and the presence of KRAS mutated cells in healthy human lungs [23]. Hence a substantial fraction of KRAS mutated cells remain dormant until additional signals/events initiate the cell division cycle and promote the process of tumor growth. My work suggests that activation of PI3K signaling is sufficient to provide these required accessory signals.

An analysis of downstream effectors that might explain these cooperations identified key components of the cell division machinery that control entry and transit through S phase as being cooperatively regulated by MAPK and PI3K signaling. In particular, PIK3CA^{H1047R}-mediated regulation of p27^{KIP1} and cooperative regulation of c-MYC, cyclin D1, survivin and the Rb pathway were observed, all of which have been reported to play important roles in KRAS mutated NSCLC [87, 95, 96]. In addition, PIK3CA^{H1047R}-mediates suppression of BIM and upregulation of BCL2 suggest a role for PI3-lipid signaling in preventing apoptosis of KRAS mutated cells.

Lastly, BRAF/PIK3CA mutated lung cancer cells were sensitive to cell cycle arrest by single agent inhibition of either pathway. However combined pathway inhibition had a stronger effect on arresting the growth of cells and also promoting cell death. Similar anti-tumor effects were observed in vivo, where combined BRAF^{V600E} and pan class I

PI3K inhibition caused tumor regression in mice harboring BRAF and PIK3CA mutations. Interestingly, KRAS/PIK3CA mutated cells were more sensitive to growth arrest by selective PIK3CA inhibition than KRAS mutated cells, indicating that PIK3CA^{H1047R}-expressing cells are more highly dependent on PI3-lipid signaling for proliferation. However, in aggressive lung cancer models driven by KRAS and PIK3CA mutations, selective PIK3CA inhibition as a single agent was cytostatic at best, attenuating tumor growth but not causing tumor regression.

In summary, this work confirmed the requirement of RAF→MEK→ERK and PI3Kα→AKT signaling for lung cancer formation in mice and identified specific nodes of dual regulation where these pathways converge to promote the entry of lung cells into the cell division cycle and suppress apoptosis. Although the first step towards tumorigenesis is expression of mutationally-activated KRAS or BRAF which activate the MAPK pathway, PI3-lipid signaling may provide a crucial second step required to initiate the expansion of tumor cells. This might occur through PIK3CA-mediated activation of the cell division cycle, prevention of apoptosis, and/or prevention of the senescence-like proliferative arrest observed in KRAS and BRAF mutant NSCLC models [12, 17]. However, despite the profound cooperation observed in these models and the requirement for PI3-lipid signaling to sustain tumor growth, established KRAS/PIK3CA and BRAF/PIK3CA mutated tumors do not depend on the PI3K pathway for survival.

REFERENCES

1. Society, A.C., *Cancer Facts and Figures*. 2015.
2. Cancer Genome Atlas Research, N., *Comprehensive molecular profiling of lung adenocarcinoma*. *Nature*, 2014. **511**(7511): p. 543-50.
3. Sun, J.M., et al., *Prognostic and predictive value of KRAS mutations in advanced non-small cell lung cancer*. *PLoS One*, 2013. **8**(5): p. e64816.
4. Lodish H, B.A., Zipursky SL, et al. , *Molecular Cell Biology*. 4th ed. Receptor Tyrosine Kinases and Ras. 2000, New York: W. H. Freeman.
5. Cerami, E., et al., *The cBio cancer genomics portal: an open platform for exploring multidimensional cancer genomics data*. *Cancer Discov*, 2012. **2**(5): p. 401-4.
6. Vanhaesebroeck, B., L. Stephens, and P. Hawkins, *PI3K signalling: the path to discovery and understanding*. *Nat Rev Mol Cell Biol*, 2012. **13**(3): p. 195-203.
7. Gkeka, P., et al., *Investigating the Structure and Dynamics of the PIK3CA Wild-Type and H1047R Oncogenic Mutant*. *PLoS Comput Biol*, 2014. **10**(10).
8. Carracedo, A. and P.P. Pandolfi, *The PTEN-PI3K pathway: of feedbacks and cross-talks*. *Oncogene*, 2008. **27**(41): p. 5527-41.
9. Charles, R.P., et al., *Activating BRAF and PIK3CA mutations cooperate to promote anaplastic thyroid carcinogenesis*. *Mol Cancer Res*, 2014. **12**(7): p. 979-86.
10. Dankort, D., et al., *Braf(V600E) cooperates with Pten loss to induce metastatic melanoma*. *Nat Genet*, 2009. **41**(5): p. 544-52.
11. Jackson, E.L., et al., *Analysis of lung tumor initiation and progression using conditional expression of oncogenic K-ras*. *Genes Dev*, 2001. **15**(24): p. 3243-8.
12. Dankort, D., et al., *A new mouse model to explore the initiation, progression, and therapy of BRAFV600E-induced lung tumors*. *Genes Dev*, 2007. **21**(4): p. 379-84.
13. Kinross, K.M., et al., *An activating Pik3ca mutation coupled with Pten loss is sufficient to initiate ovarian tumorigenesis in mice*. *J Clin Invest*, 2012. **122**(2): p. 553-7.
14. Chapman, H.A., et al., *Integrin alpha6beta4 identifies an adult distal lung epithelial population with regenerative potential in mice*. *J Clin Invest*, 2011. **121**(7): p. 2855-62.
15. Xu, X., et al., *Evidence for type II cells as cells of origin of K-Ras-induced distal lung adenocarcinoma*. *Proc Natl Acad Sci U S A*, 2012. **109**(13): p. 4910-5.
16. Trejo, C.L., et al., *MEK1/2 inhibition elicits regression of autochthonous lung tumors induced by KRASG12D or BRAFV600E*. *Cancer Res*, 2012. **72**(12): p. 3048-59.
17. Courtois-Cox, S., et al., *A negative feedback signaling network underlies oncogene-induced senescence*. *Cancer Cell*, 2006. **10**(6): p. 459-72.

18. Blasco, R.B., et al., *c-Raf, but not B-Raf, is essential for development of K-Ras oncogene-driven non-small cell lung carcinoma*. *Cancer Cell*, 2011. **19**(5): p. 652-63.
19. Hollander, M.C., et al., *Akt1 deletion prevents lung tumorigenesis by mutant K-ras*. *Oncogene*, 2011. **30**(15): p. 1812-21.
20. Castellano, E., et al., *Requirement for interaction of PI3-kinase p110alpha with RAS in lung tumor maintenance*. *Cancer Cell*, 2013. **24**(5): p. 617-30.
21. Juan, J., et al., *Diminished WNT -> beta-catenin -> c-MYC signaling is a barrier for malignant progression of BRAFV600E-induced lung tumors*. *Genes Dev*, 2014. **28**(6): p. 561-75.
22. Guerra, C., et al., *Tumor induction by an endogenous K-ras oncogene is highly dependent on cellular context*. *Cancer Cell*, 2003. **4**(2): p. 111-120.
23. Yakubovskaya, M.S., et al., *High frequency of K-ras mutations in normal appearing lung tissues and sputum of patients with lung cancer*. *Int J Cancer*, 1995. **63**(6): p. 810-4.
24. To, M.D., et al., *Progressive genomic instability in the FVB/Kras(LA2) mouse model of lung cancer*. *Mol Cancer Res*, 2011. **9**(10): p. 1339-45.
25. Finney, R.E. and J.M. Bishop, *Predisposition to neoplastic transformation caused by gene replacement of H-ras1*. *Science*, 1993. **260**(5113): p. 1524-7.
26. Cohen, J.B. and A.D. Levinson, *A point mutation in the last intron responsible for increased expression and transforming activity of the c-Ha-ras oncogene*. *Nature*, 1988. **334**(6178): p. 119-24.
27. Huang, H., et al., *Oncogenic K-Ras requires activation for enhanced activity*. *Oncogene*, 2014. **33**(4): p. 532-5.
28. Jackson, E.L., et al., *The differential effects of mutant p53 alleles on advanced murine lung cancer*. *Cancer Res*, 2005. **65**(22): p. 10280-8.
29. Schuster, K., et al., *Nullifying the CDKN2AB locus promotes mutant K-ras lung tumorigenesis*. *Mol Cancer Res*, 2014. **12**(6): p. 912-23.
30. Ji, H., et al., *LKB1 modulates lung cancer differentiation and metastasis*. *Nature*, 2007. **448**(7155): p. 807-10.
31. Iwanaga, K., et al., *Pten inactivation accelerates oncogenic K-ras-initiated tumorigenesis in a mouse model of lung cancer*. *Cancer Res*, 2008. **68**(4): p. 1119-27.
32. Pacheco-Pinedo, E.C., et al., *Wnt/beta-catenin signaling accelerates mouse lung tumorigenesis by imposing an embryonic distal progenitor phenotype on lung epithelium*. *J Clin Invest*, 2011. **121**(5): p. 1935-45.
33. Sanchez-Rivera, F.J., et al., *Rapid modelling of cooperating genetic events in cancer through somatic genome editing*. *Nature*, 2014. **516**(7531): p. 428-31.

34. Molina-Arcas, M., et al., *Coordinate direct input of both KRAS and IGF1 receptor to activation of PI3 kinase in KRAS-mutant lung cancer*. *Cancer Discov*, 2013. **3**(5): p. 548-63.
35. Li, S., et al., *Coexistence of EGFR with KRAS, or BRAF, or PIK3CA somatic mutations in lung cancer: a comprehensive mutation profiling from 5125 Chinese cohorts*. *Br J Cancer*, 2014. **110**(11): p. 2812-20.
36. Wang, L., et al., *PIK3CA mutations frequently coexist with EGFR/KRAS mutations in non-small cell lung cancer and suggest poor prognosis in EGFR/KRAS wildtype subgroup*. *PLoS One*, 2014. **9**(2): p. e88291.
37. Herbst, R.S., J.V. Heymach, and S.M. Lippman, *Lung cancer*. *N Engl J Med*, 2008. **359**(13): p. 1367-80.
38. Heist, R.S. and J.A. Engelman, *SnapShot: non-small cell lung cancer*. *Cancer Cell*. **21**(3): p. 448 e2.
39. Network, T.C.G.A.R., *Diversity of Lung Adenocarcinoma Revealed by Integrative Molecular Profiling*. *Nature*, 2013. **Under Review**.
40. Chaft, J.E., et al., *Coexistence of PIK3CA and other oncogene mutations in lung adenocarcinoma-rationale for comprehensive mutation profiling*. *Mol Cancer Ther*, 2011. **11**(2): p. 485-91.
41. Altomare, D.A. and J.R. Testa, *Perturbations of the AKT signaling pathway in human cancer*. *Oncogene*, 2005. **24**(50): p. 7455-64.
42. Ji, H., et al., *Mutations in BRAF and KRAS converge on activation of the mitogen-activated protein kinase pathway in lung cancer mouse models*. *Cancer Res*, 2007. **67**(10): p. 4933-9.
43. Engelman, J.A., et al., *Effective use of PI3K and MEK inhibitors to treat mutant Kras G12D and PIK3CA H1047R murine lung cancers*. *Nat Med*, 2008. **14**(12): p. 1351-6.
44. Jonkers, J., et al., *Synergistic tumor suppressor activity of BRCA2 and p53 in a conditional mouse model for breast cancer*. *Nat Genet*, 2001. **29**(4): p. 418-25.
45. Trotman, L.C., et al., *Pten dose dictates cancer progression in the prostate*. *PLoS Biol*, 2003. **1**(3): p. E59.
46. Sutherland, K.D., et al., *Cell of origin of small cell lung cancer: inactivation of Trp53 and Rb1 in distinct cell types of adult mouse lung*. *Cancer Cell*, 2011. **19**(6): p. 754-64.
47. Fasbender, A., et al., *Incorporation of adenovirus in calcium phosphate precipitates enhances gene transfer to airway epithelia in vitro and in vivo*. *J Clin Invest*, 1998. **102**(1): p. 184-93.
48. Ullman-Cullere, M.H. and C.J. Foltz, *Body condition scoring: a rapid and accurate method for assessing health status in mice*. *Lab Anim Sci*, 1999. **49**(3): p. 319-23.

49. Capper, D., et al., *Assessment of BRAF V600E mutation status by immunohistochemistry with a mutation-specific monoclonal antibody*. *Acta Neuropathol*, 2011. **122**(1): p. 11-9.
50. Morita, S., T. Kojima, and T. Kitamura, *Plat-E: an efficient and stable system for transient packaging of retroviruses*. *Gene Ther*, 2000. **7**(12): p. 1063-6.
51. Zhu, J., et al., *Senescence of human fibroblasts induced by oncogenic Raf*. *Genes Dev*, 1998. **12**(19): p. 2997-3007.
52. Gopal, Y.N., et al., *Basal and treatment-induced activation of AKT mediates resistance to cell death by AZD6244 (ARRY-142886) in Braf-mutant human cutaneous melanoma cells*. *Cancer Res*, 2010. **70**(21): p. 8736-47.
53. Deng, W., et al., *Role and therapeutic potential of PI3K-mTOR signaling in de novo resistance to BRAF inhibition*. *Pigment Cell Melanoma Res*, 2011. **25**(2): p. 248-58.
54. Ohren, J.F., et al., *Structures of human MAP kinase kinase 1 (MEK1) and MEK2 describe novel noncompetitive kinase inhibition*. *Nat Struct Mol Biol*, 2004. **11**(12): p. 1192-7.
55. Hirai, H., et al., *MK-2206, an allosteric Akt inhibitor, enhances antitumor efficacy by standard chemotherapeutic agents or molecular targeted drugs in vitro and in vivo*. *Mol Cancer Ther*, 2010. **9**(7): p. 1956-67.
56. Halilovic, E., et al., *PIK3CA mutation uncouples tumor growth and cyclin D1 regulation from MEK/ERK and mutant KRAS signaling*. *Cancer Res*. **70**(17): p. 6804-14.
57. Wee, S., et al., *PI3K pathway activation mediates resistance to MEK inhibitors in KRAS mutant cancers*. *Cancer Res*, 2009. **69**(10): p. 4286-93.
58. Drahl, C., *LGX818, Made To Fight Melanoma*. *Chemical & Engineering News*, 2013. **91**(16): p. 14.
59. Koul, D., et al., *Antitumor activity of NVP-BKM120--a selective pan class I PI3 kinase inhibitor showed differential forms of cell death based on p53 status of glioma cells*. *Clin Cancer Res*, 2011. **18**(1): p. 184-95.
60. Hofmann, I., et al., *K-RAS mutant pancreatic tumors show higher sensitivity to MEK than to PI3K inhibition in vivo*. *PLoS One*, 2012. **7**(8): p. e44146.
61. Collisson, E.A., et al., *A central role for RAF-->MEK-->ERK signaling in the genesis of pancreatic ductal adenocarcinoma*. *Cancer Discov*, 2012. **2**(8): p. 685-93.
62. Kissil, J.L., et al., *Requirement for Rac1 in a K-ras induced lung cancer in the mouse*. *Cancer Res*, 2007. **67**(17): p. 8089-94.
63. Meylan, E., et al., *Requirement for NF-kappaB signalling in a mouse model of lung adenocarcinoma*. *Nature*, 2009. **462**(7269): p. 104-7.

64. Nikitin, A.Y., et al., *Classification of proliferative pulmonary lesions of the mouse: recommendations of the mouse models of human cancers consortium*. *Cancer Res*, 2004. **64**(7): p. 2307-16.
65. Livet, J., et al., *Transgenic strategies for combinatorial expression of fluorescent proteins in the nervous system*. *Nature*, 2007. **450**(7166): p. 56-62.
66. Raynaud, F.I., et al., *Biological properties of potent inhibitors of class I phosphatidylinositide 3-kinases: from PI-103 through PI-540, PI-620 to the oral agent GDC-0941*. *Mol Cancer Ther*, 2009. **8**(7): p. 1725-38.
67. Morris, E.J., et al., *Discovery of a novel ERK inhibitor with activity in models of acquired resistance to BRAF and MEK inhibitors*. *Cancer Discov*, 2013.
68. Eser, S., et al., *Selective requirement of PI3K/PDK1 signaling for Kras oncogene-driven pancreatic cell plasticity and cancer*. *Cancer Cell*, 2013. **23**(3): p. 406-20.
69. Snyder, E.L., et al., *Nkx2-1 represses a latent gastric differentiation program in lung adenocarcinoma*. *Mol Cell*, 2013. **50**(2): p. 185-99.
70. Winslow, M.M., et al., *Suppression of lung adenocarcinoma progression by Nkx2-1*. *Nature*, 2011. **473**(7345): p. 101-4.
71. Thiery, J.P., et al., *Epithelial-mesenchymal transitions in development and disease*. *Cell*, 2009. **139**(5): p. 871-90.
72. Gupta, S., et al., *Binding of ras to phosphoinositide 3-kinase p110alpha is required for ras-driven tumorigenesis in mice*. *Cell*, 2007. **129**(5): p. 957-68.
73. Mirza, A.M., et al., *Cooperative regulation of the cell division cycle by the protein kinases RAF and AKT*. *Mol Cell Biol*, 2004. **24**(24): p. 10868-81.
74. Ebi, H., et al., *Not just gRASping at flaws: finding vulnerabilities to develop novel therapies for treating KRAS mutant cancers*. *Cancer Sci*, 2014. **105**(5): p. 499-505.
75. Trejo, C.L., et al., *Mutationally activated PIK3CA(H1047R) cooperates with BRAF(V600E) to promote lung cancer progression*. *Cancer Res*, 2013. **73**(21): p. 6448-61.
76. Muzumdar, M.D., et al., *A global double-fluorescent Cre reporter mouse*. *Genesis*, 2007. **45**(9): p. 593-605.
77. Lamouille, S., et al., *TGF- β -induced activation of mTOR complex 2 drives epithelial-mesenchymal transition and cell invasion*. *Journal of Cell Science*, 2012. **125**(5): p. 1259-1273.
78. Mendoza, A., et al., *Modeling metastasis biology and therapy in real time in the mouse lung*. *J Clin Invest*, 2010. **120**(8): p. 2979-88.

79. Irwin, R.S., et al., *Spread the word about the journal in 2013: from citation manipulation to invalidation of patient-reported outcomes measures to renaming the Clara cell to new journal features*. Chest, 2013. **143**(1): p. 1-4.
80. Young, N.P., D. Crowley, and T. Jacks, *Uncoupling cancer mutations reveals critical timing of p53 loss in sarcomagenesis*. Cancer Res, 2011. **71**(11): p. 4040-7.
81. Furet, P., et al., *Discovery of NVP-BYL719 a potent and selective phosphatidylinositol-3 kinase alpha inhibitor selected for clinical evaluation*. Bioorg Med Chem Lett, 2013. **23**(13): p. 3741-8.
82. Hanahan, D. and R.A. Weinberg, *Hallmarks of cancer: the next generation*. Cell, 2011. **144**(5): p. 646-74.
83. Thompson, N. and J. Lyons, *Recent progress in targeting the Raf/MEK/ERK pathway with inhibitors in cancer drug discovery*. Curr Opin Pharmacol, 2005. **5**(4): p. 350-6.
84. Folkes, A.J., et al., *The identification of 2-(1H-indazol-4-yl)-6-(4-methanesulfonyl-piperazin-1-ylmethyl)-4-morpholin-4-yl-t hieno[3,2-d]pyrimidine (GDC-0941) as a potent, selective, orally bioavailable inhibitor of class I PI3 kinase for the treatment of cancer*. J Med Chem, 2008. **51**(18): p. 5522-32.
85. Yan, L., *MK-2206: A potent oral allosteric AKT inhibitor*. American Association for Cancer Research; April 19; Denver, CO, 2009.
86. Silva, J.M., C. Bulman, and M. McMahon, *BRAFV600E cooperates with PI3K signaling, independent of AKT, to regulate melanoma cell proliferation*. Mol Cancer Res, 2014. **12**(3): p. 447-63.
87. Soucek, L., et al., *Inhibition of Myc family proteins eradicates KRas-driven lung cancer in mice*. Genes Dev, 2013. **27**(5): p. 504-13.
88. Zajac-Kaye, M., *Myc oncogene: a key component in cell cycle regulation and its implication for lung cancer*. Lung Cancer, 2001. **34 Suppl 2**: p. S43-6.
89. Chu, I.M., L. Hengst, and J.M. Slingerland, *The Cdk inhibitor p27 in human cancer: prognostic potential and relevance to anticancer therapy*. Nat Rev Cancer, 2008. **8**(4): p. 253-67.
90. Mita, A.C., et al., *Survivin: key regulator of mitosis and apoptosis and novel target for cancer therapeutics*. Clin Cancer Res, 2008. **14**(16): p. 5000-5.
91. Giaccone, G., et al., *Multicenter phase II trial of YM155, a small-molecule suppressor of survivin, in patients with advanced, refractory, non-small-cell lung cancer*. J Clin Oncol, 2009. **27**(27): p. 4481-6.
92. Basu, A., et al., *An interactive resource to identify cancer genetic and lineage dependencies targeted by small molecules*. Cell, 2013. **154**(5): p. 1151-61.
93. Gustafson, A.M., et al., *Airway PI3K pathway activation is an early and reversible event in lung cancer development*. Sci Transl Med, 2010. **2**(26): p. 26ra25.


94. Tsao, A.S., et al., *Increased phospho-AKT (Ser(473)) expression in bronchial dysplasia: implications for lung cancer prevention studies*. *Cancer Epidemiol Biomarkers Prev*, 2003. **12**(7): p. 660-4.
95. Puyol, M., et al., *A synthetic lethal interaction between K-Ras oncogenes and Cdk4 unveils a therapeutic strategy for non-small cell lung carcinoma*. *Cancer Cell*, 2010. **18**(1): p. 63-73.
96. Kelly-Spratt, K.S., et al., *Inhibition of PI-3K restores nuclear p27Kip1 expression in a mouse model of Kras-driven lung cancer*. *Oncogene*, 2009. **28**(41): p. 3652-62.
97. Brana, I. and L.L. Siu, *Clinical development of phosphatidylinositol 3-kinase inhibitors for cancer treatment*. *BMC Med*, 2012. **10**: p. 161.
98. Klempner, S.J., A.P. Myers, and L.C. Cantley, *What a tangled web we weave: emerging resistance mechanisms to inhibition of the phosphoinositide 3-kinase pathway*. *Cancer Discov*, 2013. **3**(12): p. 1345-54.
99. Wu, L., et al., *Specific small molecule inhibitors of Skp2-mediated p27 degradation*. *Chem Biol*, 2012. **19**(12): p. 1515-24.
100. *First CDK 4/6 Inhibitor Heads to Market*. *Cancer Discov*, 2015. **5**(4): p. 339-40.
101. Marsh Durban, V., et al., *Differential AKT dependency displayed by mouse models of BRAFV600E-initiated melanoma*. *J Clin Invest*, 2013. **123**(12): p. 5104-18.

Publishing Agreement

It is the policy of the University to encourage the distribution of all theses, dissertations, and manuscripts. Copies of all UCSF theses, dissertations, and manuscripts will be routed to the library via the Graduate Division. The library will make all theses, dissertations, and manuscripts accessible to the public and will preserve these to the best of their abilities, in perpetuity.

Please sign the following statement:

I hereby grant permission to the Graduate Division of the University of California, San Francisco to release copies of my thesis, dissertation, or manuscript to the Campus Library to provide access and preservation, in whole or in part, in perpetuity.



Author Signature

7-29-5
Date